TWO-DIMENSIONAL ELECTRODE ARRAY STUDIES OF PROPAGATING EPILEPTIFORM NEURAL ACTIVITY IN THE RAT HIPPOCAMPAL SLICE

BY

JAMES LAWRENCE NOVAK

B.S., University of Illinois, 1983
M.S., University of Illinois, 1985

THESIS

Submitted in partial fulfillment of the requirements
for the degree of Doctor of Philosophy in Electrical Engineering
in the Graduate College of the
University of Illinois at Urbana-Champaign, 1988

Urbana, Illinois

UNIVERSITY OF ILLINOIS AT URBANA-CHAMPAIGN

THE GRADUATE COLLEGE

JANUARY 1988

WE HEREBY RECOMMEND THAT THE THESIS BY

JAMES LAWRENCE NOVAK

ENTITLED TWO-DIMENSIONAL ELECTRODE ARRAY STUDIES OF PROPAGATING EPILEPTIFORM NEURAL ACTIVITY IN THE RAT HIPPOCAMPAL SLICE

BE ACCEPTED IN PARTIAL FULFILLMENT OF THE REQUIREMENTS FOR THE DEGREE OF DOCTOR OF PHILOSOPHY

Bruce C Wheeler
Director of Thesis Research

Timothy N. Trick
Head of Department

Committee on Final Examination†

Bruce C Wheeler
Chairperson

Burdette Oade II

Charles A Law

William J Greenough

† Required for doctor's degree but not for master's.

O-517

TWO-DIMENSIONAL ELECTRODE ARRAY STUDIES OF PROPAGATING EPILEPTIFORM NEURAL ACTIVITY IN THE RAT HIPPOCAMPAL SLICE

James Lawrence Novak, Ph.D.
Department of Electrical and Computer Engineering
University of Illinois at Urbana-Champaign, 1988

A technique has been developed in which a planar array of 32 microelectrodes, arranged in a 4 by 8 pattern with 200 μm separation, is used to record from and to stimulate the rat hippocampal slice preparation at multiple sites. Active suppression circuitry is used to prevent device saturation due to large stimulation artifacts. Control of media flow past the tissue is critical to observe signals and to preserve viability. The field potentials recorded are spatially unique and provide a two-dimensional description of the underlying population activity in the various pyramidal cell strata and subpopulations. The application of current source density analysis to the potential data permits accurate determination of peak times, in addition to the estimation of local current sources and sinks. Propagation delays of the compound action potential, first, and second population spikes along CA1 calculated using these peak times are not uniform, and may indicate differences and directionality in coupling mechanisms.

ACKNOWLEDGMENTS

I thank my wife, Julie, for treating me as a mature adult during this research, even though I was a graduate student. She was always ready to lift me up when nothing worked, as well as to keep my head from swelling when great discoveries were made. Her stabilizing influence has undoubtedly added years to my professional and personal life.

Professor Bruce Wheeler provided invaluable guidance as I performed the brain slice experiments with the planar electrode array. I now realize that this freedom is somewhat rare, and I sincerely appreciate his support during this project.

I thank Fen-Lei Chang for his assistance when I faced biological problems. Our discussions regarding technique and data interpretation were vital to the completion of this project.

The Bioacoustics Research Laboratory houses a most wonderful combination of people. I am truly grateful for the opportunity to work with the BRL staff, faculty, and especially the students. I hope that I have been as supportive of them as they have been of me.

Finally, now that I have what some may call a terminal degree, I am certain my parents are resting more easily. I could not have succeeded without the self-confidence and desire to learn which they instilled in me.

This project was supported by a 3M Faculty Development grant and a research grant from the Epilepsy Foundation of America. The Pyralin polyimide was donated by DuPont.

TABLE OF CONTENTS

CHAPTER 1

MULTICHANNEL RECORDINGS FROM NEURAL TISSUE

1.1 Multielectrode Arrays

The nervous system is composed of a bewildering variety of neurons and other cells arranged in intricate structures. Neuroscientists have long studied both the organization of and projections connecting the structures of the brain. The spatial variations, both intra- and interstructural, reflect their diversity of function. It is now generally accepted that the power of the nervous system stems from massive amounts of parallel processing in time and space.

This spatial aspect of processing has motivated attempts to fabricate arrays of electrodes for recording simultaneously from multiple neural sites. "Bed of nails" structures, made of conventional extracellular electrodes, have been used for recording from visual and olfactory cortex (Freeman, 1980; Kruger and Bach, 1981; Kruger, 1982; Bach and Kruger, 1986) as well as in the hippocampal slice (Bragin et al., 1977; Knowles et al., 1985a). These devices consisted of individual metal or glass electrodes which were bonded together using epoxy. They were relatively fragile and required painstaking hand fabrication, especially as the number of desired electrodes increased.

Rapid development of integrated circuit fabrication technology prompted its use in fabricating sensors for use in neurophysiology to overcome these difficulties. Mass production of high-density electrode arrays in a variety of geometries can

be achieved. Furthermore, integration of electronics, possibly including buffering, amplification, and multiplexing, can potentially improve signal-to-noise ratio and make the sensing system more compact. A review of some techniques for fabrication of multielectrode arrays was given by Pickard (1979).

Probe-type microelectrode arrays inserted into neural tissue are becoming increasingly common. One of the first reports of such a device was given by Wise and Angell (1975) in which they described the fabrication and design criteria for a three-pronged "fork" electrode. The center prong contained two recording electrode sites while the outer prongs were used for stimulation. Another variety of probe, a depth electrode, was fabricated on the outer surface of a single micropipette using electron beam lithography. It was used to record unit activity from the cat marginal gyrus (Pochay et al., 1979).

As micromachining techniques improve, probes with multiple recording sites on a single tip are being developed. Small, thin tips are necessary to minimize tissue damage upon insertion. A probe consisting of a 100 μm by 1 mm molybdenum tip with 2 columns of 12 microelectrodes has been used to elucidate neural group properties in the rat hippocampus (Kuperstein and Eichenbaum, 1985; Kuperstein et al., 1986). Design considerations for a probe consisting of four conductor sites on a single prong with on-chip multiplexing, as well as tests of preliminary designs, were described by Bement et al. (1986).

Planar microelectrode arrays, which are placed in contact with tissue but not inserted into it, may also be fabricated

using photolithographic techniques, and are particularly conducive to mass production with high numbers and density of electrodes. In their simplest form, these devices are passive, and consist of a planar supporting substrate with photopatterned metal conductors covered by an insulating material except for the electrode and connector sites. Differences between these passive arrays arise principally from insulation materials, deinsulation techniques and electrode geometries. Significant effort has been made to use these devices to record from neural cultures (Thomas et al., 1972; Pine, 1980; Gross, 1979; Lucas et al., 1985; Droge et al., 1986). Single unit potentials from molluscan ganglia have also been recorded using passive planar arrays (Gross et al., 1982, Novak and Wheeler, 1986a). The use of a flexible polyimide substrate permitted another planar array of electrodes to be shaped to follow the contour of the human cochlea (Shamma-Donoghue et al., 1982).

Planar arrays fabricated on silicon wafers offer simple integration of on-chip electronics together with recording electrodes. The use of such an array with a hippocampal slice was reported by Jobling et al. (1981), who recorded evoked population spikes with a 3 by 3 matrix of field-effect transistors spaced 1 mm apart. The gates of these transistors served as the electrodes and were exposed to the hippocampal slice surface. Another innovative device, the transsubstrate microelectrode array, overcame the problem of passivation of active elements necessary to prevent saline media from

contaminating the gates (Kim et al., 1985). The electrode contacts were made through a silicon wafer to the reverse side. Conductive p-type dopant zones were migrated through the n-type material, using an infrared laser, producing local increases in conductivity. This device was used to record action potentials from crayfish giant axons.

1.2 Multichannel Recordings from Brain Slices

The hippocampal slice has proved to be a useful tool for the study of synchronized epileptiform activity (Prince, 1978; Traub et al., 1985; Knowles et al., 1985a). Slice recordings made with conventional microelectrodes have provided a great deal of information regarding membrane properties and local neural population circuitry (MacVicar and Dudek, 1980a; Turner and Schwartzkroin, 1980). However, there exist few studies which focus on the slice at a macroscopic, systems level, due largely to a lack of simultaneous recordings (Schneiderman, 1986). The electrophysiology of the slice is quite dynamic and involves changes in membrane level events as well as neural circuitry. Thus spatially sampled records which have been serially reconstructed from multiple stimuli (e.g., Swann et al., 1986) may be misleading in systemic investigations of the slice.

There has been only one previous report of multichannel recording from brain slices using microelectrode arrays. As mentioned above, the array fabricated by Jobling et al. (1981) was used to record field potentials from hippocampal slices. However, recording sessions lasted only 20 min and the presence

of signals was interpreted only as a demonstration of the technique. No details of the recording protocol or recording capabilities of the system were given. The lack of information regarding the benefits and limitations of surface recording device clouds the issue of whether the advantages are outweighed by increased cost and the relative fragility of active electronic devices directly exposed to salt solutions.

Described in this thesis is a technique in which a passive planar array of 32 microelectrodes was used to record from the hippocampal slice preparation at multiple sites within the strata in the pyramidal cell subfields. The array was durable and was used for stimulation as well as recording. Experiments have been performed to define the advantages and limitations of the technique itself, as well as to study the propagation of epileptiform activity through a hippocampal slice. This work has provided the motivation for new array designs (e.g., Ficht, 1987), which attempt to improve the recording capabilities. Many of the aspects of this project have been reported, including fabrication of the device (Novak and Wheeler, 1986a), the recording system (Novak and Wheeler, 1987a), the experimental methodology (Novak and Wheeler, 1987b,c), a multichannel signal processing technique (Wheeler and Novak, 1986), and the results of the propagation study (Novak and Wheeler, 1987d; Novak et al., 1987).

1.3 Thesis Organization

The development of any new recording technique for use in neurophysiology first requires the characterization of the signals acquired, and then the establishment of scientific relevance of these signals. This thesis is thus organized to reflect both the engineering and biological results of the work. Chapters 1 and 2 serve as introductory material, providing a survey of important results from the multielectrode and hippocampal literature, respectively.

Chapter 3 provides information on the specialized hardware constructed to acquire, process, and display the multichannel signals. The technical aspects of the multichannel recording system are discussed, providing a framework for future system designs. A summary of the biological protocol is given in Chapter 4, particularly with respect to those techniques unique to this system. The operations used in extracting the peak time information from the large amount of data are outlined in Chapter 5.

The results of the investigation are presented in two main sections in Chapter 6. The first of these deals with the recording technique itself, and the characteristics of the signals which are recorded by the array. Information on tissue viability and sensitivity to slicing angle is also given. This section also demonstrates the capability for stimulation using the array.

The second portion of this chapter deals with the analysis of the data acquired in an effort to isolate differences between

two classes of hippocampal slice models of epilepsy. The first model involves the addition of drugs to antagonize inhibition mediated by gamma-amino-butyric acid (GABA), while the second increases post-synaptic excitability by removing Mg^{++} from the medium. Measurements of conduction delays through region CA1 of the hippocampal slice for various components of the epileptiform bursts reveal differences between the two models. By utilizing the current source density technique discussed in Chapter 5, differences in the slope of conduction delay versus distance can be observed. These measurements are obscured by using field potentials alone.

Finally, Chapter 7 contains a discussion of the results, with emphasis on the power of the recording technique, not merely because of the increased number of signals, but also due to the ability to apply spatial filtering techniques (e.g., CSD analysis) to the data, in order to highlight specific types of information. Differences between hippocampal slice models, as well as implications regarding the appropriate choice of a particular model, are also explored. Experiments designed to further investigate these biological results are also outlined in addition to recommendations for future work in this area.

CHAPTER 2

THE HIPPOCAMPAL BRAIN SLICE EPILEPSY MODEL

2.1 Epilepsy and the Hippocampal Slice

Epilepsy is a condition which results in the abnormal synchronous firing of many neurons within structures of the central nervous system. Epileptic seizures are divided into two categories, based upon the amount of cortex involved. Focal epilepsy involves discrete cortical abnormalities while the generalized form appears to involve deep subcortical grey matter which projects diffusely to the forebrain. Thus, both types involve foci of abnormal activity, although there are significant differences in the location of the affected regions. Recent work in the field has been devoted to understanding the abnormal physiology of cortical foci, in an effort to develop pharmacological agents to control epileptiform activity (Prince, 1978; Dichter and Ayala, 1987).

Electroencephalographic (EEG) recordings reveal two characteristic types of electrical activity associated with an epileptic event. The interictal spike discharge appears to be a marker for regions of the brain which are particularly prone to the second EEG characteristic, the seizure or ictal discharges. In some forms of epilepsy, seizures appear to begin at sites of interictal discharge. Although many types of epilepsy do not appear to display a simple transition from interictal to ictal discharges, the interictal event has been extensively studied as the earliest and simplest phenomenon in epilepsy.

Attempts to understand epilepsy from a cellular perspective have been made using the in-vitro brain slice technique. Because of similarities with some forms of human epilepsy, brain slice models of cortical focal epilepsy have been extensively studied (Prince, 1978). The hippocampal brain slice preparation, in particular, has been the predominant model for many of the membrane and cellular studies of epilepsy. This is not only because of its uniform, laminar anatomy, but also because it can be made to generate population bursts, in which large numbers of neurons burst in tight synchrony. It is generally believed that these population bursts are closely related to the interictal discharges observed in EEG recordings (Alger, 1984). Furthermore, hippocampal slices contain relatively large neurons and are planar, making them well-suited for use with the planar microelectrode array.

2.2. Anatomy of the Hippocampal Slice

The hippocampus is organized as a series of roughly parallel lamellae, which makes it possible to cut transverse slices containing an intact neural circuit (Andersen et al., 1971a). These may be kept viable for long periods (up to 24 h) and many of the cells within a slice appear to retain their in-vivo properties (Schwartzkroin, 1975). Although fibers not lying in the plane of section are severed, they are believed to exert only modulatory influences on the major excitatory pathways (Andersen et al., 1971a). A schematic diagram of a transverse hippocampal slice is shown in Figure 2.1. The principal cells within the

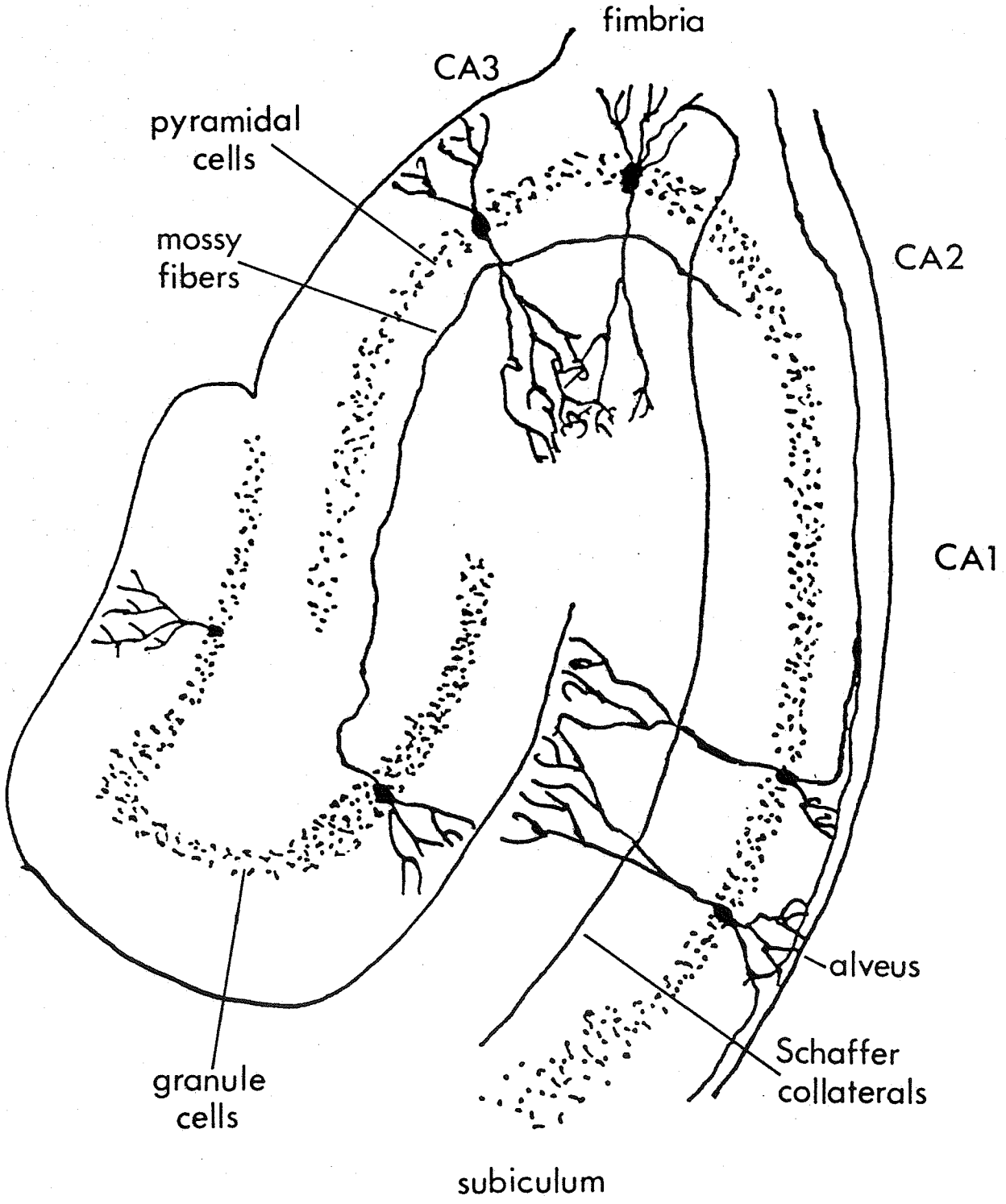

Figure 2.1 Schematic diagram of the rat hippocampal slice.

hippocampus are organized into two interlocking "C" shaped layers, containing the pyramidal cells and the granule cells of the dentate gyrus (Lorente de No, 1934). The granule cells will not be discussed further because they possess high thresholds for bursting and are not considered in most studies of epileptiform activity (Alger, 1984).

The somata of the pyramidal cells are contained in densely packed bands, indicated by dotted regions in Figure 2.1. The dendritic branches of hippocampal pyramidal cells extend perpendicularly from these bands, forming layers of locally uniform cellular structures. The nomenclature for the various strata in region CA1 is illustrated in Figure 2.2. The layer of cell bodies is termed stratum pyramidale (s. pyr.) and that of the basilar dendritic tree is the stratum oriens (s. or.). The apical dendritic region is termed the stratum radiatum (s. rad.), and is often further divided into proximal and distal segments, because the various afferent fibers innervate different levels.

The curved arrangement of pyramidal cells consists of a number of different cell types, but clear distinctions between these regions are not always made (Alger, 1984). The pyramidal cells are divided into three regions, CA1, CA2, and CA3. The CA1 pyramidal cells are located nearest the subiculum. The CA2 region borders CA1 near the point where the s. pyr. begins to curve; however, it is difficult to identify the CA2/CA1 border without histological manipulations. The anatomical differences between CA3 and CA2 pyramidal cells are even less clear, leading to interpretation problems when recording in this area.

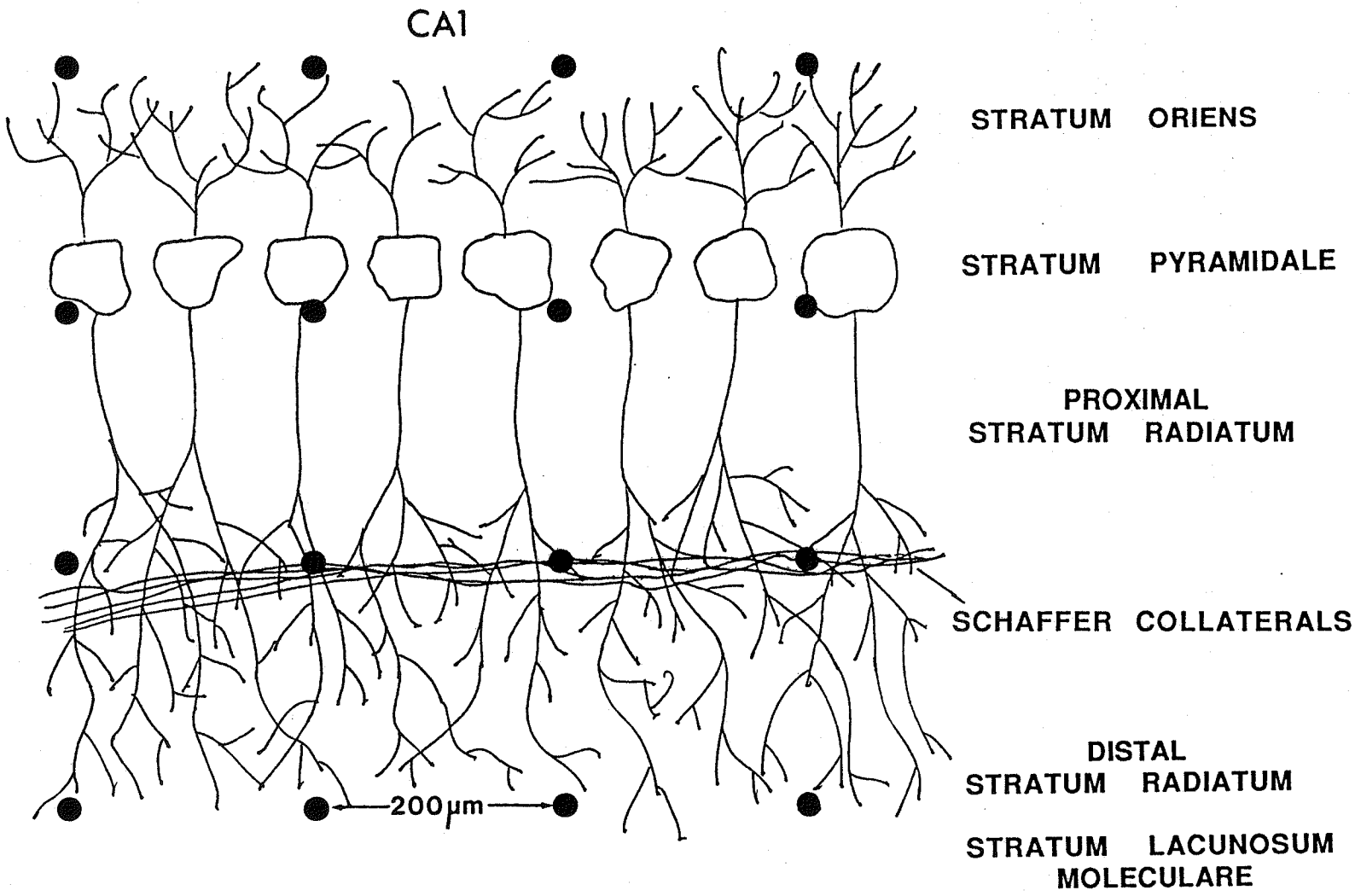

Figure 2.2 CA1 strata nomenclature.

Pyramidal cells in region CA1 of the hippocampus possess electrophysiolgical and anatomical properties distinct from cells within CA2 and CA3 (Masukawa et al., 1982). Cells within CA2 and CA3 exhibit bursting behavior to both direct current injection and synaptic activation. Cells at either end of region CA1, near the subiculum (CA1a) or CA2 (CA1c) burst when stimulated by current injection, but not in response to synaptic input. In contrast, CA1b cells, which are located in the center of the CA1 region, will fire single spikes in response to current injection, while those in CA2 and CA3 will burst.

Furthermore, experiments indicate that CA1, CA2, and CA3 display different epileptiform responses (Schwartzkroin and Prince, 1978; Wong and Traub, 1983; Schneiderman, 1986). Differences in epileptiform activity are observed between CA1a and the rest of CA1 under low-Ca^{++} conditions (Konnerth et al., 1986). In the experiments described here, efforts were made to record from CA1b, the middle of CA1, both because of its linear extent and to avoid interpretation problems.

The pyramidal cells are connected by an excitatory bisynaptic pathway (Figure 2.1). The axons of the granule cells project to the pyramidal cells of CA3, and are termed mossy fibers because of their bumpy, spiny appearance. The CA3 axons bifurcate near the somata and send one branch into the fimbria. The other branches from the CA3 axons double back to CA1, and form the Schaffer collateral tract. These synapse "en passant" on the dendrites of CA1 pyramidal cells. Lastly, the axons of CA1 cells form the alvear fiber tract and project toward both the

fimbria and subiculum.

The pyramidal cells are also interconnected within a region. Cells within CA3 and CA2 reciprocally innervate one another with excitatory synapses and electrotonic junctions (MacVicar and Dudek, 1980a, 1980b; Knowles et al., 1982a; Barnes et al., 1987). Such reciprocal excitation has not been found in CA1 (Knowles and Schwartzkroin, 1981), although it has not been ruled out. However, all regions contain inhibitory basket cells located within the s. or. and s. rad. These cells elicit powerful inhibitory post-synaptic potentials (IPSPs) (discussed later) in the pyramidal cells via both feed-forward and feedback connections (Schwartzkroin and Mathers, 1978; Alger and Nicholl, 1982a; Knowles et al., 1984; Schwartzkroin, 1986).

2.3 Electrophysiology of the "Normal" Hippocampal Slice

Normal hippocampal pyramidal cells display intrinsic capacities for bursting, which vary from dendrite to soma as well as between the anatomical regions. (For the purposes of this thesis, the term "normal" will designate a cell or slice which has not been intentionally made to display epileptiform activity.) Intradendritic and intrasomatic recordings demonstrate that both the somata and dendrites of CA2 and CA3 cells may be induced to burst by short (2-20 ms) depolarizing pulses (Wong et al, 1979). Although the dendrites of CA1 cells also may be induced to burst by slightly longer pulses (10-20 ms), the CA1 somata do not burst. These dendritic bursts appear to be all-or-nothing responses, i.e., once triggered,

their time course and amplitude are independent of the stimulus (Wong and Prince, 1979; Fujita and Iwasa, 1977).

Under normal conditions, activation of pyramidal cells will activate the inhibitory basket cells within the region. The powerful GABA-mediated recurrent and feed-forward IPSPs induced in the pyramidal cells by these basket cells will inhibit or terminate the expression of intrinsic pyramidal burst. Because of this, afferent excitation of pyramidal cells typically evokes only a single action potential, even though the pyramids themselves might otherwise burst (Dingledine and Langmoen, 1980; Schwartzkroin, 1986). The balance between excitation and inhibition is essential to the normal function of the hippocampus.

The pyramidal cells and their associated fiber pathways are closely spaced and aligned in parallel and can fire synchronously, producing currents which result in voltage drops across the extracellular space (Andersen et al., 1971b). The extracellular potentials produced by the pyramidal cells themselves are termed population spikes, and their amplitude and duration reflect the number of active cells and the degree of synchrony among them. Similarly, the coherent activation of the Schaffer collateral fibers by an external stimulating electrode produces a propagating compound action potential (CAP) which is often visible just before the onset of a population spike. This potential is small compared to a population spike, but has been used to estimate the conduction velocity of the Schaffer

collaterals in the guinea pig as 0.1-0.3 m/s (Andersen et al., 1978).

Stimulation of the Schaffer collaterals in a normal slice produces population spikes with latencies that increase with the distance from the stimulus. The resulting serial release of neurotransmitter is presumed to result in the propagation of population spikes through the CA1 region at a rate reflecting the conduction velocity of the Schaffer collateral fibers (Schneiderman, 1986). The particular neurotransmitter is uncertain, but candidates appear to include glutamate and related compounds (Dingledine, 1984; Koerner and Cotman, 1982; Collingridge et al., 1983).

There appears to be a secondary, more slowly acting receptor located in the s. rad. which is specific for N-methyl-D-aspartate (NMDA), and may play a role in the generation of other types of activity (see Dingledine, 1986; Cotman and Iversen, 1987, for reviews). It appears that this receptor is activated by the same neurotransmitter as the fast-acting receptor discussed above (Collingridge et al., 1983; Olverman et al., 1984). Binding studies have determined that s. rad. of CA1 has the highest density of NMDA receptors in the rat brain (Monaghan and Cotman, 1985; Cotman et al., 1987). This receptor is blocked in a voltage-sensitive manner by extracellular Mg^{++} (Ault et al., 1980; Mayer et al., 1984), and its effects can be unmasked by lowering extracellular Mg^{++} (Herron et al., 1985a; Hamon et al., 1987). It may also be selectively blocked by the compound D-2-amino-5-phosphonovalerate (DAPV) (Collingridge et

al., 1983). The NMDA receptor is implicated in studies of long-term potentiation and epileptiform activity in hippocampal slices and is further discussed in the next section.

2.4 Generation of Epileptiform Activity

The hippocampal brain slice is widely used as a model for research into fundamental issues in epileptiform neural activity (Schwartzkroin and Prince, 1978; Andersen et al., 1978; Schwartzkroin, 1986). The electrophysiology of the tissue displays a number of features which are believed to play a significant role in the generation and spread of epileptiform activity. Generation of such activity includes membrane-level events involving intrinsic cellular properties, the predisposition of cells to fire bursts, and the local synchronization of populations of cells through synaptic or environmental effects. Once generated, this abnormal activity propagates through different anatomical regions. The resolution of conventional recording techniques makes them most useful for investigating local generation phenomena, and most previous efforts have been directed toward this end.

A variety of manipulations may be performed to permit the expression of abnormal bursting in hippocampal slices. Epileptiform phenomena are the result of alterations in the balance between inhibition and excitation. The application of drugs, various manipulations of the slice environment, hypoxia, and patterned electrical stimulation can all evoke synchronous seizure-like activity. Each of these manipulations alters a

different intrinsic mechanism, and although no one model is likely to be useful in all situations, comparisons of these models may reveal basic components of epileptiform activity (Prince, 1978; Dichter and Ayala, 1987).

Evoked or spontaneous population bursts in hippocampal slice models of epilepsy display similar characteristics. An example of such an event recorded in a slice bathed in media containing the convulsant drug picrotoxin is shown in Figure 2.3 (Snow and Dudek, 1984). The pyramidal cells experience a large long-lasting depolarization that triggers multiple action potentials. The corresponding extracellular event displays population spikes that occur due to the synchronous bursting of many cells. The population spikes are negative, corresponding to the extracellular somatic recording of an action potential. Note that individual cells may burst asynchronously and not produce such an extracellular event.

The first class of models studied in this thesis involves the addition of drugs to the incubation media to reduce or to abolish synaptic inhibition. The powerful recurrent and feed-forward IPSPs discussed above are primarily GABA-mediated, and as such, may be reduced with a number of relatively specific GABA-antagonists. These drugs lessen the degree of inhibition in the slice to a point where the intrinsic bursting properties and excitatory coupling of the pyramidal cells permit the expression of their intrinsic bursting properties.

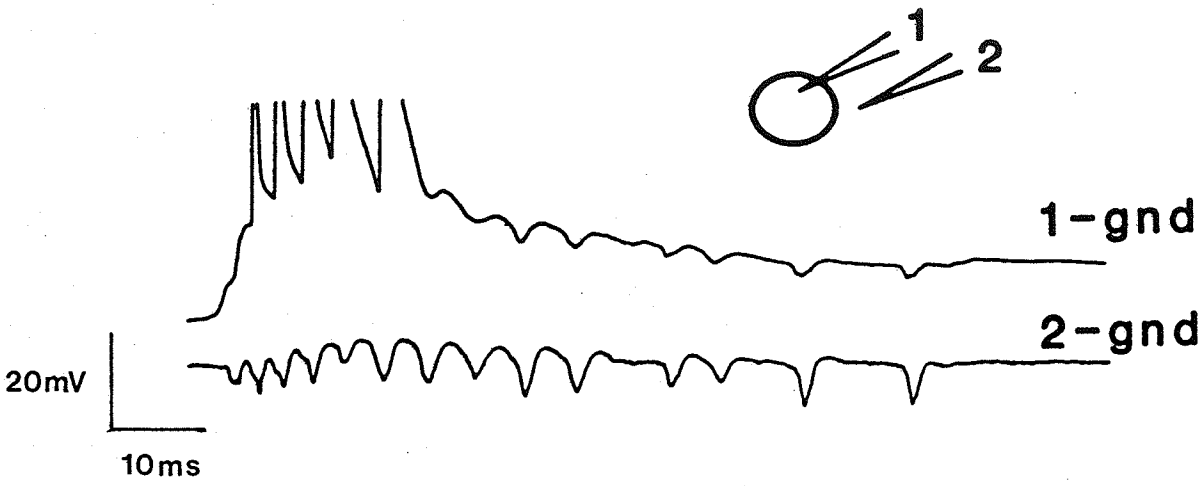

Figure 2.3 Simultaneous intracellular and extracellular potentials during a population burst. (Adapted from Snow and Dudek, 1984).

Although penicillin was widely used as the epileptic agent in slice studies, it appeared to have some effect on the intrinsic membrane properties of the pyramidal cells (Dingledine and Gjerstad, 1979; Hablitz, 1984). For this reason, the less commonly used drug picrotoxin (PTX) was used in this study. Picrotoxin appeared to antagonize GABA-mediated recurrent inhibition more completely than penicillin, while having little effect on cellular properties (Hablitz, 1984). However, inhibition is not totally blocked, as a PTX-resistant IPSP does exist in CA1 (Alger and Nicholl, 1982b).

The other convulsant drug used was pentylenetetrazol (PTZ), which has been used as the convulsant agent in studies involving the NMDA receptor. In one study, the first population spike within a burst recorded from slices in PTZ appeared only marginally sensitive to the application of DAPV, while the subsequent spikes (presumably abnormal) were abolished (Herron et al., 1985a). This finding suggested that a single epileptiform burst may be composed of a "normal" as well as an "epileptic" component, and that comparisons between these components of bursts may reveal mechanisms involved exclusively in "normal" or "epileptic" activity. However, PTX-induced population bursts appeared insensitive to DAPV in slices of cerebral cortex (Thomson and West, 1985), demonstrating that NMDA receptor involvement was sufficient, but not necessary for synchronized activity.

In contrast with the reduced inhibition models, increasing the level of excitation in the slice also results in the

generation of epileptiform activity. The third model of epilepsy studied in this thesis involved using 0-Mg^{++} medium to eliminate the blocking effect of the ions on the NMDA receptors. GABA-mediated inhibition was not antagonized in 0-Mg^{++} medium, unlike the PTX and PTZ models. The large and long duration excitatory post-synaptic potentials (EPSPs) resulting from NMDA receptor activation produced population bursts similar to those observed in the drug models (Coan and Collingridge, 1985; Herron et al., 1985b; Mody et al., 1987) as well as seizure-like events which appeared to be related to the ictal EEG waveform (Anderson, et al., 1986; Mody et al., 1987; Swartzwelder et al., 1987). As was the case in the PTZ model, 0-Mg^{++} induced bursts were altered using the NMDA antagonist DAPV (Coan and Collingridge, 1985).

2.5 Propagation of Population Bursts

Once generated using either PTX, PTZ or 0-Mg^{++}, epileptiform bursts evoked by stimulation of the s. rad. near CA3 propagated through CA1 via the Schaffer collateral fibers (Schwartzkroin and Prince, 1978; Mesher and Schwartzkroin, 1980; Wong and Traub, 1983; Hablitz, 1984). The multipeaked bursts propagated through CA1, changing shape presumably due to variations in the local synchronization of pyramidal cells. The propagation velocity of the first population spike in penicillin-treated slices has been measured as 0.08-0.15 m/s between CA2 and CA1 using field potentials on pairs of microelectrodes (Schwartzkroin and Prince, 1978).

Principally because of the uniform anatomy, it has been postulated that CA1 bursts consist of serially activated, stereotypical responses (Schneidermann, 1986). However, no detailed analyses of propagation of population bursts through CA1 have been performed. Further, although the mechanisms underlying the generation of bursts in terms of membrane and synaptic events have been widely studied, the mechanisms for the apparent propagation of the secondary components of a population burst remain unclear.

A variety of candidate excitatory coupling mechanisms has been proposed. Recurrent excitatory synapses or gap junctions in CA1 have not been found in CA1 (Knowles and Schwartzkroin, 1981), although they appeared to exist in CA3 and CA2 (MacVicar and Dudek, 1980a). Ephaptic or electric field coupling has been demonstrated to play a role in the synchronization of bursting CA1 pyramidal cells (Snow and Dudek, 1984). In this mechanism, the extracellular field produced by synchronously firing cells altered the transmembrane potential of adjacent cells, effectively bringing the cells closer to threshold. The dense packing of CA1 pyramidal cells and the resulting high extracellular resistivity presumably enhanced this effect (Holsheimer, 1987). Significant changes in extracellular K^+ and Ca^{++} concentrations have also been observed during intense activity (Somjen and Giacchino, 1985; Aitken and Somjen, 1986; Balestrino et al., 1986). Further, moderately high K^+ medium itself resulted in synchronized activity (Rutecki et al., 1985). The raised levels of K^+ appeared to increase the excitability of

neighboring neurons, promoting synchronization.

Recently, studies of epileptiform burst propagation in slices of neocortex have been reported. In these experiments, pairs of single microelectrodes were used to observe the conduction delay between the onset of population bursts. In parietal neocortical slices, saltatory conduction of population bursts was observed at similar locations, irrespective of direction of propagation (Gutnick and Wadman, 1986). In another study involving cortical slices from other regions, saltatory propagation was not reported, although velocities varied in a highly periodic manner (Connors and Chervin, 1986). Interestingly, although the periodicity was preserved during propagation in either direction, the patterns were 180 degrees out of phase, i.e., places with the highest velocity in one direction had the slowest velocity in the opposite direction. The authors in both studies cited above hypothesized that these observed differences in propagation velocity of epileptiform bursts reflect underlying inhomogeneities in the density or strength of intracortical excitatory connections.

2.6 Significance of Electrode Array Data

The electrode array is best suited for studying mechanisms involved in the synchronization and propagation of seizure-like activity because of its recording resolution and overall dimensions. Recordings may be made at 200 μm intervals along the linear extent of hippocampal region CA1, permitting a detailed study of propagation over a distance of 1.0 mm.

Additionally, the spatial sampling achieved by the array permits the use of CSD estimates to identify accurately the peak times of synchronized neuronal activity. As demonstrated in Section 6.3, field potential recordings alone cannot provide the resolution necessary to observe propagation on this scale.

Questions remain as to the uniformity of cells within the CA1 region. As discussed earlier, significant variations exist between neurons in subregions of CA1. Additionally, region CA1a (nearest the subiculum) is the site of initiation of spontaneous events in a low extracellular Ca^{++} model (Konnerth et al., 1986). Possible differences in neuronal or synaptic properties within CA1 could be inferred by propagation differences.

It is also unclear whether common mechanisms underlie the propagation of the first and second population spikes. If mechanisms involved are alike, one would expect similar conduction delays for the waveform components. Similarly, differences in propagation within CA1 would reflect local changes in excitatory coupling. Because it appears that these components of an epileptiform burst in CA1 are pharmacologically distinguishable (Herron et al., 1985a), it is possible that the coupling mechanisms may play time-variant roles during the progress of a single burst. A particular mechanism involved in propagation coupling during the first population spike may be less important for the synchronization of the second event. Additionally, it seems likely that the various models would propagate epileptiform activity in a unique manner. Common

mechanisms among these models might permit generalization, providing a more unified theory of propagation.

Conduction delays can also be used to restrict the candidate propagation phenomena. The proposed coupling mechanisms may be divided into two groups, based upon their directionality. Isotropic mechanisms would include ephaptic effects and ionic changes, while synaptic connections and gap junctions would presumably be anisotropic, depending upon the actual interconnection patterns. The presence or absence of propagation symmetry would suggest a greater role of isotropic or anisotropic mechanisms, respectively.

This study of propagation is one of the first to deal with the mechanisms of epileptiform propagation in the hippocampal slice. The current focus on the mechanisms for generation and not propagation of the bursts is presumably due to the technical recording limitations. The electrode array removes these limits, making it suitable for studies of propagation of epileptiform activity because of its multisite recording ability. The experiments reported in Chapter 6 determine conduction delays, and then compare population bursts propagating in the forward and reverse directions to identify the dominant coupling mechanism in three different slice models of epileptiform activity.

CHAPTER 3

THE ELECTRODE ARRAY AND RECORDING SYSTEM

Fully utilizing the recording capability of the electrode array required a 32-channel computer-based recording system. As the equipment currently available to support multichannel neurophysiological recording was quite limited, most of the hardware was constructed locally. The principal components of the system included the array, the analog amplifiers, the analog-to-digital (A/D) converter, the host computer, and the stimulation apparatus (Figure 3.1).

3.1 Array Description and Fabrication

Fabrication of the electrode array has been described in detail (Novak and Wheeler, 1986a). Briefly, titanium (10-30 nm) and gold (150-300 nm) were evaporated onto a clean 3 inch square glass plate and were photopatterned using standard techniques. This resulted in a pattern of metal conductors running from connector pads at the edges of the glass plate to the electrode matrix at the center. The tips of these conductors served as the electrodes (20 μm diameter) and were arranged in a 4 by 8 matrix on 200 μm centers. Polyimide insulation (DuPont Pyralin 2555) was applied over the entire surface of the plate, partially cured, photopatterned to create openings over the tips of the conductors, and fully cured. Polyimide thickness was measured using the focal plane of a Nikon Labophot microscope and was estimated as approximately 2 μm. Regions distant from the recording surfaces were hand-painted with additional insulation.

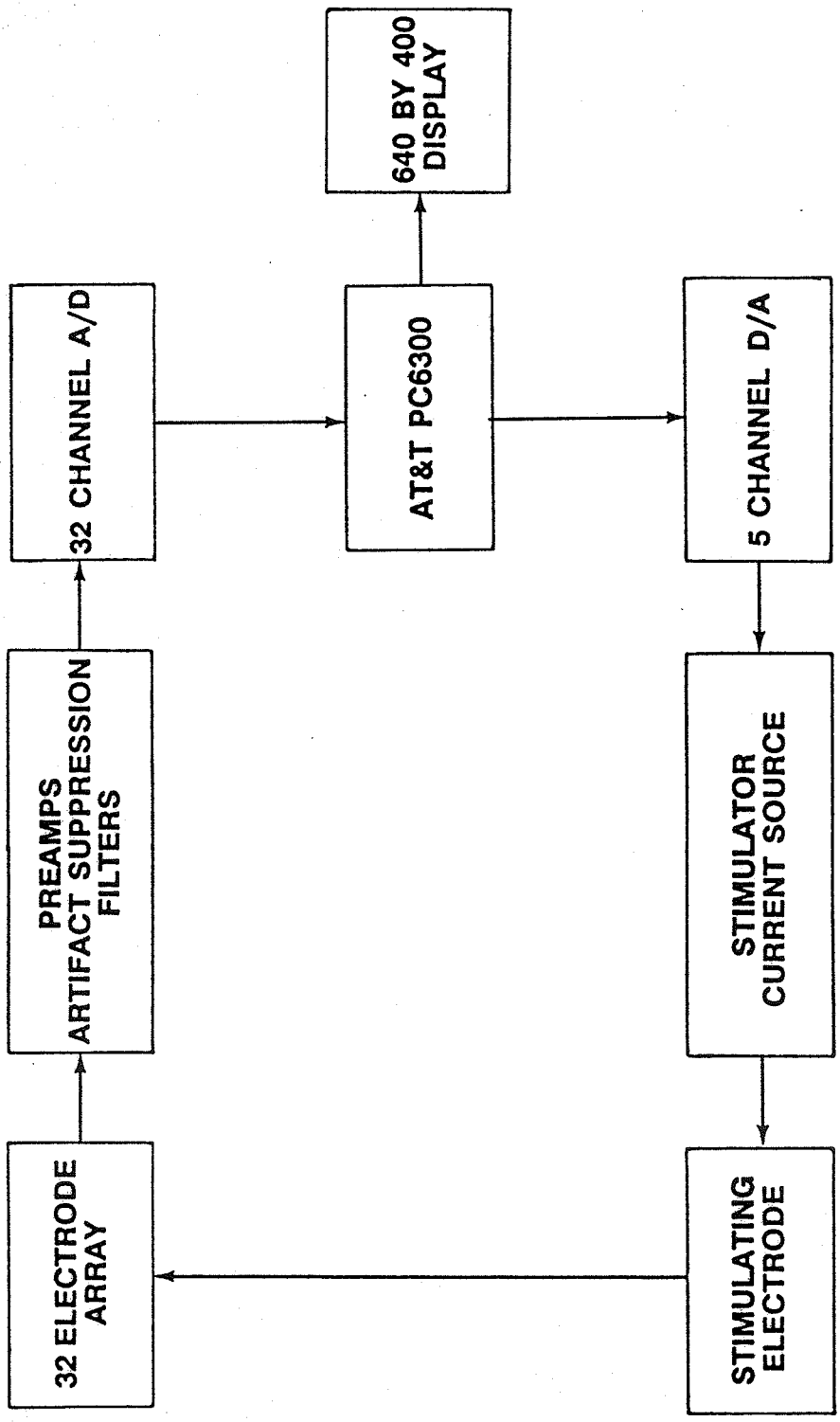

Figure 3.1 System block diagram.

New arrays (Figure 3.2) were routinely soaked overnight in saturated NaCl solution to leach out possible contaminants.

The electrodes were electroplated with platinum black, using a 0.025 N HCl solution containing 3.0% $PtCl_6$ $2H_2O$ and 0.025% $Pb(CH_3OH)_2$, and approximately 0.1 $\mu A/\mu m^2$ current density. Plating was monitored optically under a microscope and usually required 25-35 s to achieve a sufficient coating. Typical impedance magnitudes were about 10 kΩ at 1000 Hz in normal saline medium (Novak and Wheeler, 1986a).

3.2 Amplifiers and Artifact Reduction Circuitry

Signals recorded by the array electrodes were amplified using 32 identical amplification and filtering channels (gain 2000, 5000; BW (-3dB) 2-1000 Hz). Each channel consisted of a junction field effect transistor (JFET) preamplifier, a track and hold artifact suppression circuit, an instrumentation amplifier, and filters with switchable gain (Figure 3.3). The JFET input stage and the track and hold circuitry served to decouple the electrode from the recording system as well as to decouple the later stages of gain and filtering during the stimulus. Using the track and hold, the output from the JFET was fixed at its prestimulus level during the delivery of the stimulus. This prevented saturation, with a recovery period of up to 200 ms, and nonlinear operation of the later high-gain amplification and filtering stages due to the stimulus artifact. Without the circuitry it was often impossible to observe the neural response, particularly in normal medium, where signal size was small.

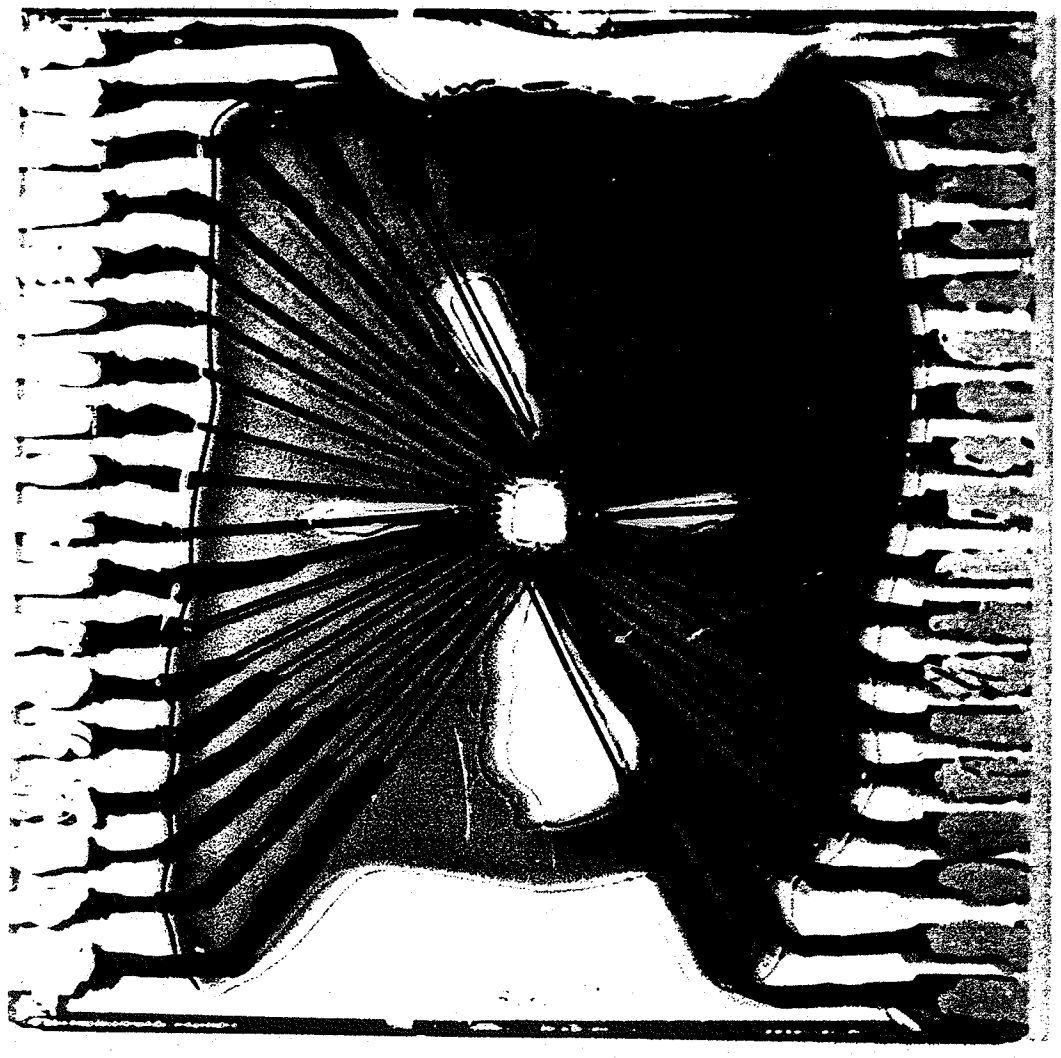

Figure 3.2 The planar microelectrode array.

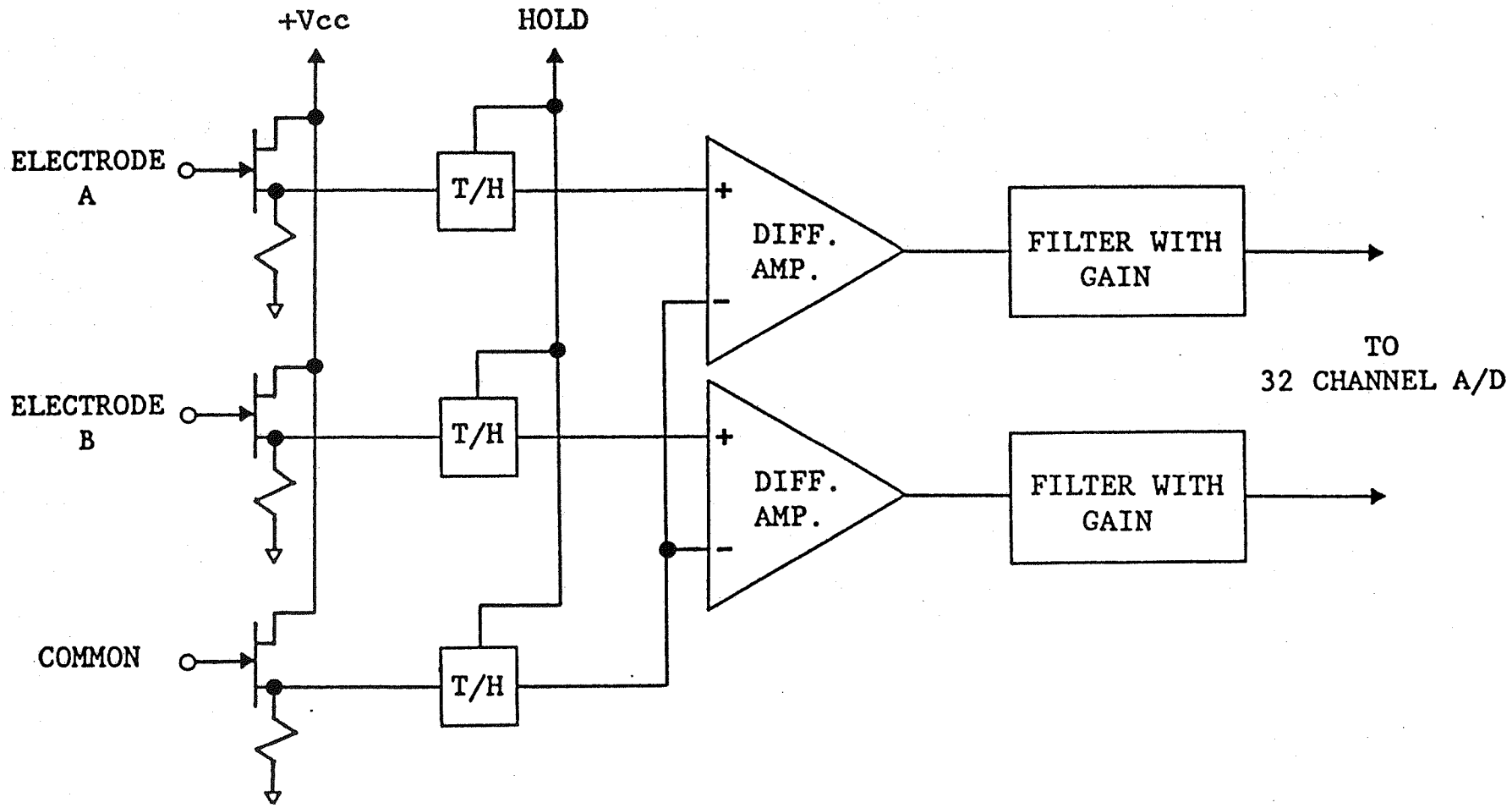

Figure 3.3 Analog front-end circuitry with active artifact suppression.

The external signal return electrode (Ag/AgCl) was also connected to an additional channel of preamplification and track and hold circuitry (Figure 3.3). This design resulted in common-mode noise of less than 10 μV because of the matched impedances at the array and signal return electrodes. The common-mode return path to earth-ground was made using another Ag/AgCl electrode. The gain of the final filtering stage was adjusted to maximize the dynamic range of the signal within the $\pm$5 V limits of the digitization circuitry.

3.3 Digitization and Acquisition System

The amplified signals were digitized using a specially constructed 32 channel 8-bit A/D card and an AT&T PC6300 (IBM PC compatible) computer. In order to provide fast visual feedback of the signals to the experimenter, it was necessary to sample at a rate sufficiently fast to permit direct interpretation of the graphics display. Fast sampling also permitted more accurate resolution of peak times. Since the 6300 uses an 8086 microprocessor and a 16-bit data bus, the use of 8-bit samples permitted packing two samples into a single word, doubling the throughput as compared with a 12- or 16-bit converter. The maximum sampling rate of 8.25 ksamples/s/channel was used for the data presented in this thesis unless otherwise indicated. The gains of the analog amplifiers were adjusted to take maximum advantage of the dynamic range.

Because 8.25 ksamples/s over 32 channels was not sufficient to permit use of this system for action potential recording

(about 10 kHz bandwidth), a faster A/D card using direct memory access (DMA) transfers was designed and was recently incorporated into the system. With the new card, which is transparent to the experimenter, the system functioned similarly, except for the increased maximum sampling rate of 20.4 ksamples/s on 32 channels (Novak and Wheeler, 1987a).

System software was written in FORTRAN and 8086 assembly languages. Low-level system functions such as graphics displays, sampling, and data file I/O were primarily written in assembly code. These routines provided direct access to the system hardware, and were used where speed was critical. Most of the signal processing was performed in FORTRAN, which greatly simplified floating point calculations.

The 32 channel data were treated as images in time, and stored in one of four data arrays. One data buffer was reserved for raw data, i.e., new samples or data retrieved from disk. The remaining three buffers were FORTRAN integer arrays. The use of three buffers permitted flexible processing on single responses as well as multiple data files. Any of the four (1 raw, 3 FORTRAN) data buffers could be displayed on the monochrome graphics monitor as 32 channels of voltage versus time plots arranged in a 4 by 8 array. The 640 by 400 pixel resolution permitted the display of 150 points per channel. User-selectable horizontal and vertical scaling as well as window location within the maximum 2000 points (240 ms) per channel were performed using the cursor control keys.

A typical recording session proceeded as follows. After the slice was placed on the array and responses were observed, the 32 amplified evoked neural signals were connected at the A/D board inputs. Sampling was initiated manually or automatically after delivery of a stimulus to the preparation. Once sampling was triggered by the stimulator, an assembly language software routine stored a 240 ms window of data per channel following the stimulus. The acquired signals were then displayed on the monitor and keyboard entries controlled further processing. If the data were not acceptable, resampling and display could have been repeated indefinitely. Once acceptable signals were observed, the data were further processed or stored on disk for future off-line analysis.

While displaying the raw or processed data, the user could have entered an on-screen analysis mode. This mode permitted operator-controlled peak and feature detection and interval measurements by moving a cursor on each of the 32 waveforms displayed. As the cursor was adjusted to the point of interest on the display, the value of the sample at each point for each channel was displayed adjacent to the waveform.

Menu-driven FORTRAN routines provided quick, easy calculation and display of many derived functions (Table 3.1). Preprocessing manipulations such as interpolation of missing channels, scaling and addition of data buffers, and subtraction of artifact templates were available. The processing functions included temporal and spatial filtering (e.g., CSD), subtraction of adjacent columns or rows of data within a buffer to estimate

Table 3.1 Digital signal processing function menu.

Signal Processing Menu

1. Subtraction of scaled artifact template
2. Interpolation of missing signal channels
3. Five-point Laplacian (current source density estimation)
4. Spatial derivatives (current density estimates)
5. Spatial filtering using arbitrary function
6. Correlation (pairs of channels)
7. Power and cross-power spectra
8. Coherence (pairs of channels)
9. Cursor control and data readout
10. Overlay of signals for data comparison
11. Timer for automated acquisition
12. Peak detection and regression analysis

current densities, temporal correlations and spectral analyses, contour mapping using grey scales, and a peak detection and linear regression package for propagation analysis (described in Section 5.3). After processing, these data arrays could have been displayed immediately and interpreted using the analysis mode.

The data displayed on the monitor may also be plotted (HP7440 ColorPro plotter). After adjusting display parameters using the monochrome screen, the displayed data were communicated to the plotter for hard-copy output.

3.4 Conventional Stimulating and Recording Electrodes

Stimulation for array recordings was performed using a bipolar stainless steel electrode with 100 μm tip diameters and a 400 μm tip separation. In these experiments, monopolar constant current pulses (100 μs) were used for stimulation (100-400 μA).

In experiments designed to test the stimulating capabilities of the array, responses evoked using array stimulation were recorded using a 3-5 MΩ, 3M NaCl filled glass micropipette electrode. Voltage pulses (100 μs) were applied either between array electrodes or between an array electrode and an external Ag/AgCl electrode. Stimulation was limited to less than 20 V to avoid damage to the array. These single-channel responses were amplified (gain 100, 1000; BW (-3dB) 10-3000 Hz) and stored on FM tape for off-line analysis.

CHAPTER 4

THE BRAIN SLICE PREPARATION

4.1 Array Recording Chamber and Media

The electrode array served as the bottom of the recording chamber and was covered by cotton gauze. In early experiments, filter paper and coffee filters were also used and found to be slightly inferior for control of flow of medium over the array. A number of different cotton gauzes were tested, but only one type currently manufactured (Kendall Curity eye pads) was found to possess the appropriate balance between absorbancy and fluid conducting ability.

A flap was cut in the gauze, forming an approximately 7 mm square hole over the electrode matrix. Saline medium was bubbled with a 95% O_2/5% CO_2 mixture and perfused the gauze, flowing over the array surface and dripping into a waste container at a rate of about 1 drop every 2 seconds, or about 0.25 ml/min. Surface tension permitted the medium to remain over the hydrophobic array surface. The array and gauze were covered by a Plexiglas cover, and a warmed, moist gas mixture was passed through the enclosed chamber (Figure 4.1). An access hole in the cover permitted the use of external stimulating and recording electrodes and could be covered with a microscope slide to prevent drying. A heated water bath beneath the array served to control the chamber temperature at either $36\pm1\ ^{\circ}C$ or $31\pm1\ ^{\circ}C$.

Normal medium consisted of (in mM) 124 NaCl, 5 KCl, 1.25 NaH_2PO_4, 26 $NaHCO_3$, 0.8 $MgSO_4$, 1.5 $CaCl_2$, and 10 Dextrose.

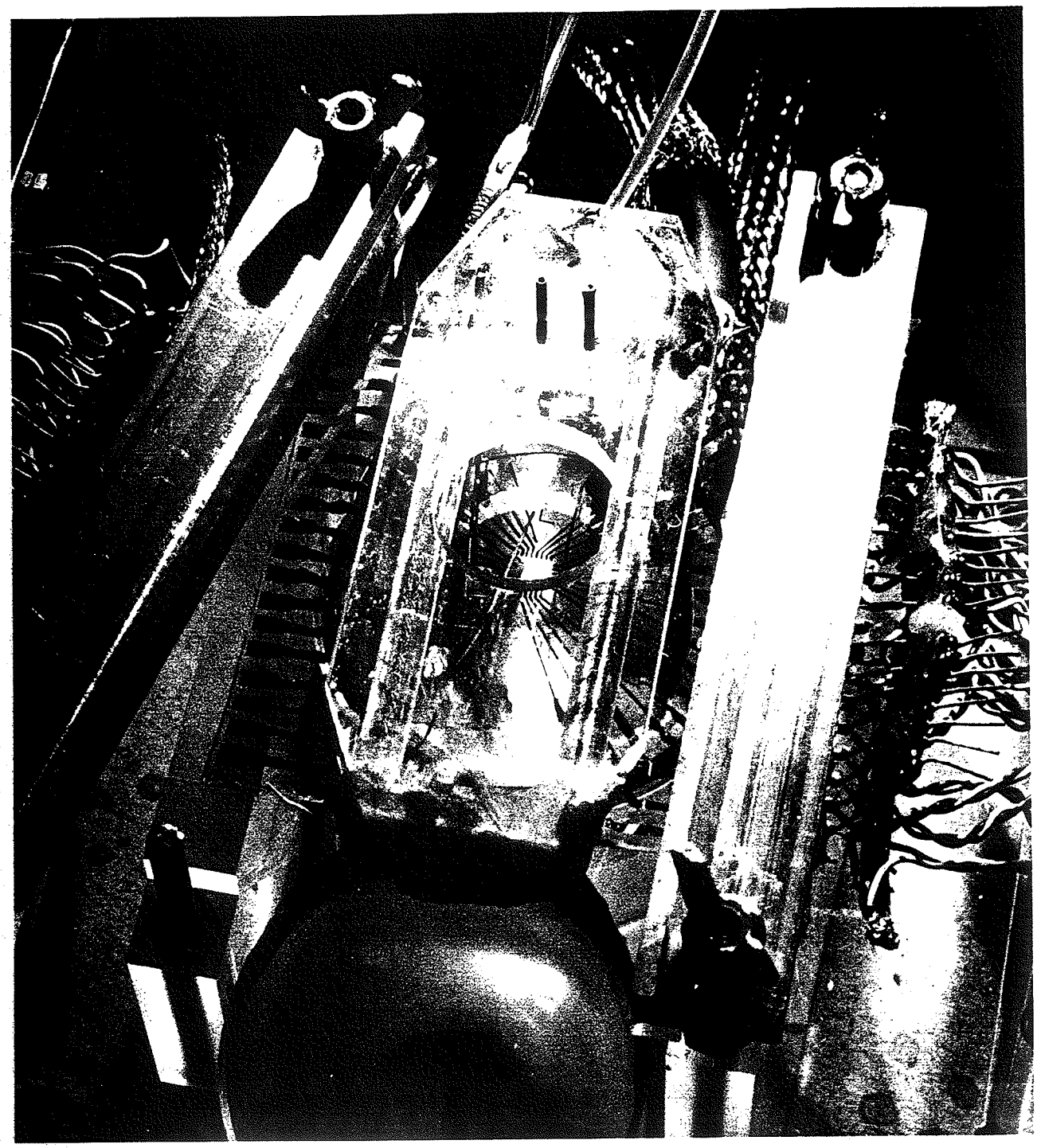

Figure 4.1 . Photograph of array recording chamber. Cotton gauze (not shown) is positioned within the chamber over the array and carries media flowing from the upper inlet to the waste container. Electrical connections to the array are made via the edge connectors.

Epileptiform activity was induced by the addition of 100 μM picrotoxin (PTX) or 2.0 mM pentylenetetrazol (PTZ). Two ionic manipulations were also used to produce abnormal activity. These were elevating KCl to 7 mM and omitting $MgSO_4$ from the normal medium to produce a 0-Mg^{++} formula.

4.2 Biological Preparation

Transverse slices from male Sprague-Dawley rat (250-450g) hippocampi were obtained using standard techniques (Teyler, 1980). After halothane anesthesia, the rat was decapitated, the skull opened, and the brain removed and placed into a dish of cold (approximately 0 °C), oxygenated medium for approximately 1 min. Next, the right hippocampus was removed and placed on the slicing platform.

The angle at which the hippocampus was sliced critically affected the ability to record evoked responses over the entire array surface. As illustrated in Figure 4.2, if the hippocampus was sliced at angle A, the Schaffer collaterals ran "into" the plane of the array and responses evoked from the forward stimulus could not be recorded in CA1 near the subiculum. If angle C was used, the collaterals ran "out" of the slice, limiting reverse propagating responses (reverse stimulation) near CA3. Slicing angle B, which was parallel to the alvear striations observed prior to slicing, ran parallel to and preserved much of the Schaffer collateral tract and provided activation to most of CA1 during forward or reverse stimulation.

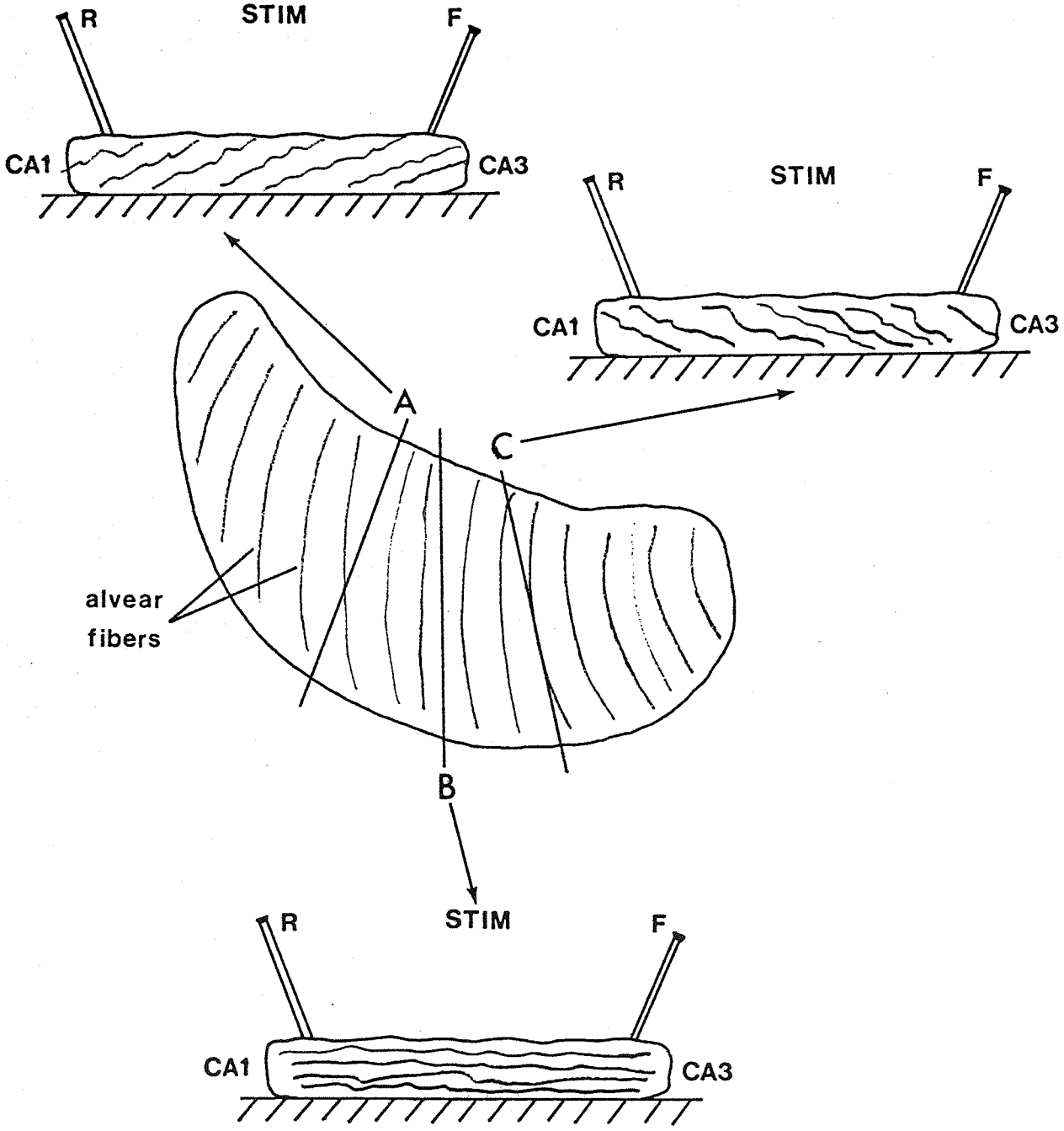

Figure 4.2 Diagram illustrating the correct slicing angle.

To facilitate such accurate slicing of the hippocampus, it was first placed on the slicing stage with the rostral end forward and dorsal side up. The alvear striations were visible over most of the hippocampal surface, and the striations in the septomedial portion were aligned parallel to the blade. Starting at the temporal end, the hippocampus was typically sliced into 12-15 400 μm sections. These were placed into three separate chambers in a holding dish at room temperature (21 °C), in order to retain the spatial identity of the slices. Slices from the middle chamber (medial hippocampus) were used for experiments reported here. Confirmation of a proper slicing angle was provided by the ability to record evoked propagating signals over the length of the array, and the appearance of small capillaries near the hippocampal fissure.

After permitting the slices to recover for 1-2 h, a single slice was transferred to the recording chamber using a camel's hair brush. A standard orientation was adopted for positioning the hippocampal slice on the recording electrodes. Figure 4.3a) is a photograph of a slice in such a position, and Figure 4.3b) is a schematic representation of the slice anatomy and forward and reverse stimulation sites. In this position, the long axis of the array was aligned with the Schaffer collaterals, which permitted recordings of propagating activity from 8 sites along a 1.4 mm length of CA1. The four electrodes normal to this axis provided signals from different strata within the CA1 region. The s. pyr. was positioned over the third column of electrodes, in order to permit two-dimensional calculation of the CSD profile

a)

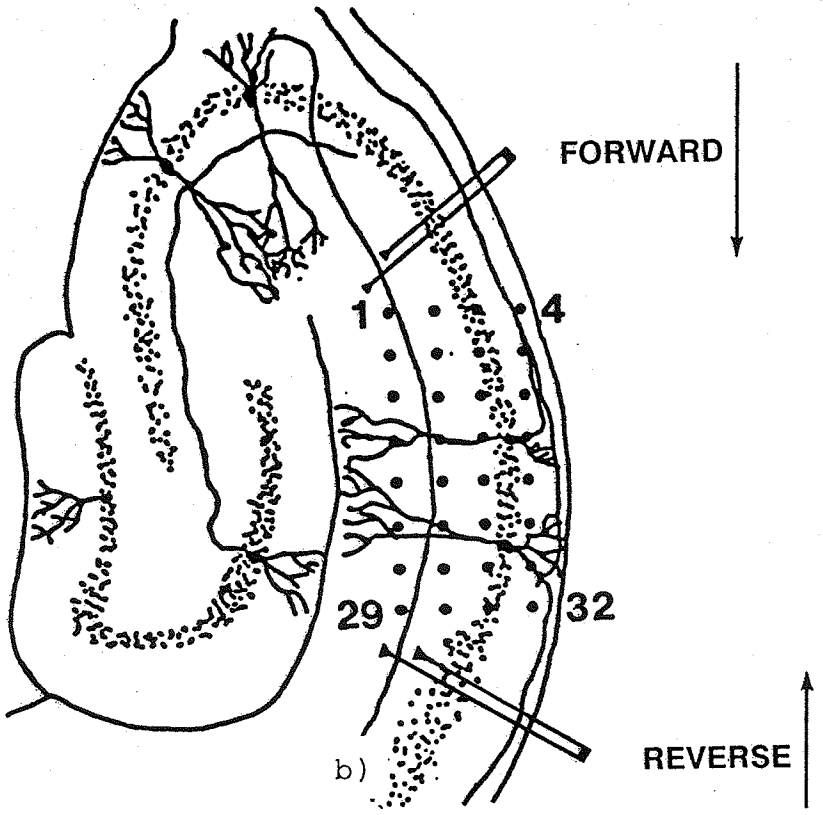

Figure 4.3 Standard orientation of slice on the array. A photograph of a slice on the array is given in a). Forward and reverse stimulus sites as well as array electrode locations are shown in b).

at sites along s. pyr. without the edge effects mentioned later in Chapter 5. While stability test stimuli were being applied to the Schaffer collaterals (discussed later), the resulting CSD profiles were used to electrophysiologically confirm the location of the slice on the array (Chapter 6) and any necessary position adjustments were made.

Initial experiments were performed at 36±1 °C using normal medium in both the holding and array chambers. The stimulating electrode was positioned either for forward or reverse stimulation (Figure 4.3a) and lowered until it just contacted the thin layer of medium over the tissue. Improper fluid levels in the chamber were readily apparent at this point, and resulted in either dimpling under too dry conditions or poor tissue contact if the slice was too moist. After positioning the stimulating electrode, a single stimulus was delivered to ascertain the state of the tissue. If necessary, amplifier gains were then adjusted to fill the dynamic range of the digitization system. Every 2 min an additional pulse was delivered, and this response was compared with the previous one as a test for stability. Slices were considered acceptable only if responses stabilized within 20 min. Once the signal levels were stable, the experimental medium was introduced through a tee valve attached to another reservoir. Because of the relatively slow flow rate required to keep the slice from moving, the slice was on the array for 30-45 min before experimental recordings could be made. Examples of stabilization and the wash-in of PTX are given later in Chapter 6.

In the propagation experiments reported in Section 6.5, the slices were placed in the experimental medium in the holding chamber immediately after slicing. This allowed experimental recording to begin immediately after the slice stabilized following placement on the array. All necessary measurements could then be made before slice spreading (discussed later) occurred. Experiments using the three manipulations (PTX, PTZ, 0-Mg^{++}) were intermixed, and some using PTX and 0-Mg^{++} were performed by another experimenter.

After positioning the slice in the chamber, the above stability test procedure was followed to assure stable recordings. Only slices which stabilized within 20 min and demonstrated clearly defined CSD source/sink relationships at the six electrodes in s. pyr. (Section 6.4) were analyzed. Furthermore, the negative peaks of spikes 1 and 2 were required to be sufficiently sharp to permit accurate peak location.

The stimulus pulse intensity was increased from 50 μA to produce maximal multipeaked population bursts and was typically 300 μA (range 200-400 μA; 100 μs monopolar pulses). Five stimuli were delivered at 1 min intervals to evoke both forward and reverse propagating population bursts. A window of 500 samples (60 ms) for each channel beginning 1 ms before the stimulus was stored for off-line analysis using the methods of Chapter 5. Following this, photographs of the chamber were taken to provide a visual record of slice position. Finally, after 5-10 min, one pulse was given to reconfirm response stability. In some experiments involving the PTX model, additional slices from the

same hippocampus were tested using the same protocol as indicated in the data in Chapter 6. However, experiments with the PTZ or 0-Mg^{++} models were performed on a one slice per animal basis.

CHAPTER 5

DATA ANALYSIS

5.1 Current Source Density Analysis

The signals recorded with the array from the slice are field potentials that are produced as a result of current flows in a resistive media. The synchronous activation of large numbers of densely packed, oriented, laminar cells permits the active regions of hippocampal pyramidal CA1 cells to be modelled as highly localized current sinks, coupled with diffuse passive sources. Although potential data can reveal some properties of the underlying neural activity, a more accurate description is provided if one inverts the volume conduction problem and computes estimates of the locations and time courses of the underlying neural current sources (Plonsey, 1969; Nicholson, 1973; Nicholson and Freeman, 1975; Freeman, 1980).

The inverse volume conduction problem can be formulated as a spatial filtering operation. Since the multipoint data acquired with this microelectrode recording system permit spatial as well as temporal filtering, estimates of the current sources present in a slice may be computed using appropriate filters. In the neurobiological literature, this technique has become known as current source density (CSD) analysis (Freeman and Stone, 1969; Freeman and Nicholson, 1975; Breckow et al., 1982). Because the hippocampal slice satisfies many of the assumptions in the CSD model, this filtering technique is being applied more frequently in slice studies using arrays of three conventional electrodes

(Swann et al., 1986; Miyakawa and Kato, 1986, Holsheimer, 1987), and the array described here (Wheeler and Novak, 1986).

Modelling the relationship between the recorded potentials and the underlying neural events requires the assumptions that the neural events themselves can be described as current sources. Furthermore, it is assumed that the spatial variation of the CSD is such that it can be adequately sampled at the interelectrode spacing of the array.

The current source assumption is valid, particularly in the hippocampal slice. The hippocampal pyramidal cells are densely packed and laminar, and are activated synchronously as a population. Such stratified neural structures possess active regions, which act as local current sinks or sources coupled with opposing sources or sinks due to passive conduction along or through distant processes (Plonsey, 1969; Nicholson, 1973; Nicholson and Freeman, 1975; Freeman, 1980). The decline of the resulting extracellular potential with distance, even in the highly branched dendritic trees, is scaled by the effective electrotonic space constant (Rall, 1973). In the near field (up to several space constants distant) potentials produced by the local monopole may be observed, but at greater distances the potentials are those of a dipole and attenuate more rapidly. In the CA1 region of the guinea pig hippocampus, the effective electrotonic lengths of the dendritic trees are on the order of 200 μm (Turner and Schwartzkroin, 1980) which is the interelectrode separation of the array. The electrotonic lengths for rat CA1 pyramidal cells are assumed to be similar.

Furthermore, the thickness of the dead cell layer due to slicing trauma is between 50-100 μm. Thus the array is likely to be able to report current source/sink information, not merely the presence of dipoles.

To simplify the modelling below, it is assumed that the conductivity of the tissue is homogeneous and isotropic, i.e., the conductivity matrix is the identity matrix. Significant inhomogeneities and anisotropicities in the conductivity matrix appear to exist, as shown in studies using pairs of conventional microelectrodes. However, the inclusion of the specific values for conductivity in CSD calculations has been reported to only slightly change the magnitudes of the CSD profiles (Jefferys, 1984; Holsheimer, 1987).

The electric field produced by bioelectric phenomena may be regarded as quasistatic and the media as purely resistive (Plonsey, 1969). For a point current source in an infinite, homogeneous, isotropic medium with conductivity σ , the extracellular potential is inversely proportional to the distance between the source and the observation point. Assuming that the current source is located at a distance z directly above the origin of the x-y plane in which the electrodes are located, the potential, p(x,y,z), due to a current source of unit strength is

$$p(x,y,z) = \frac{-1}{4\pi\sigma} \cdot \frac{1}{(x^2+y^2+z^2)^{1/2}}$$

The field potentials recorded at the array electrodes are the superposition of potentials produced by all of the active neural sources in the slice, and thus reflect gross and not local neural activity. Because of this superposition, it is likely that a potential recorded at an electrode would merely be a result of adjacent activity and yet be interpreted as a synchronous local event.

Locally, the volume current source density (CSD), I(x,y,z), may be represented by Poisson's equation,

$$I(x,y,z) = -\sigma \nabla^2 \rho(x,y,z)$$

Using this equation, the CSD may be inferred by calculating the Laplacian of the potential distribution (Freeman and Stone, 1969; Llinas and Nicholson, 1974). Furthermore, the slice is assumed to be synchronously active normal to the slicing plane (z direction), permitting a two-dimensional (2-D) formulation. Because the potential distribution is rectangularly sampled in space, the discrete approximation for the Laplacian may be used and the CSD is given by

$$I(i,j) = K\left[4\rho(i,j) - \rho(i-1,j) - \rho(i+1,j) - \rho(i,j-1) - \rho(i,j+1)\right]$$

where I(i,j) is the CSD and P(i,j) is the potential at the i,j th electrode, and K is a constant incorporating the conductivity and the interelectrode spacing. As stated above, the constant K will be neglected (K=1) and relative measures of CSD amplitude will be reported in units of mV/mm^2. Using this assumption, one may equivalently regard the CSD calculation as the discrete spatial convolution of the potential "image" with the kernel

$$\begin{matrix} & -1 & \\ -1 & 4 & -1 \\ & -1 & \end{matrix}$$

Calculation of the CSD at the edges of the array electrodes requires the potential at positions with no electrode. An additional assumption (tested in Section 6.4) regarding the hippocampal slice preparation must be made at the edges. Since the standard array position relative to the slice spans most of the active regions of the CA1 pyramidal cells (Figure 5.1), it is assumed that imaginary electrodes located 200 μm farther into the s. or. or the s. rad. (left/right edges) would record passively generated signals similar to the edge electrode. This assumption is also made for CSD calculations at the top and bottom edges of the array; however, it is rather poor, as will be demonstrated later in Chapter 6.

5.2 Peak Detection

Detailed study of the propagation of the epileptiform burst

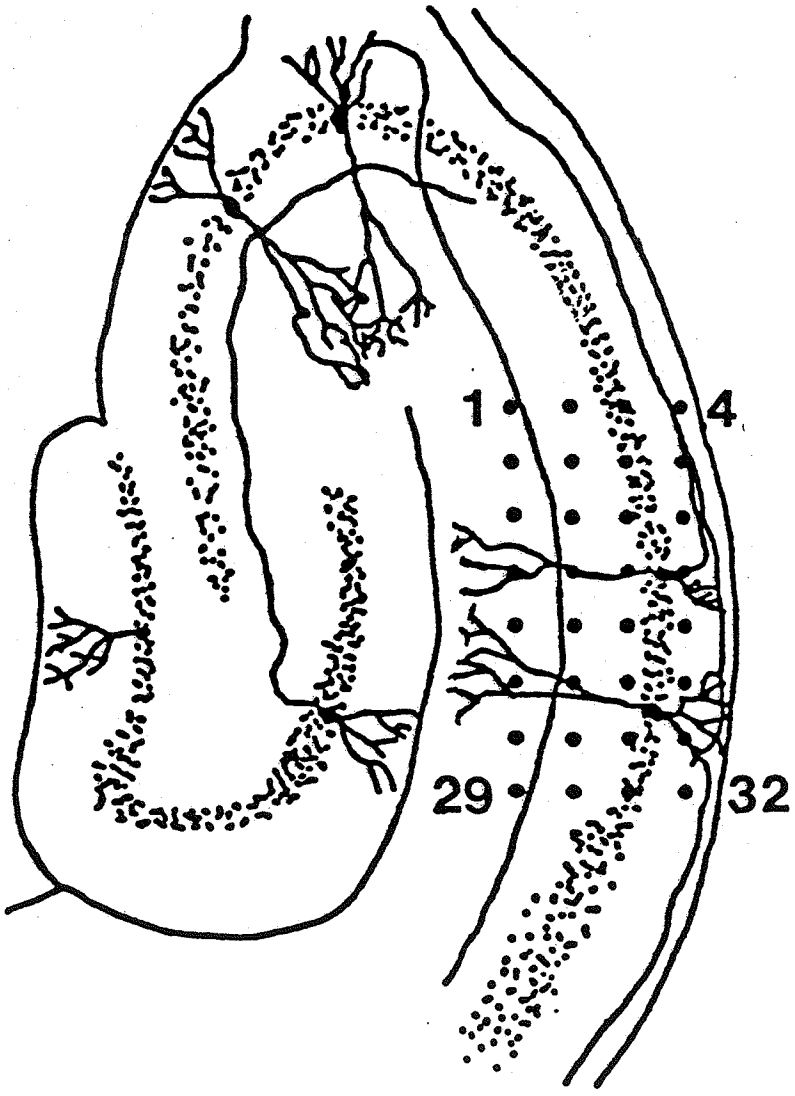

Figure 5.1 Schematic of hippocampal slice indicating the locations of array electrodes in CA1.

through the slice required measurement of peak times for each component on each channel. Because of the large amount of data collected and the time-intensive nature of manual peak detection, a technique has been developed to permit automated detection with human override. The technique consisted of filtering CSD profiles followed by peak identification using a zero-slope detection algorithm with visual operator intervention.

Peak detection relied on locating a portion of a waveform with zero slope. The CSD profiles were essentially second spatial derivatives and were subsequently noisy, both in the temporal and spatial domains. The additional differentiation necessary for peak detection resulted in an unacceptably large number of false peak detections. Fortunately, the offending temporal high frequency noise was sufficiently above the CSD signal bandwidth to permit temporal filtering prior to automated peak detection. The most significant requirement for the filter was that it possess zero phase shift, since unequal shifting of frequency components could have resulted in errors in peak times. A 9-point symmetrical rectangular filter (first zero = 916 Hz) was found to remove the high-frequency noise without shifting the peaks or significantly altering the waveform and was consistently applied to CSD data before further analysis. The endpoints of the filtered CSD sequence were computed assuming a zero-padded input CSD profile, but were not used in quantitative analyses.

After filtering, the zero crossings of the derivatives of the CSD profiles were computed, and markers were introduced into the data display so that the peak locations could be verified

visually on the CRT display. At this point, the operator typically needed to edit the peaks, removing those which did not correspond to physiological events, or adding points which did not meet the zero-slope condition due to numerical errors, but which were obvious to the eye. Following this editing, the locations of the peaks were interpolated using a cubic spline algorithm (Wheeler and Smith, 1987), which reduced some of the error due to the asynchronous sampling times with respect to the peak arrivals. Finally, the peak times and amplitudes were stored on disk for later analysis.

5.3 Conduction Delays and Significance Tests

The CAP, first (spike 1), and second (spike 2) population spike were the three components of the epileptiform bursts at the s. pyr. which were chosen for analysis. To prevent errors due to incomplete CSD estimates along the direction of propagation, the CSD profiles at top and bottom edges of the array (Figure 5.1) were not used, leaving 6 valid measurements for each burst component in a response. However, preliminary tests indicated that significance measures varied unacceptably between stimuli, although the observations themselves were similar. This variation was eliminated by computing the mean peak times and amplitudes for 5 stimuli which produced similar CSD profiles, suggesting that the variations were due to the asynchronous sampling with respect to peaks as well as the small number of observations.

Because a serial model of CA1 activation appeared likely from previous studies (Wong and Traub, 1983; Schneiderman, 1986), a standard least-squares linear regression analysis was performed on the mean peak times ($t_1 \ldots t_6$) of each component with the electrode position as the independent variable ($d_1 \ldots d_6$) (Sokal and Rohlf, 1969). Differences between the regression coefficients (b_{CAP}, $b_{spike\ 1}$, and $b_{spike\ 2}$) for pairs of burst components (a,b) were then tested using the measure

$$F_{\alpha[1,8]} = \frac{(b_a - b_b)^2}{\frac{\sum_i d_{a_i}^2 + \sum_i d_{b_i}^2}{\left(\sum_i d_{a_i}\right)^2 \left(\sum_i d_{b_i}\right)^2} S^2}$$

where

$$S^2 = \frac{1}{8} \cdot \left[\sum_i t_{a_i}^2 - \frac{\left(\sum_i d_{a_i} t_{a_i}\right)^2}{\sum_i d_{a_i}^2} + \sum_i t_{b_i}^2 - \frac{\left(\sum_i d_{b_i} t_{b_i}\right)^2}{\sum_i d_{b_i}^2} \right]$$

Next, correlations between peak times and peak amplitudes were determined using the product-moment correlation coefficient, r (Sokal and Rohlf, 1969), for each component of a burst (CAP, spike 1, spike 2). It was given by

$$r = \frac{\sum_i t_i c_i}{\sqrt{\left(\sum_i t_i^2\right)\left(\sum_i c_i^2\right)}}$$

where t_i and c_i were the peak time and amplitude of the component, respectively, at the i^{th} electrode. However, because the distribution of sample values for the correlation coefficient is very asymmetrical for nonzero values of r, a transform due to Fisher (1954), which has the form

$$Z = \frac{1}{2} \ln \left(\frac{1+r}{1-r} \right),$$

was applied. Additionally, because the number of valid measurements was small (n = 6), the resulting z values were again transformed using an approximation for small n (Hotelling, 1953) to z^*, given by

$$Z^* = Z - \frac{3Z + r}{24}$$

The variance of this measure is 1/(n - 1). Significance of the statistic z^* was ascertained by using the Student's t-distribution with

$$t_{\alpha,4} = \sqrt{5}\, Z^*$$

CHAPTER 6

RESULTS

The goals of this project required the following demonstrations: 1. the technical problems involved in multichannel recording were overcome; 2. the slice preparation was viable for a period of time sufficient for the acquisition of data; 3. the biological data were consistent with conventional recordings and with current understanding of neurophysiology; 4. the recordings were non-trivial, i.e., the information obtained was greater than that obtainable with conventional recordings; 5. the observations made were of potential significance in furthering the understanding of epileptiform activity in the slice.

The first three sections of this chapter deal with the former requirements, presenting general aspects of the recording system, preparation, and types of signals recordable and evokable. The fourth section involves a detailed study of an analysis technique (CSD) that utilizes the spatially-sampled multichannel recordings. Finally, after illustrating measurement techniques for extracting propagation delays, the data from a number of experiments are analyzed, providing biologically significant results which are not obtainable using conventional recording techniques.

6.1 Instrumentation

The array itself showed no noticeable deterioration under saline medium, even after repeated use in extended experiments.

The polyimide insulation proved to be stable under the medium as did the platinum-plated electrodes. Although the platinum plating wore off with use, particularly when stimulating, replatinizing the tips restored their original low-noise characteristics. Damage to the insulation by scratching with either a glass micropipette or metal stimulating electrode was the only type of failure experienced. One array was used in 28 experiments, while three other arrays were used in more than 12 experiments each.

Signals were recorded in standard medium without a slice on the array, to test the track and hold circuitry (Figure 6.1). Without suppression, the artifact is large and prolonged, while the suppressed artifact was relatively short and small. When recording with a slice on the array, the artifact was somewhat larger, presumably as a result of the greater resistivity of the tissue. In most cases, the larger unsuppressed artifact could not be merely subtracted from the recorded response, since amplifier saturation often occurred near the peaks of the biological signal. All of the results presented later in this chapter were acquired using the artifact reduction circuitry, without any additional processing such as artifact subtraction.

The ability to stimulate and to observe the signals at all 32 electrodes immediately, using the graphics monitor, greatly facilitated efficient experimentation. Adjusting flow rate and stimulus strength and location to optimize the evoked signals became routine. Additionally, fast calculation and display of

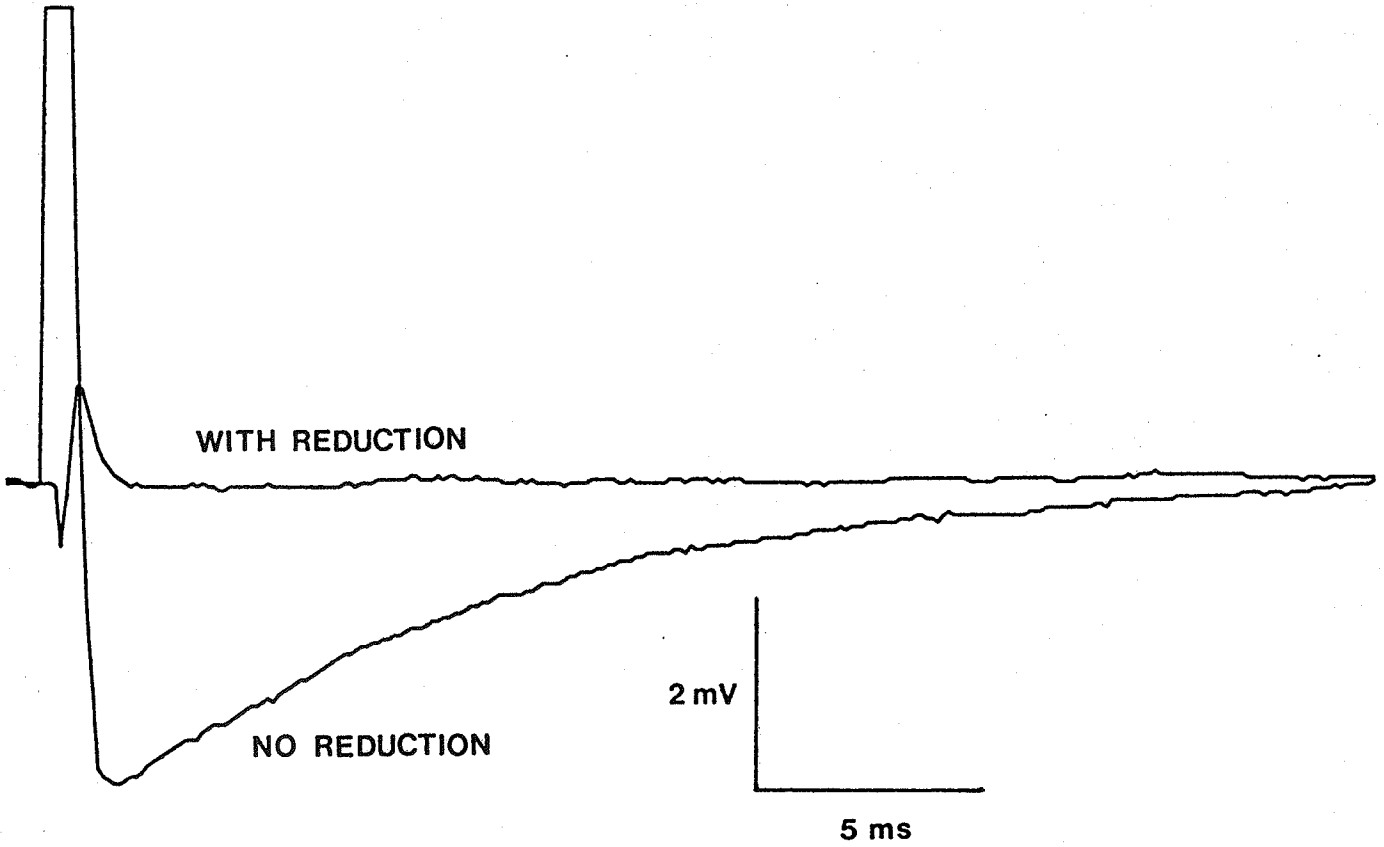

Figure 6.1 Comparison of stimulus artifact with and without active suppression circuitry.

the CSD profile permitted fine adjustment of slice position to provide consistent anatomical recording locations from slice to slice. Phase reversals seen in CSD profiles were directly related to the electrode location within the strata of CA1.

6.2 General Recording Characteristics

Although a dead layer of cells existed on either side of the slice, population responses were routinely recorded from the surface using the array. Considerable effort was expended determining environmental conditions under which controlled recordings could be made. Significant problems included keeping the slice alive and firmly on the array during perfusion, in order to increase experiment duration.

The most critical parameter for successful recording was the fluid level in the area around the slice. Since the polyimide insulation was hydrophobic, the medium tended to bead up on the surface, producing isolated pools. The size of the opening in the gauze laid over the array needed to be large enough to accommodate the slice easily, while ensuring that the surface tension of the medium was sufficient to permit fresh medium to flow past the slice. However, maximizing the signal levels recorded at the slice surface required a relatively low fluid level and flow rate to prevent the slice from floating. The low flow rate resulted in unacceptably long delays for washing-in experimental media.

A reasonable balance between keeping the slice viable and making recordings was achieved by first adjusting the fluid level

to just cover the slice, and then reducing it just enough to expose the slice surface. The gauze used was approximately the thickness of a slice and provided a reference for the fluid level. The slice environment was similar to that in a standard interface chamber (Haas et al., 1979), except that slices positioned on the array had less exposure to the medium on the bottom recording surface.

It appeared that the depth of anesthesia affected the length of the recovery period before the slices were responsive. Initially, rats were deeply anesthetized for as long as 5 min. Subsequent attempts at evoking responses from slices just placed on the array after a 90-min recovery period often produced CAPs without population spikes. Population spikes did recover in some of these cases, but epileptiform bursts were not observed. Slices from the same hippocampus placed on the array 2-4 hours after dissection produced robust responses. If rats were closely monitored during anesthesia and removed immediately after losing head support (30-60 s), slices displayed robust responses after the 90-min recovery period. This method was adopted as the standard protocol, to permit recording as soon as possible after placement on the array. This minimized the problems of slice spreading and of limited recording duration, which are discussed below.

Slices which passed the stability criteria defined in Chapter 4 typically displayed stable responses soon after being transferred from the holding chamber to the array surface (Figure 6.2a). Responses remained stable for 1-2 hours after placement

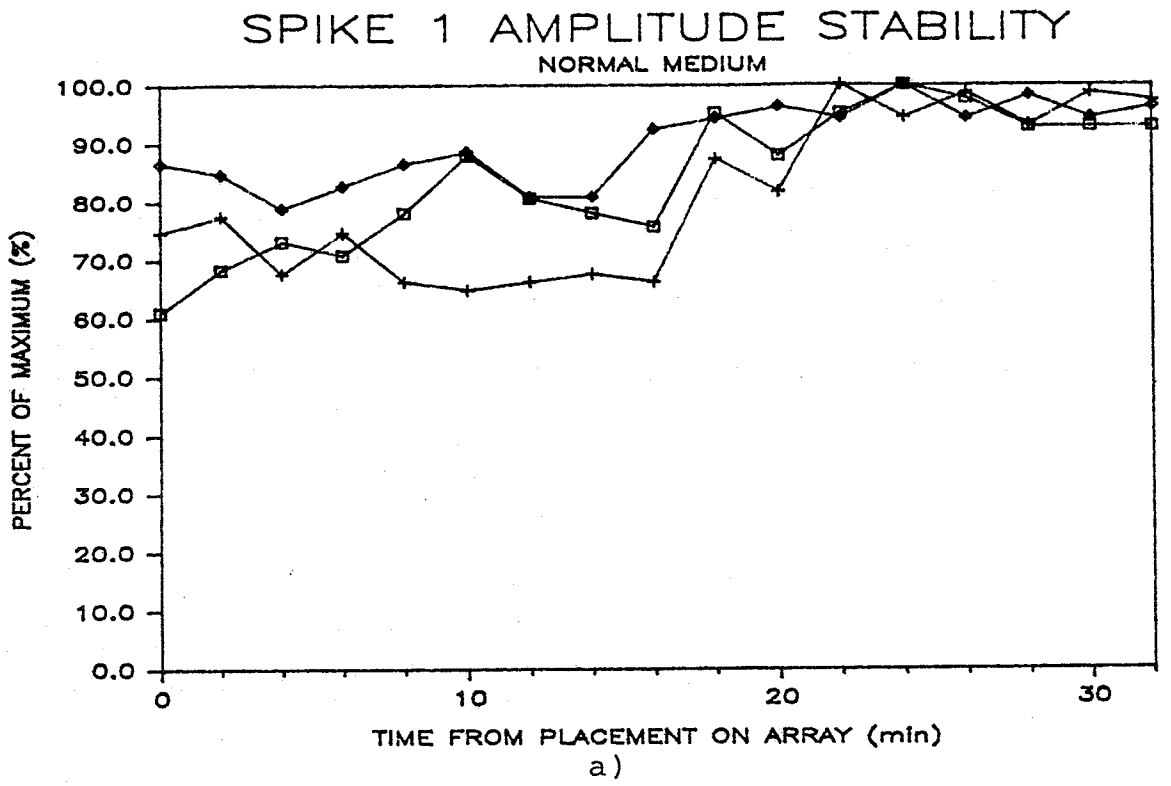

a)

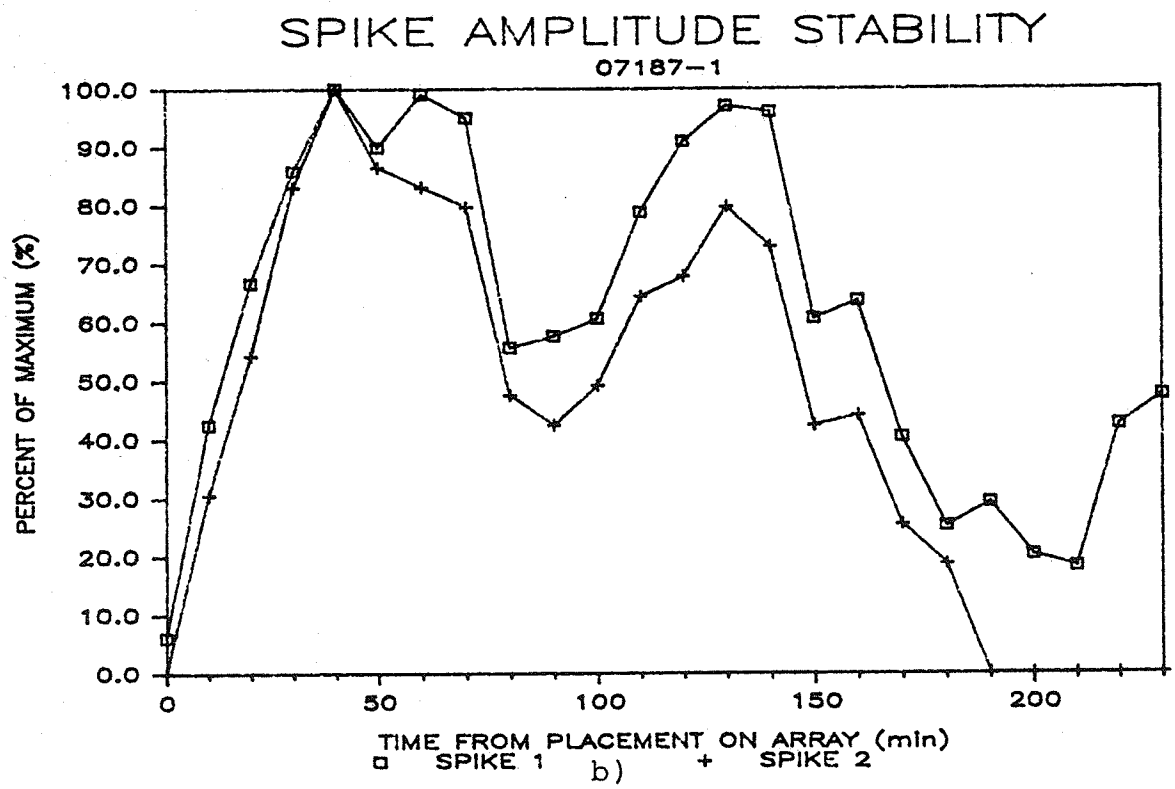

b)

Figure 6.2 CSD amplitude versus time from placement on the array. Rapid amplitude stabilization of an acceptable slice is shown in a). Slower recovery of unacceptable slice and subsequent dip during slice spreading are shown in b).

on the array. However, the extended recording session duration seemed to be limited by the presence of the nonporous recording surface (Figure 6.2b). In this experiment, the amplitude of the population spike 1 was recorded every 10 min. After a period of increasing amplitude lasting about 30 min, the signal level stabilized for nearly 40 min. The variations that occurred after 70 min are believed to be the result of a phenomenon termed slice spreading. At this time, slices began to spread out from their centers (near the s. rad. of CA1) and become transparent (Figure 6.3). Variations in signals occurred as a result of the electrodes shifting with respect to the slice. However, in experiments where slice activity was monitored using a glass micropipette, evoked responses were recorded for 10 h, presumably indicating that the penetration of the tissue by the electrode prevented shifting at the recording point, and also that cells not recordable with the array remain viable after array signals declined.

The population potentials in Figure 6.4a) were recorded in CA1 following orthodromic stimulation of the Schaffer collaterals near CA2 (Figure 6.4a). (In an effort to present multiple traces more clearly, the stimulus artifact from all evoked responses has been omitted from this and subsequent figures. The stimuli were delivered 1 ms before the beginning of the waveforms, unless otherwise indicated.) The initial deflection in the uppermost traces in Figure 6.4a) was the CAP produced by the evoked volley in the Schaffer collateral fibers (Andersen et al., 1978). As reflected by the increasing latency on electrodes distal to the

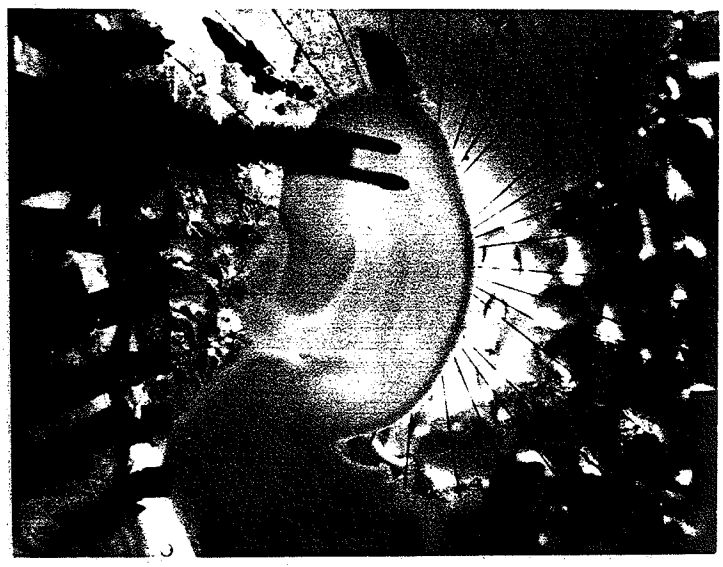

a)

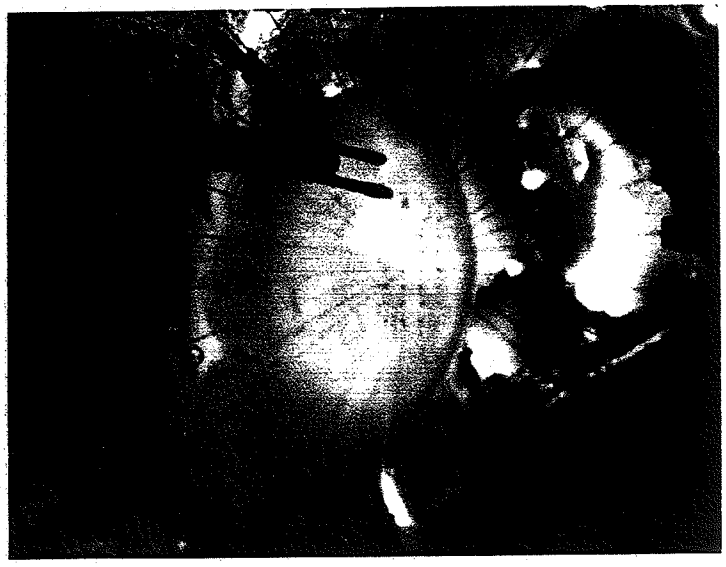

b)

Figure 6.3 The phenomenon of slice spreading. a) shows the slice just after placement on the array. After 70 min, slice spreading has occurred and the array electrodes are visible through the transparent slice b).

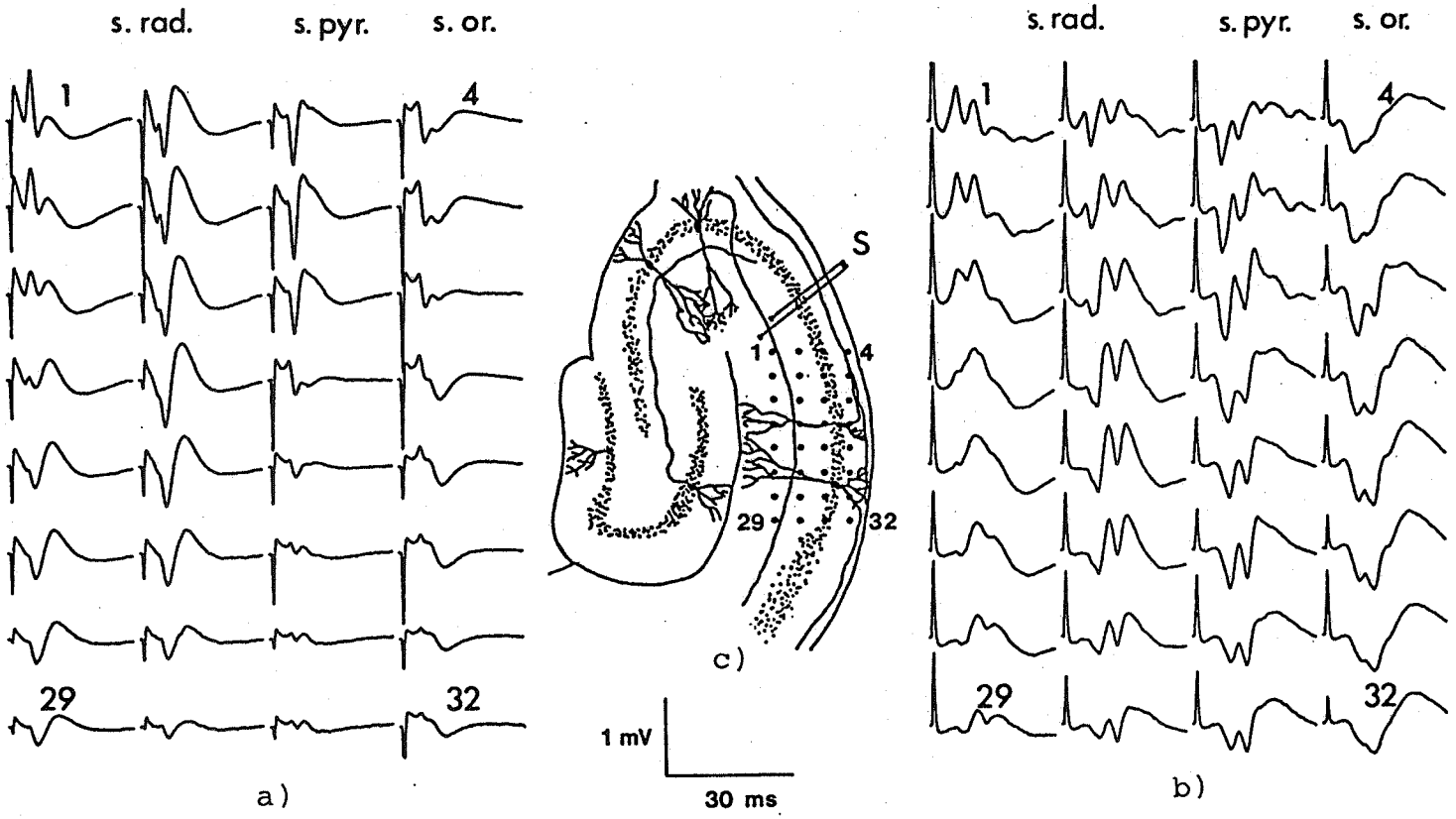

Figure 6.4 Comparison of evoked activity in normal medium a) and with the addition of 100 μM picrotoxin b). The recordings in a) were taken just prior to the addition of the picrotoxin, while those in b) were taken 10 min later. Multiple spikes and enhanced slow waves are evident in b). The approximate position of the array is shown in c).

stimulus, it propagated along the pathway, decreasing in amplitude until barely visible on electrode 29. The responses recorded in s. pyr. resembled population spikes recorded with conventional extracellular electrodes (Andersen et al., 1971b).

The signals changed to epileptiform responses 10 min after the addition of PTX-containing medium directly to the chamber (Figure 6.4b). These epileptiform potentials were composed of multiple population spikes of increased amplitude and of enhanced underlying slow waves. The CAP merged with the slow wave and stimulus artifact and was no longer visible. Both the slow waves and the population spikes exhibited a phase inversion between the s. rad. and s. pyr., while the slow components in s. pyr. and s. or. appeared to be in phase.

A time series of CSD profiles taken from the s. pyr. in another experiment revealed the gradual development of epileptiform activity during the wash-in of experimental medium (Figure 6.5). At t=0, PTX-containing medium was introduced into the medium intake tubing as close as was possible to the chamber. At the flow rate used in this experiment, a full 12 min was required for spike 2 to develop and to stabilize. The CAP was not visible in these recordings. Unfortunately, the rapid flow rate also caused the tissue to shift during an attempt at washing out the drug. Because of this type of problem with fluid level as well as the short recording time, the alternative method of placing the slice directly in medium containing drug was adopted (Chapter 4).

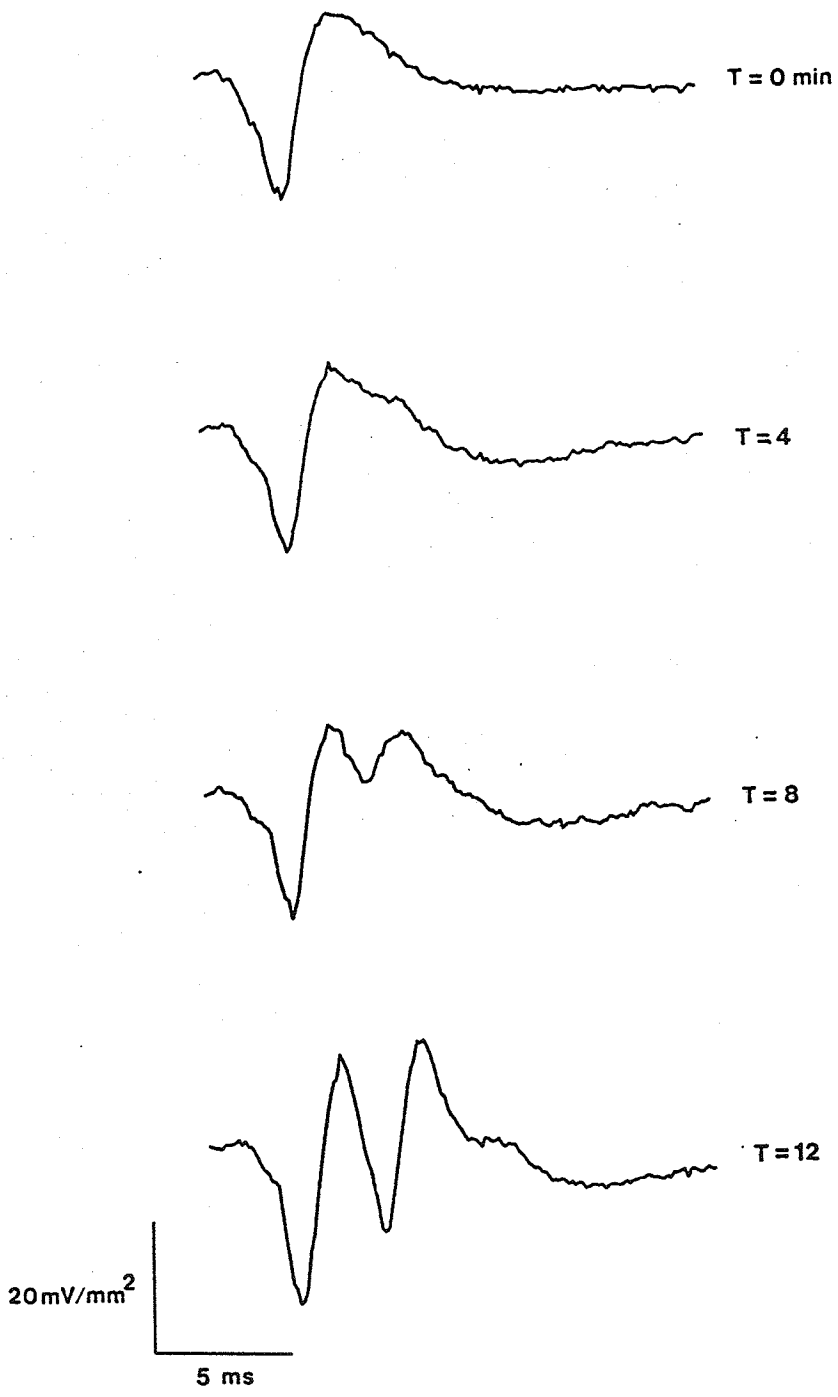

Figure 6.5 Changes in CSD profile on an electrode in s. pyr. during wash-in of PTX. A single population spike is evoked in normal media at t=0. A second population has developed 12 min after changing to media containing 100 μm PTX.

Spontaneous epileptiform potentials were observed in slices bathed in high KCl medium (Figure 6.6a). These demonstrated that low-level signals were recordable at the surface of the slice. The electrodes straddled CA2 and extended into both CA3 and CA1 (Figure 6.6b). This spontaneous event occurred at a frequency of approximately 2.6 Hz and persisted for over 1 h. The area of greatest signal amplitude corresponded to the CA2/CA3 region. The activity nearer the s. pyr. of CA2 also exhibited larger amplitude fast activity, although the underlying slow wave was larger within the s. or. of CA2/CA3. Electrodes located in distal s. rad. (electrode 13) recorded slow wave potentials inverted in phase from those nearer the s. pyr. (electrode 15).

The recordings plotted in Figure 6.7 provided a striking example of the systemic nature of the laminar hippocampal slice. First, the Schaffer collaterals were stimulated in the reverse direction with intensity sufficient to evoke population bursts in CA1 via the en passant synapses (Figure 6.7a). A subthreshold stimulus applied to the same location evoked the response seen in Figure 6.7b). This subthreshold stimulation antidromically activated CA3, which in turn orthodromically reactivated the Schaffer collaterals, and produced a response in CA1 which propagated toward the stimulating electrode.

6.3 General Stimulating Characteristics

The effectiveness of array stimulation was assessed by positioning the Schaffer collateral tract in CA2 over a group of array electrodes and monitoring the antidromically elicited a

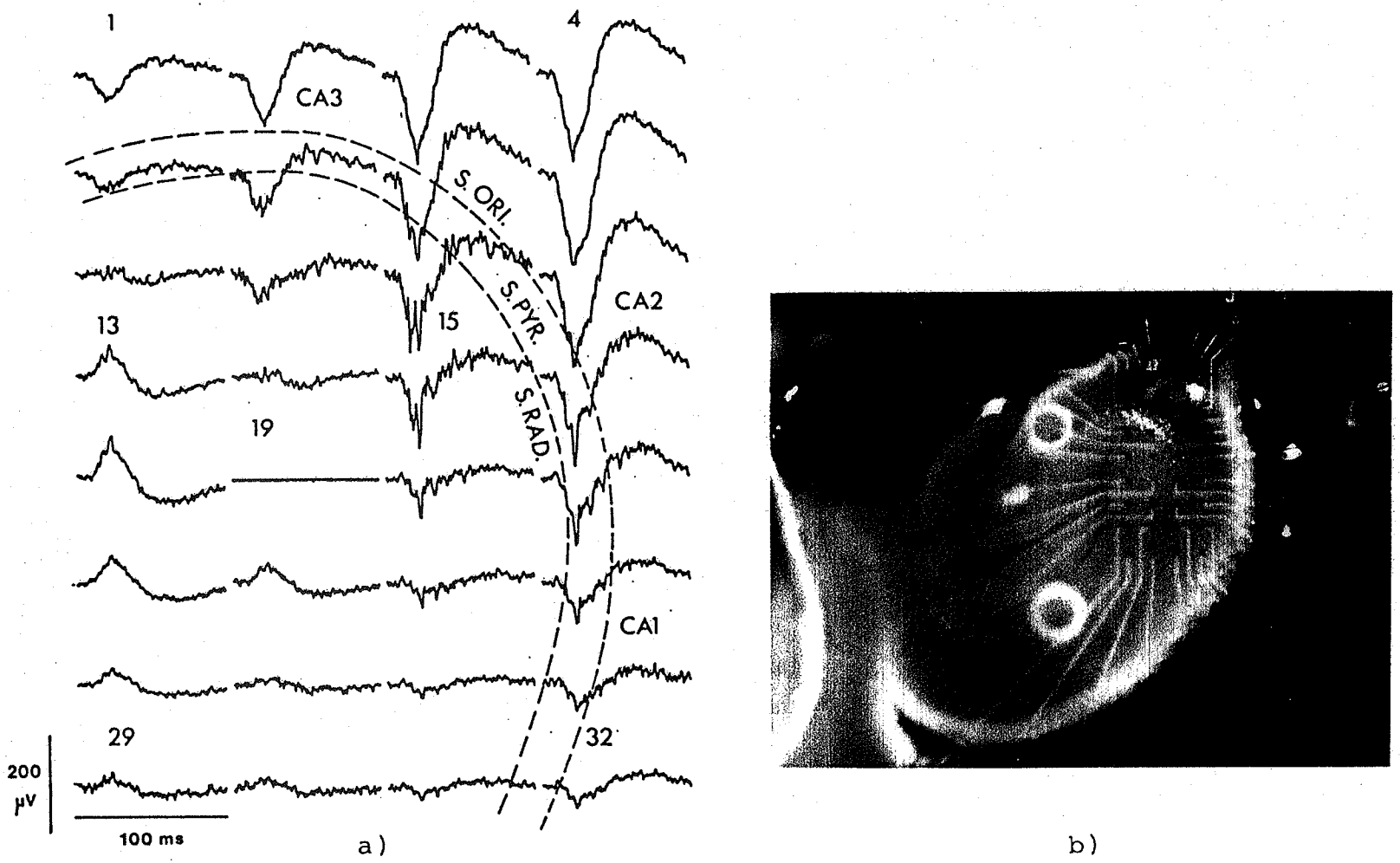

Figure 6.6. Spontaneous burst recorded in 7.0 mM KCl solution a) and a photograph of the slice as positioned on the electrode array b). The array straddles both CA3 and CA2, and that activity nearer CA3 has a larger slow component and reduced population spikes compared with that in CA2. Slow wave phase inversions between the electrodes in the center rows (e.g., electrodes 13 and 15) are also evident.

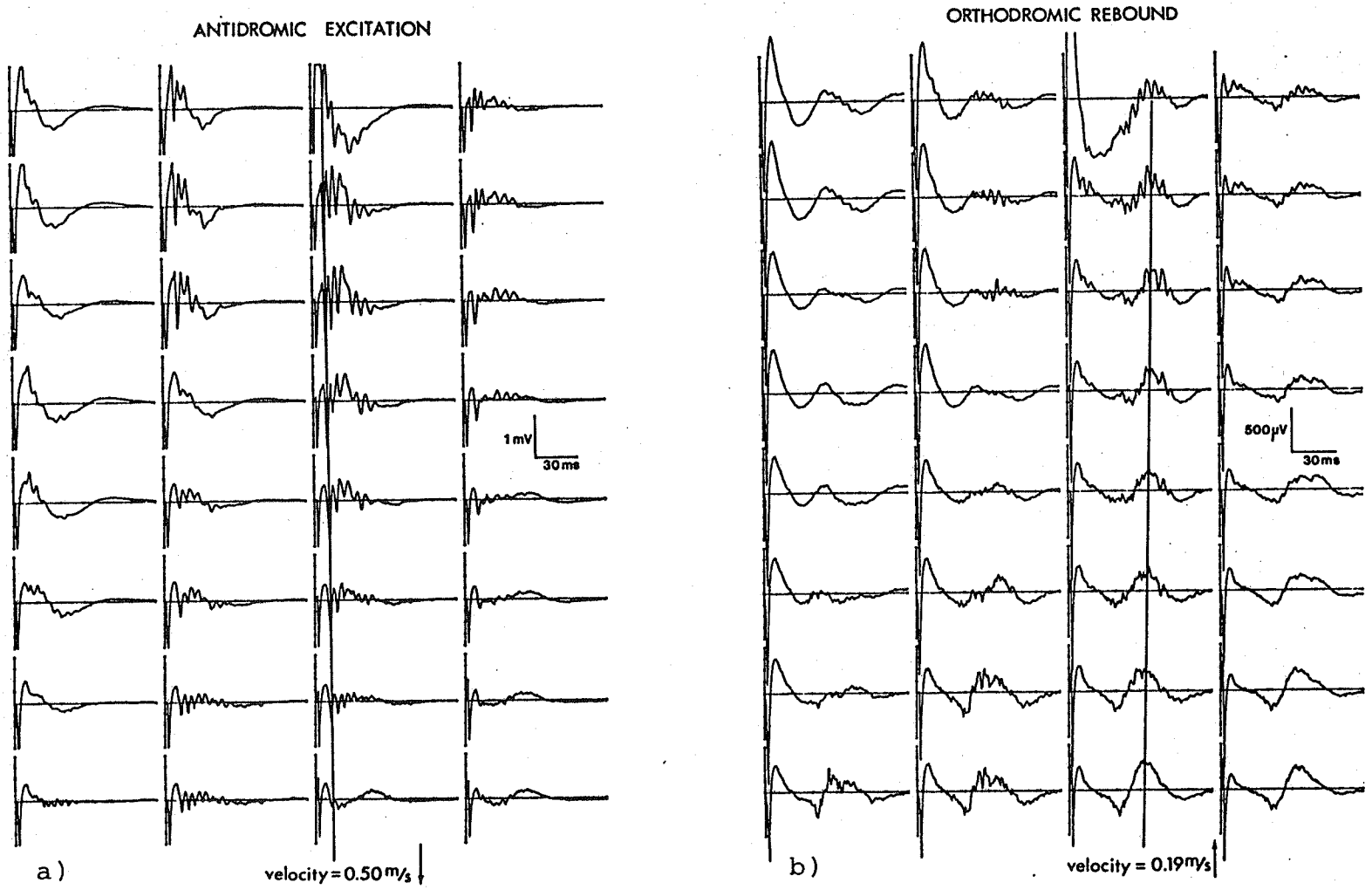

Figure 6.7 Differences in evoked responses due to variations in stimulus intensity. In a), the reverse stimulus was sufficient to evoke population spikes in CA1. At a lower stimulus intensity b), population spikes propagate in the forward direction toward the stimulating electrode. It appears that CA3 was activated antidromically and reactivated the Schaffer collaterals sufficiently to excite CA1.

population spike in CA3 using a glass microelectrode. The electrodes were positioned as indicated in Figure 6.8a). Monopolar voltage pulses (100 μs) were applied between pairs of electrodes indicated by the filled circles. Unfilled circles were used to indicate unused array electrodes. In the first experiment, the center electrode was negative (cathodal), while the outer eight electrodes were sequentially selected as the anode. All anodal positions were successful at eliciting similar amplitude population responses at about the same intensity (5-7 V) (Figure 6.8b). The regions stimulated by the various pairs seemed to overlap to some degree near the cathodal center electrode.

Next, the center electrode was made positive (anodal), and the surrounding electrodes cathodal (Figure 6.8c). These responses were strikingly different from those recorded with the cathodal center electrode. The electrodes located farthest off the Schaffer collateral tract evoked only small responses up to the 20 V limit. These data indicated that using this geometry and these electrode polarities, the stimulated regions of tissue are very different, and do not overlap as was the case with the cathodal center electrode.

6.4 Current Source Density Calculations

Calculation of the 2-D CSD evoked response profiles revealed patterns of activity which reflected the current source nature of the underlying neural structures (Figure 6.9). The field potentials in different strata possessed similar phase

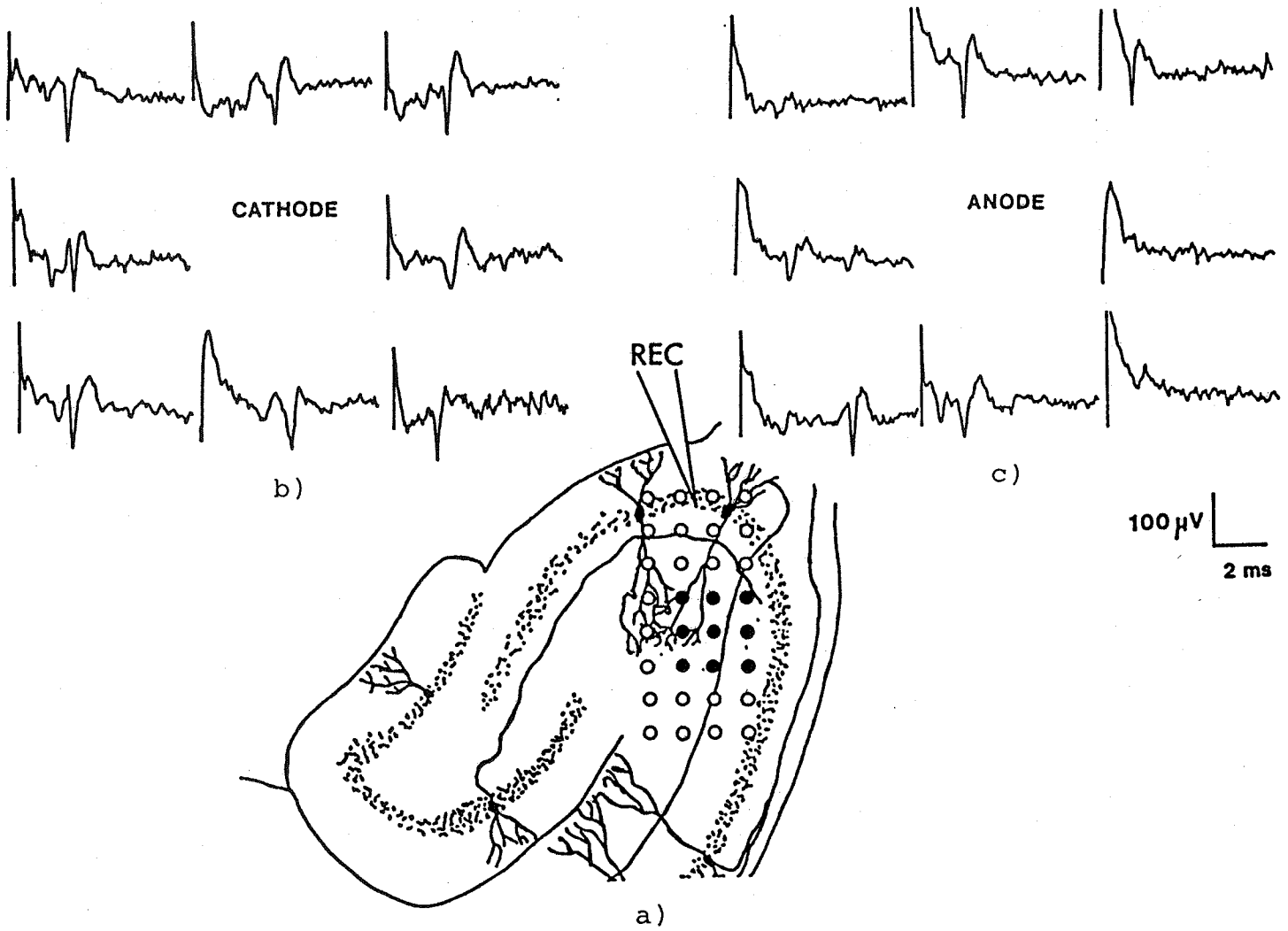

Figure 6.8 Array-evoked antidromic responses in CA3. The filled circles in a) are the electrodes chosen for stimulation. Monopolar voltage pulses were applied between the center electrode and the eight neighbors. The signals in b) and c) are those recorded at REC as a result of stimulation at the corresponding array electrode. The evoked responses in b) (cathodal center electrode) are quite similar, while those in c) (anodal center) are unique, with latencies that appear to increase with distance from the recording site.

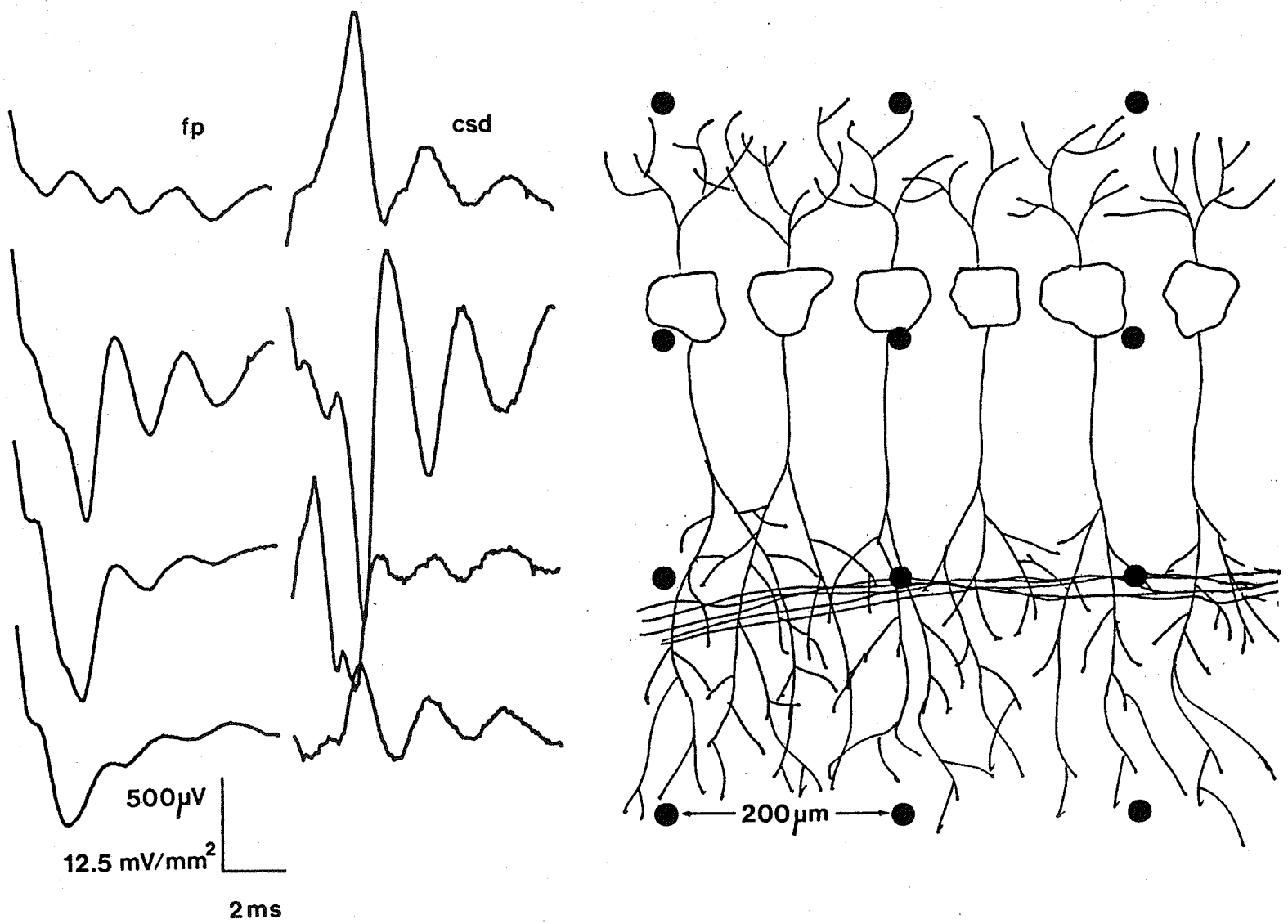

Figure 6.9 Comparison of field potentials (fp) in CA1 strata versus CSD profiles. The waveforms correspond to the anatomical level indicated. Phase reversals corresponding to activation of different strata are readily observed in the CSD profiles. These relationships are not seen in the field potential recordings.

relationships, and did not exhibit the striking source/sink phase reversals seen in the 2-D CSD profiles.

Close inspection of the 2-D CSD profiles revealed the time course of activation of the pyramidal cells (Figure 6.9). The CAP arrived in the proximal s. rad., directly producing a sink corresponding to the activation of fiber tract itself. Following the arrival of the CAP, the current flowed into the proximal s. rad., with corresponding sources in the distal s. rad. and s. pyr. Next, the somata responded to this dendritic depolarization and, in turn, became large current sinks themselves, producing the first population spike. The roughly 90° phase shift between the peaks in s. rad. and s. pyr. has also been observed by Miyakawa and Kato (1986) and was attributed to active changes in membrane properties and not to propagation of dendritic action potentials. During spike 1, the s. or. acts as a passive current source, as indicated by the 180° phase shift.

The phase relationships were quite different during the generation of spike 2. The s. pyr. appeared as a sink which was directly opposed by sources in s. or. and s. rad. Active dendritic involvement, which would be indicated by a phase angle other than 180°, was not apparent in either spike 2 or subsequent population spikes. Note that the source amplitude of the distal s. rad. was greater than proximal s. rad. during these later spikes. The synapses activated by the afferent volley were not reactivated via recurrent excitation or other mechanisms during spike 2. Further, although not directly activated, the distal s. rad. seemed to play a significant role in the generation of the

second population spike.

Because of the direct relation to anatomical features of the CA1 region, accurate calculation of the CSD profiles for the CAP, spike 1, and spike 2, required computing the 2-D CSD profile and not relying on one-dimensional (1-D) calculations as done with linear arrays of conventional electrodes (Swann et al., 1986, Miyakawa and Kato, 1986). In addition to the assumptions stated in Chapter 5 for the 2-D CSD algorithm, computing 1-D profiles required neglecting the current flows in the orthogonal direction parallel to the Schaffer collaterals (Figure 6.10). However, because the sources/sinks reflecting the CAP were in this direction (vertical), while pyramidal cell current flows are horizontal, it was not possible to estimate all three features of the burst accurately using a 1-D analysis. The 1-D vertical, 1-D horizontal, and 2-D CSD profiles for a typical response were superimposed in Figure 6.10 to illustrate this finding. The 1-D vertical calculation preserved the CAP, but provided a poor estimate of the population spikes, while the 1-D horizontal calculation provided no indication of a CAP. For these reasons, all CSD calculations in the remainder of this thesis were performed using the 2-D formula.

The CSD profiles at the edge electrodes were calculated assuming the missing potentials to be identical to the edge electrode recording. Errors in estimating the top and bottom edge CSD profiles were similar, because the missing electrodes would have been located in similar anatomical structures. Actual

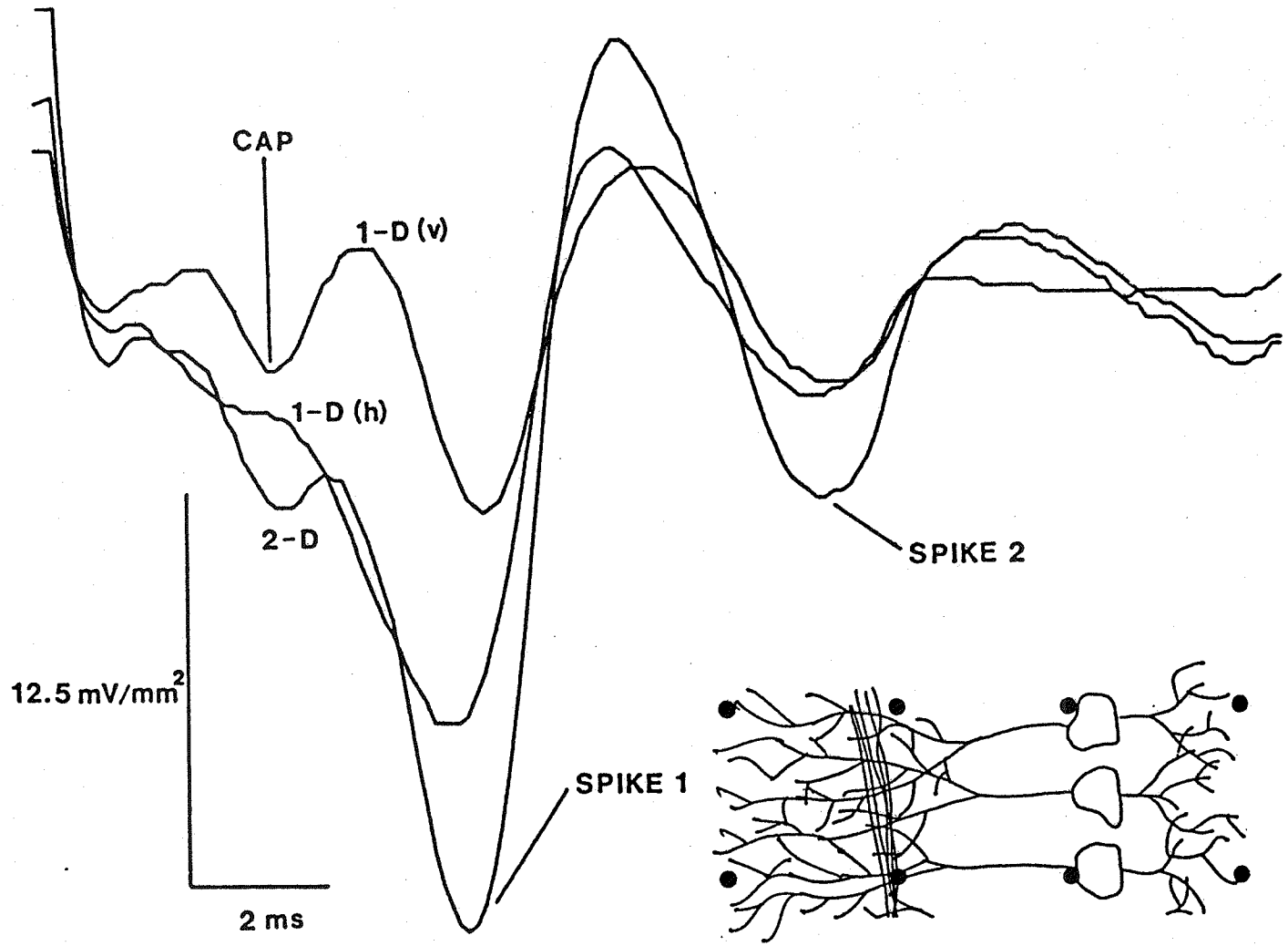

Figure 6.10 Comparison of 1-D and 2-D CSD calculations. Current flow generating the CAP is primarily in the vertical direction, while much of the population spike current is horizontal. The CSD profile calculated by ignoring the contribution in the vertical direction, 1-D (h), does not reveal the CAP. Neglecting the horizontal direction and calculating the 1-D (v) profile provide a poor estimate of the peak times of spike 1 and spike 2.

2-D CSD profiles were compared with the equivalent edge estimates to determine the accuracy of the assumptions (Figure 6.11). For top (bottom) edges, the actual 2-D CSD profile was calculated for a position in the center of the array which actually had 4 neighbors. By assuming the potential 200 μm above to be similar to that in the center, the equivalent edge estimate was calculated (Figure 6.11a). It is obvious that this top (bottom) estimate was rather poor for identifying peak times. The peaks of spikes 1 and 2 were shifted in opposite directions. The poor quality of this estimate was likely due to the the active nature of the tissue at the imaginary electrode site.

A similar procedure was performed to investigate errors in the CSD estimates for left and right edges. Because the anatomy is different in each case, they were treated separately. To provide the additional data necessary for computing 2-D profiles at the left and right edges, the slice was rotated 90° before evoked responses were recorded. Comparison of both the left and right edge estimates revealed that although there were errors in the magnitude of CSD profiles, the peak times appeared to be quite similar throughout the burst (Figures 6.11b) and 6.11c). This was expected, since the neural structures near the left and right edges were relatively small current sources when compared with the s. rad. and s. pyr. Thus, any field potentials recorded in these structures were likely to be dominated by the activity from adjacent sites, as assumed.

A powerful feature of the CSD calculation was that it permitted repositioning slices so as to span the strata of CA1 in

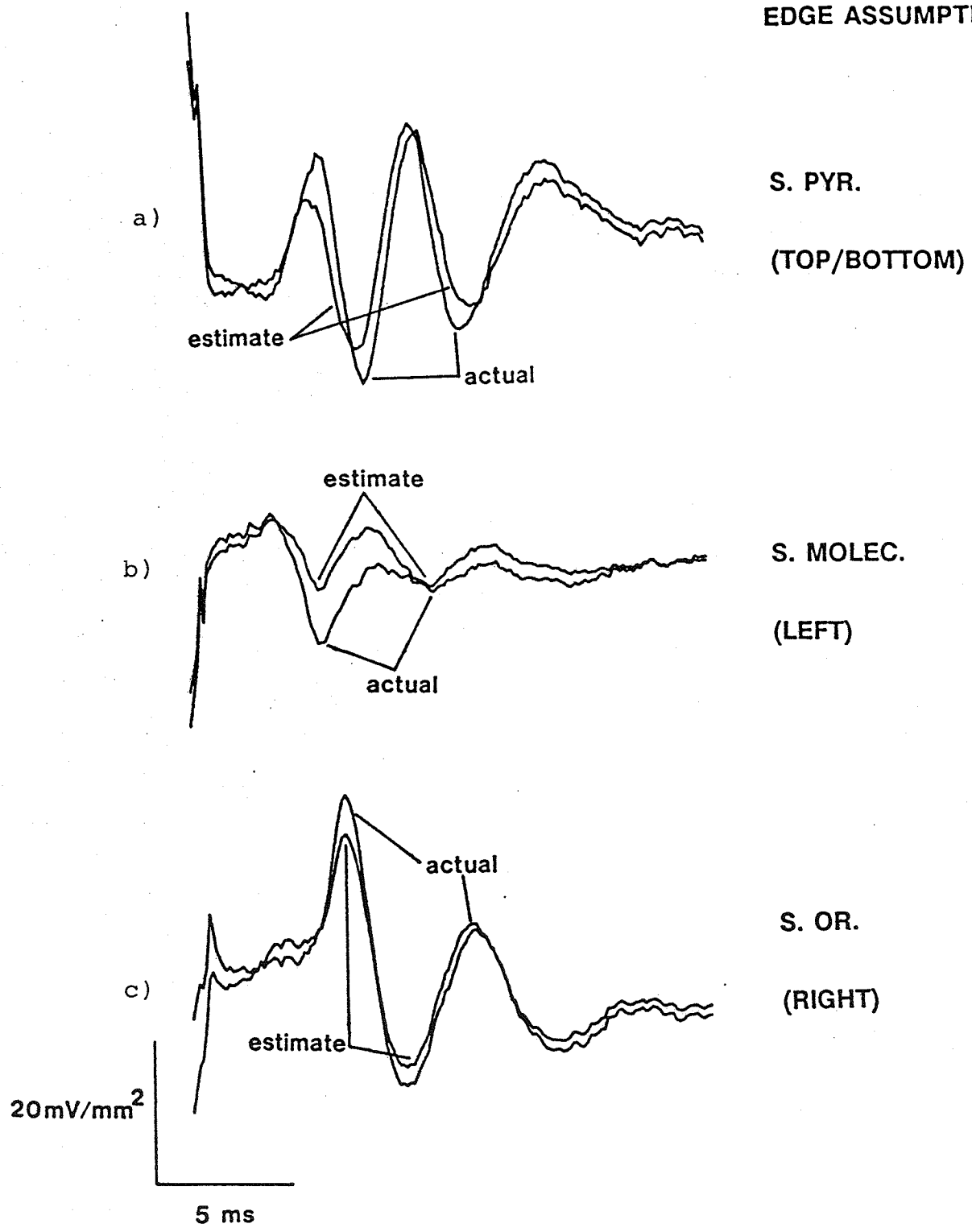

Figure 6.11 Inaccuracy of the CSD calculation at the edges of the array. The equivalent edge calculation for each case is superimposed on the actual 2-D CSD profile. In a) the peaks of the CSD profile at the top and bottom edges of the array are incorrect. The waveforms in b) and c) illustrate that the edge assumptions at the left and right edges provide CSD estimates which accurately fix peak times but not amplitude.

a consistent manner. After the slice was positioned on the array and allowed 20 min equilibration time, a stimulus was delivered and the CSD profiles calculated and displayed (Figure 6.12a). In this case, the columns of CSD profiles did not run parallel to the CA1 strata. The characteristic CSD profiles appeared to drift to the right as the activity propagated downward. After repositioning the tissue using a camel's hair brush and repeating the stimulation, the CSD profiles were similar in time course over each column of the array (Figure 6.12b). This electrophysiological technique was consistently used to position the slice accurately relative to the array.

6.5 Propagation and Amplitude Comparisons

Propagation of epileptiform bursts was studied using four adjacent CSD profiles located in the s. pyr. (Figure 6.13). The CAP, spike 1, and spike 2 occurred with increasing delay on electrodes located farther from the stimulus, and appeared to propagate downward, away from the stimulus. The conduction delays between corresponding events on neighboring electrodes and interpeak latencies between adjacent events on a single electrode were used as measures of propagation.

Regression equations for each burst component were computed for conduction delay versus electrode position. The results of a typical calculation were plotted in Figure 6.14. The latencies of all three components of the burst at a given electrode increased nearly linearly with distance from the stimulating electrode. This was expected, due to the uniform anatomy of CA1.

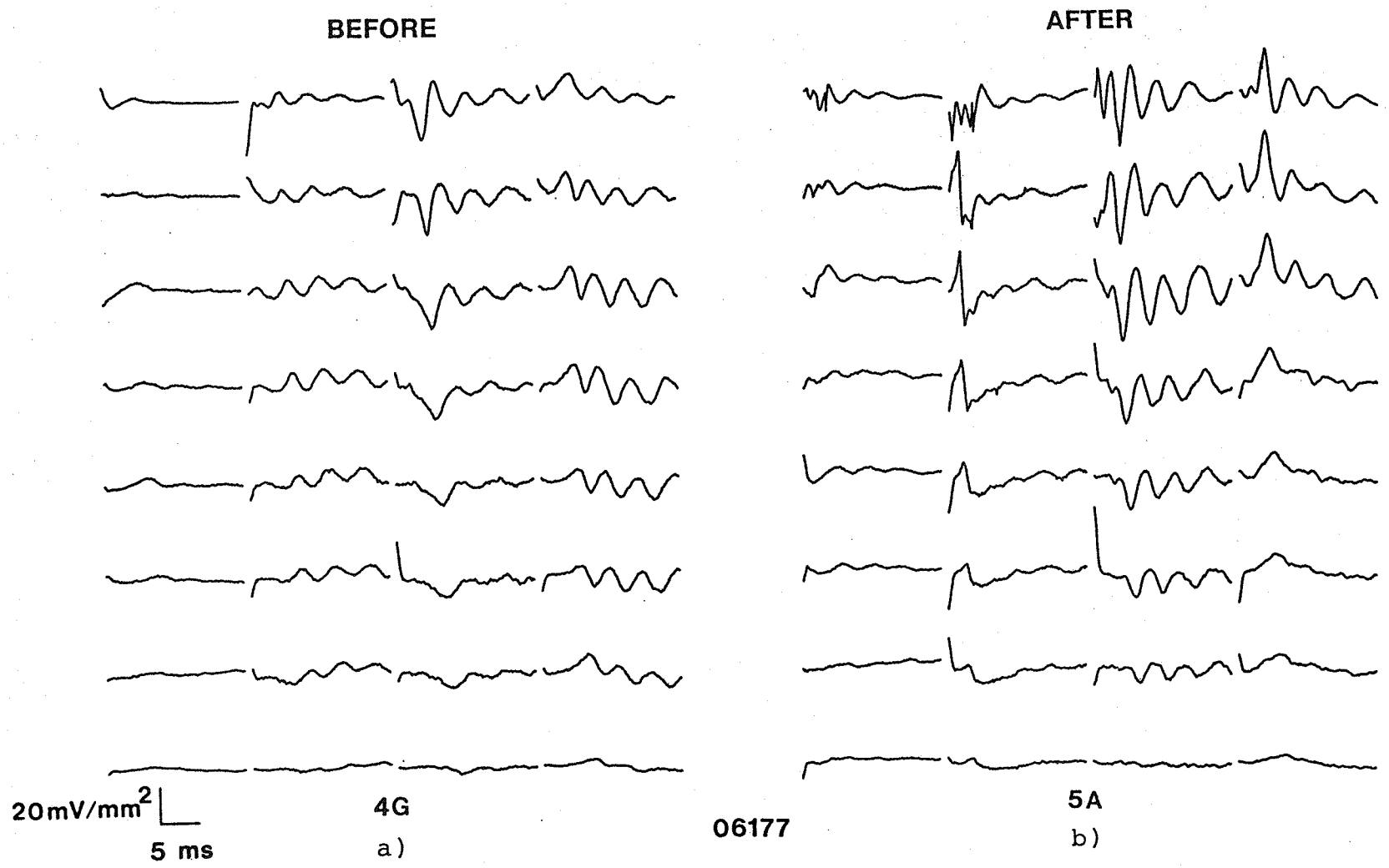

Figure 6.12 Electrophysiological determination of slice position on the array. The CSD profiles at 32 electrodes after placing the slice on the array are seen in a). The slice position in b) was adjusted such that the large amplitude signals corresponding to the s. pyr. run along the third column of array electrodes.

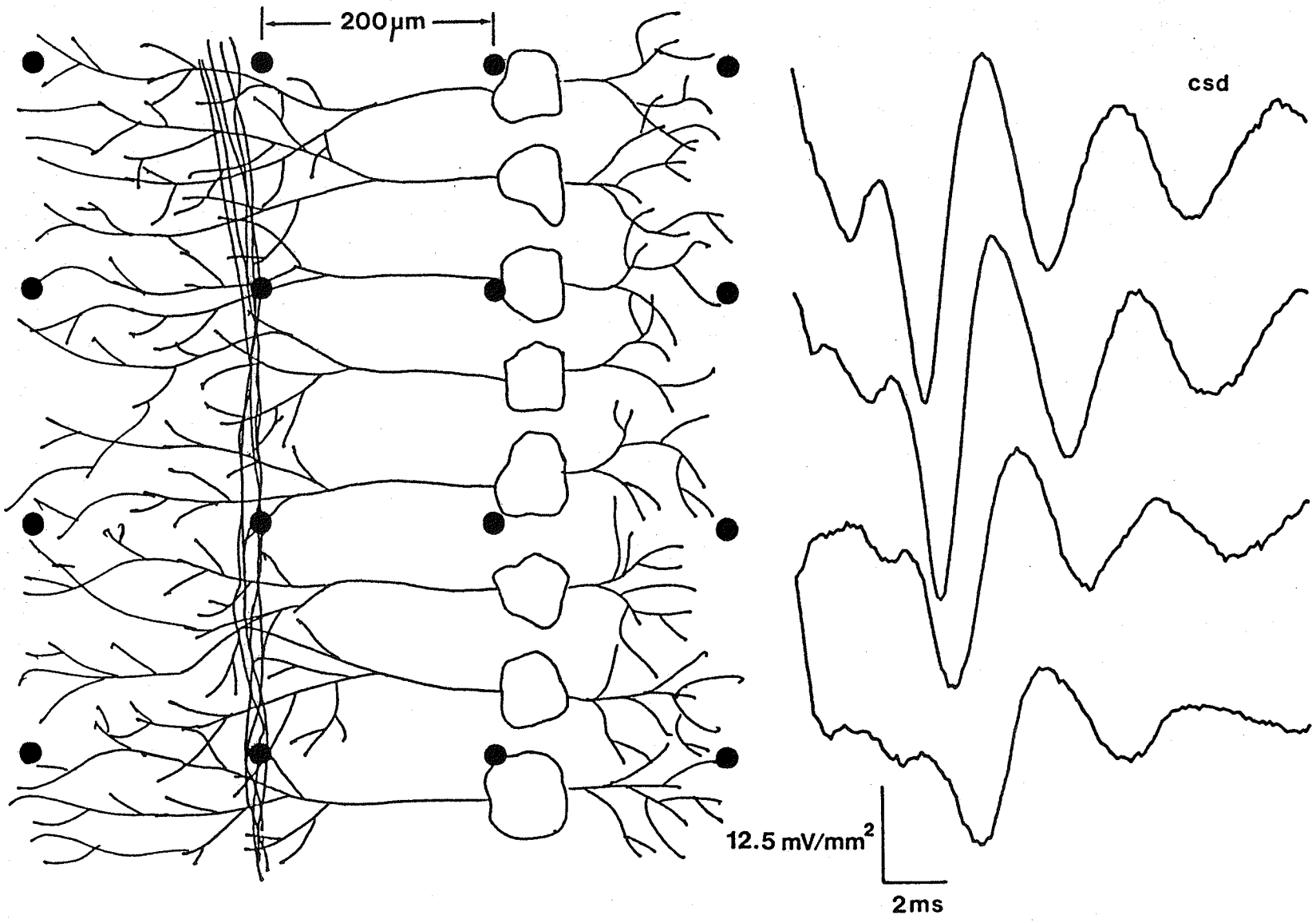

Figure 6.13 Example of apparent propagation of burst components along the s. pyr. of CA1. The four traces shown are CSD profiles at electrodes along the direction of propagation.

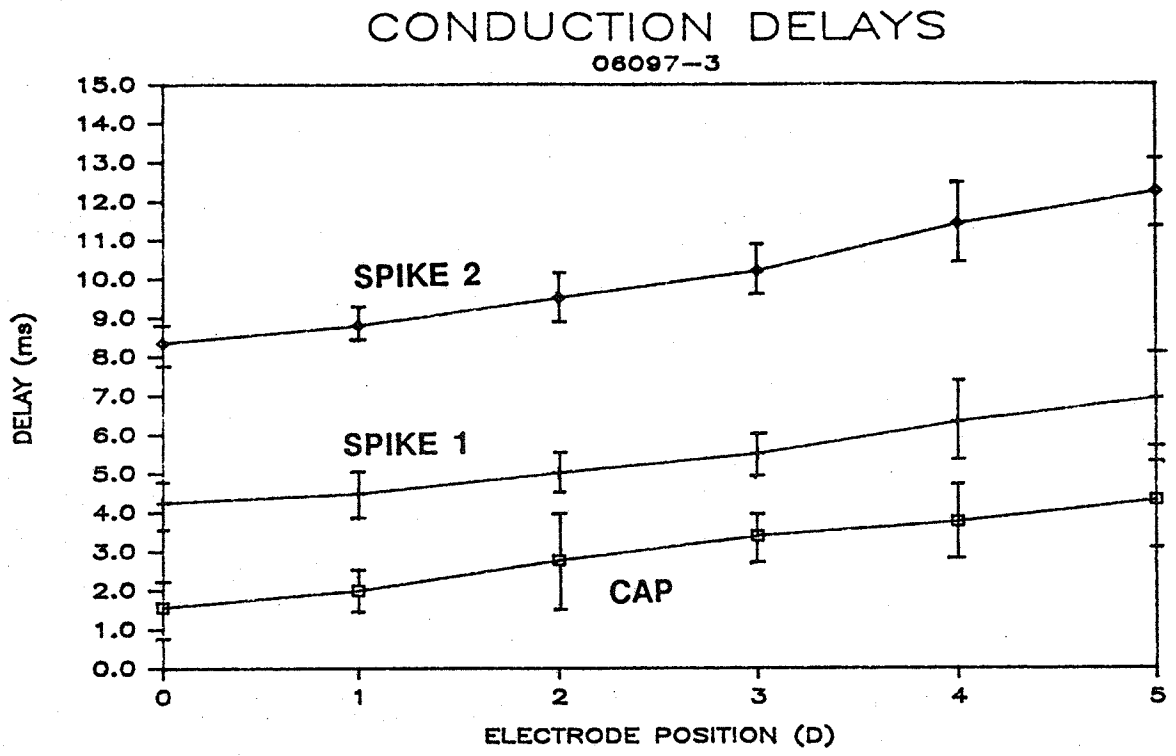

REGRESSION EQUATIONS

CAP DELAY (ms) = 0.561 * D + 1.56; r = 0.996

SPIKE 1 DELAY (ms) = 0.557 * D + 4.03; r = 0.998

SPIKE 2 DELAY (ms) = 0.800 * D + 8.08; r = 0.990

Figure 6.14 Conduction delays of the CAP, spike 1, and spike 2 measured using the peak of CSD profiles at 6 electrodes within s. pyr. in the PTX model. The delays increase nearly linearly with distance from the stimulus. Regression equations and correlation coefficients are as indicated. The error bars indicate $\pm$ 1 S.E.M. with N = 5.

The interpeak latency versus the electrode position for each slice was also plotted (Figure 6.15a). Note that while the latency between the CAP and spike 1 did not vary linearly with distance, there was an increase in the interpeak latency between spike 1 and spike 2. The burst shape changed as it propagated away from the stimulus by spreading out between the first and second population spike. There was no correlated decrease in the amplitude of the signal as the burst propagated (Figure 6.15b). Such a correlation might have indicated a common dissipative cause.

Similar analyses were performed for data obtained from other slices in PTX, PTZ, and 0-Mg^{++}. A total of 10 slices from 7 rats were used in PTX, with 5 slices from 5 rats in PTZ, and 8 slices from 8 rats in 0-Mg^{++}. However, because the actual values of the conduction delays (slopes of regression lines) varied greatly from slice to slice, conduction delays for the three burst components were compared for each individual slice. The high variability was presumably due to differences in slicing angle, which would strongly affect the actual distance from neural populations recorded by adjacent electrodes. Conduction delays for the same burst component during forward and reverse propagation were compared, as were delays for the various components in a single direction. The number of slices that fell into one of three categories (less than, equal to, greater than) at a threshold of $p < 0.01$ was tabulated in histogram format. Fewer slices provided data for the comparison of the CAP and spike 1 than for spike 1 and spike 2, because the CAP was

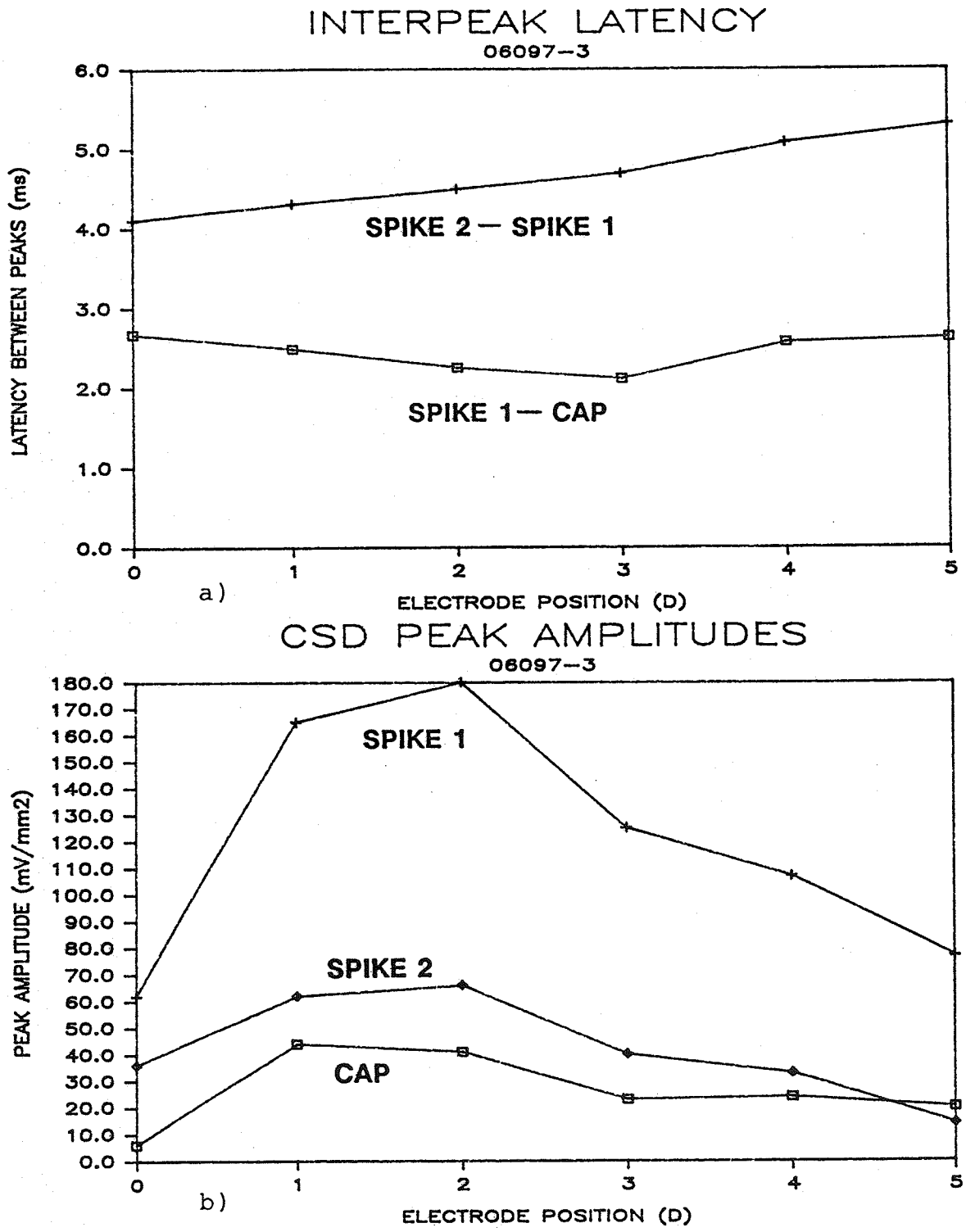

Figure 6.15 Interpeak latencies and peak amplitudes versus distance from the stimulus for the data in Figure 6.14. As shown in a), the latency between spike 1 and spike 2 (SPIKE 2-SPIKE 1) increases linearly with distance, although delays between the CAP and spike 1 (SPIKE 1-CAP) do not. The amplitudes of the peaks follow similar trends to one another b), but do not appear to be related to the interpeak latencies.

much smaller in amplitude and was often obscured by the stimulus artifact or noise.

Histograms were generated for forward and reverse stimulation in the PTX, PTZ, and 0-Mg^{++} models (Figures 6.16, 6.17, and 6.18). As experiments were performed, it became apparent that the conduction delays in the PTX model were anisotropic (Figure 6.16a). The slopes of the peak time regression equations for the CAP and spike 1 showed no significant difference, i.e., the CAP and spike 1 propagated with a fixed latency between them. This was as expected since the arrival of the CAP directly activates the synapses in s. rad. However, spike 1 had a smaller conduction delay (slope) than spike 2. The latency between the peaks of spikes 1 and 2 increased with distance from the stimulus.

There appeared to be no difference between the reverse conduction delay for spike 1 and spike 2, although the CAP delay was significantly smaller than that for spike 1 (Figure 6.16b). The onset of the population spikes following the arrival of the CAP was increasingly delayed with distance from the stimulus. Thus, although the activation of CA1 may have occurred in a serial fashion via the CAP on the Schaffer collaterals, forward and reverse bursting responses were dynamic and varied with distance from the stimulus. Although the CAP and spike 2 propagated with the same delay in both directions, the conduction delay for spike 1 in the forward direction was significantly less than in the reverse direction. These data seemed to indicate that the mechanisms of propagation of spike 1 were anisotropic,

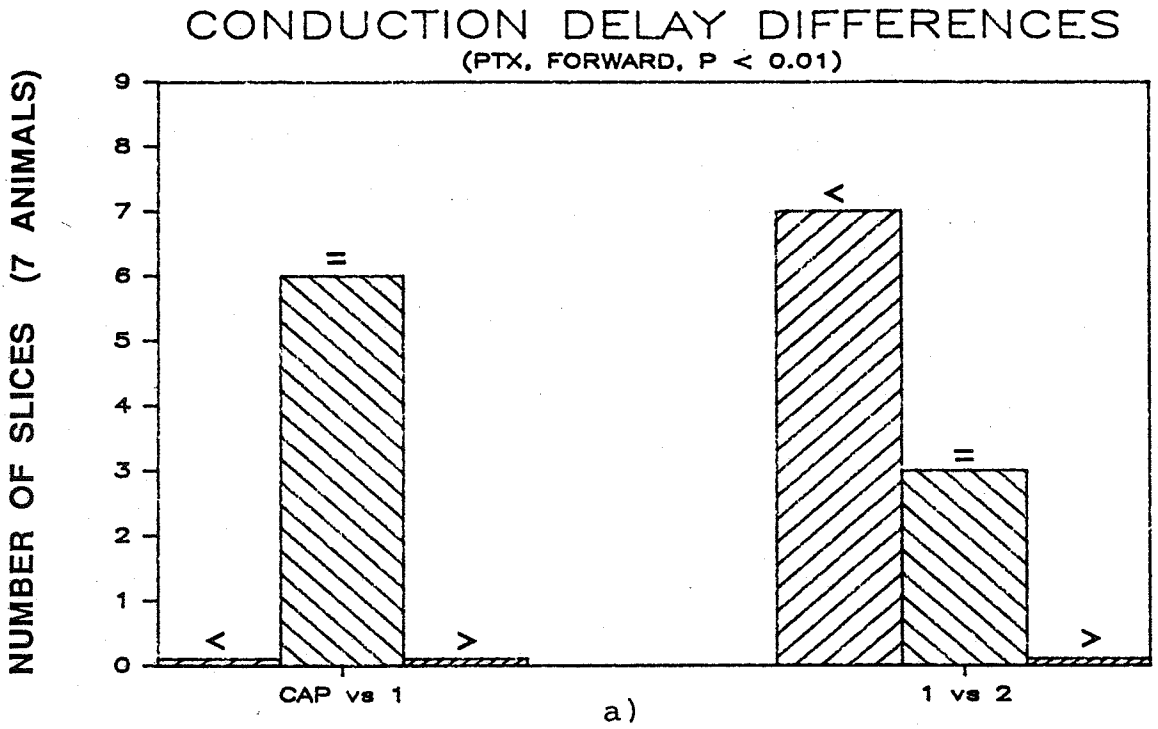

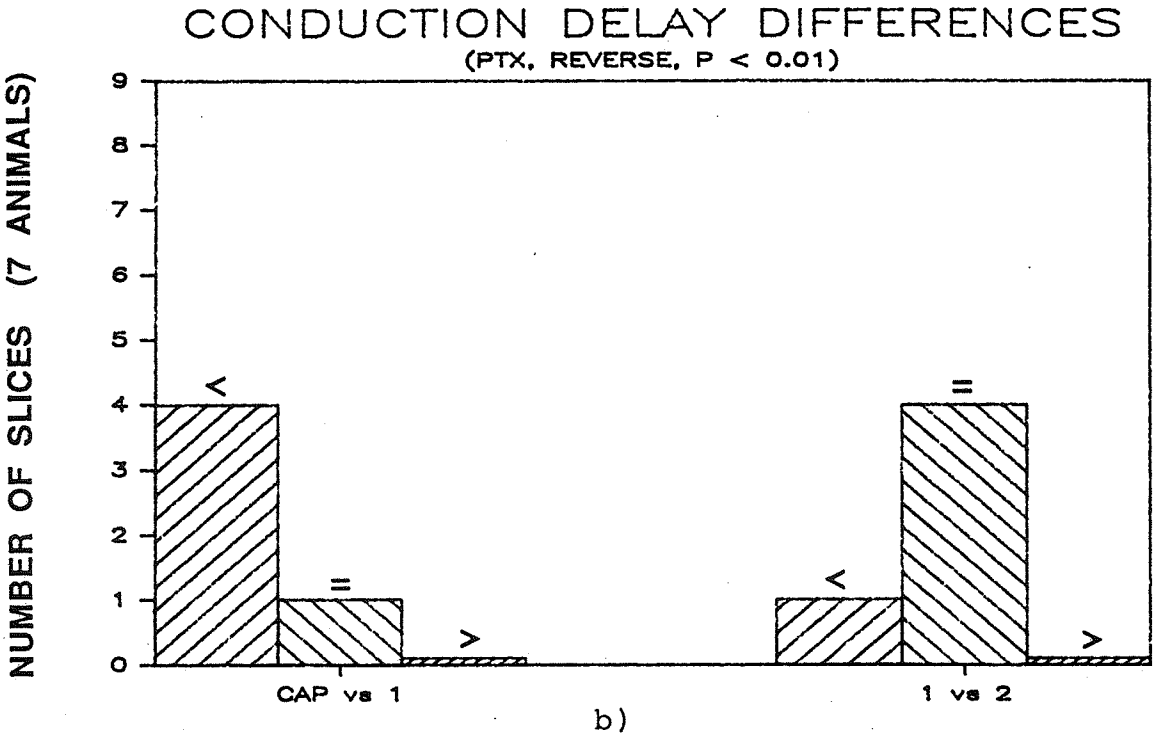

Figure 6.16 Conduction delay comparisons for the PTX model. Forward conduction is shown in a), reverse conduction in b), and a comparison of forward versus reverse delays is given in c). The data are from 10 slices obtained from 7 animals on separate occasions.

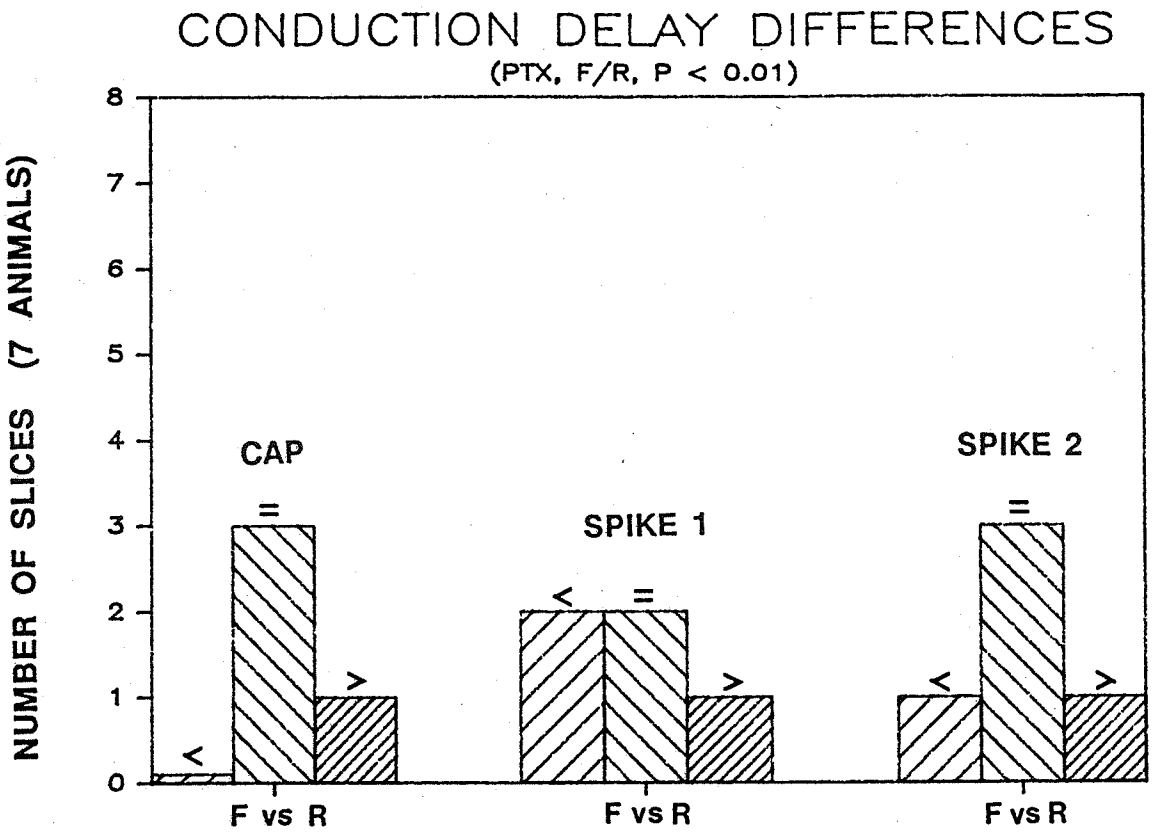

c)

Figure 6.16 Continued.

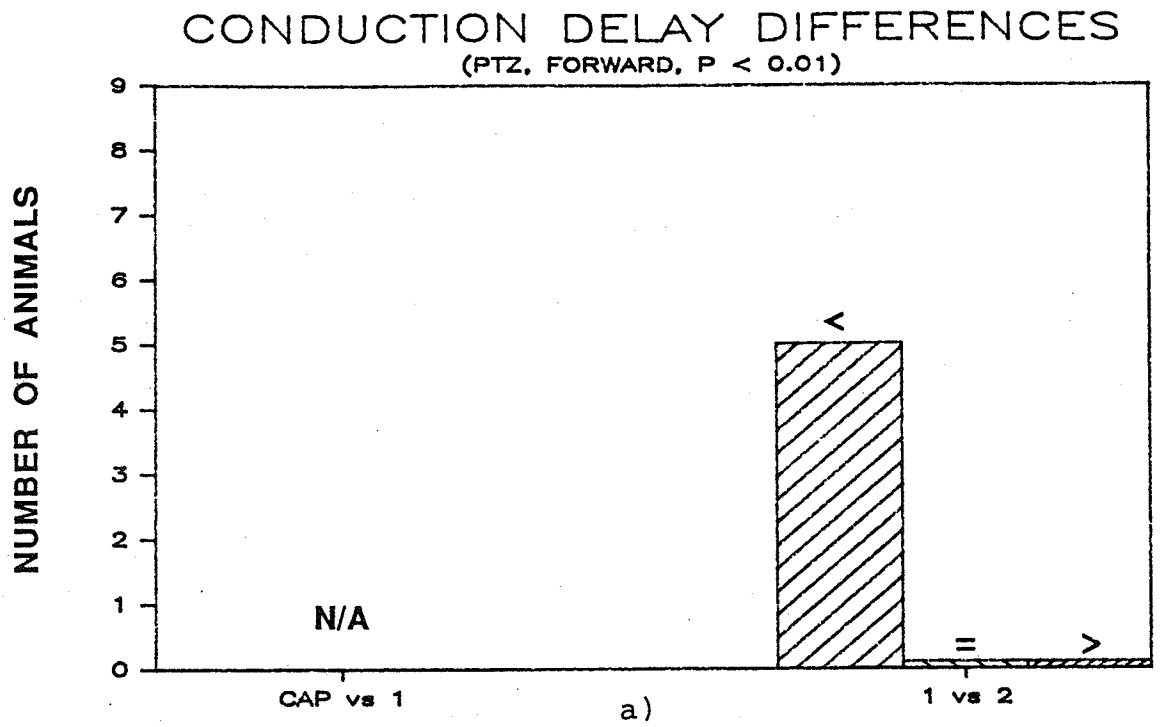

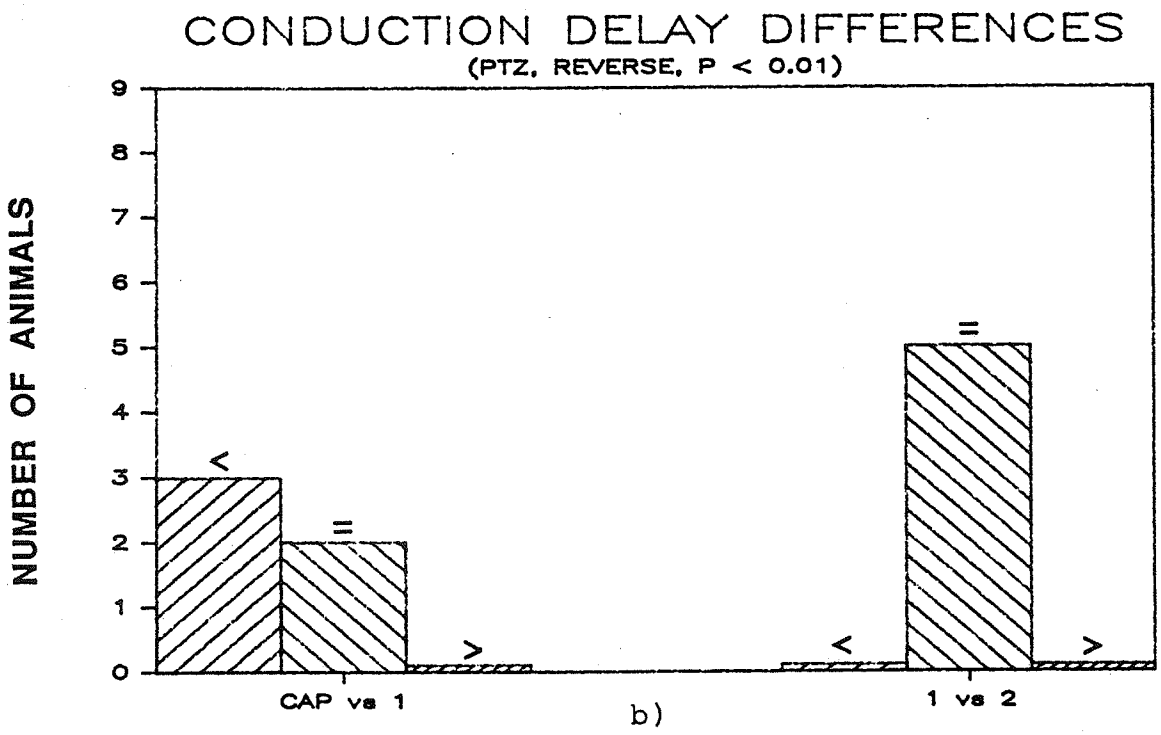

Figure 6.17 Conduction delay comparisons for the PTZ model. Forward conduction is shown in a), reverse conduction in b), and a comparison of forward versus reverse delays is given in c). The data are from 5 slices obtained from 5 animals on separate occasions.

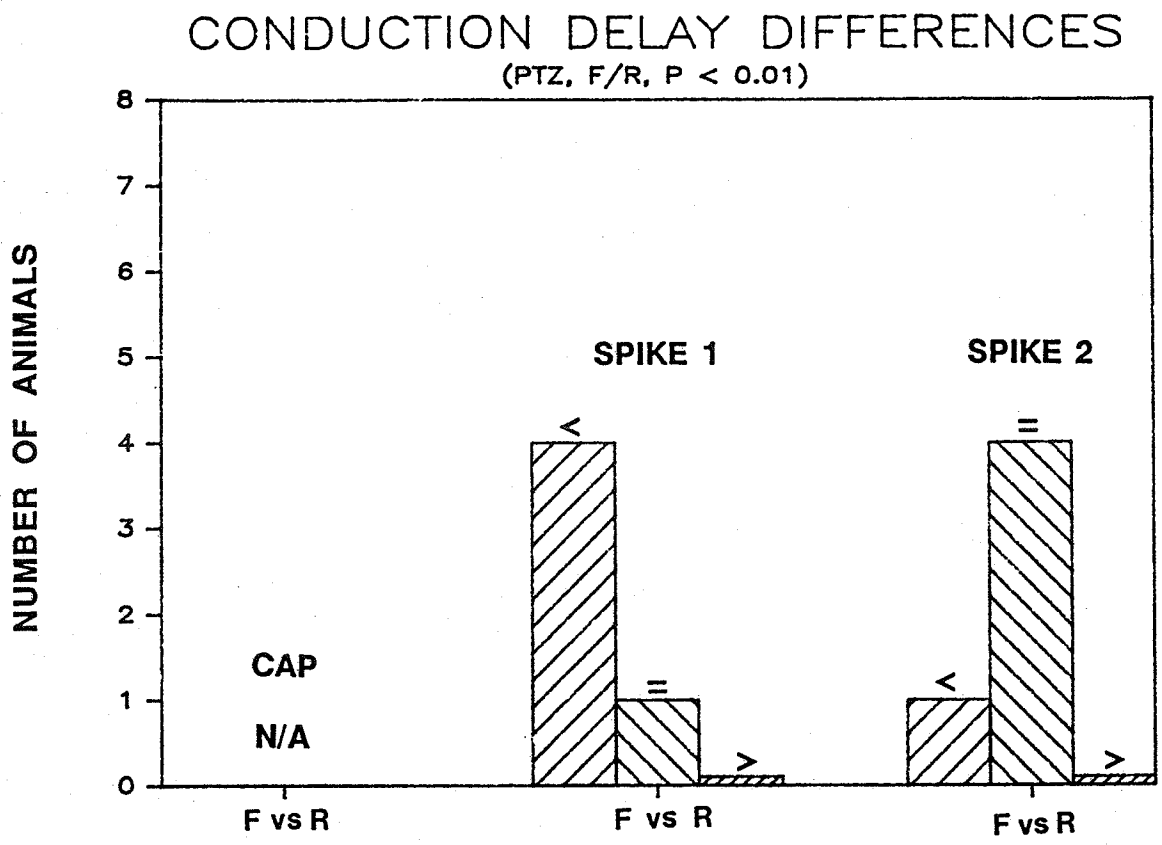

c)

Figure 6.17 Continued.

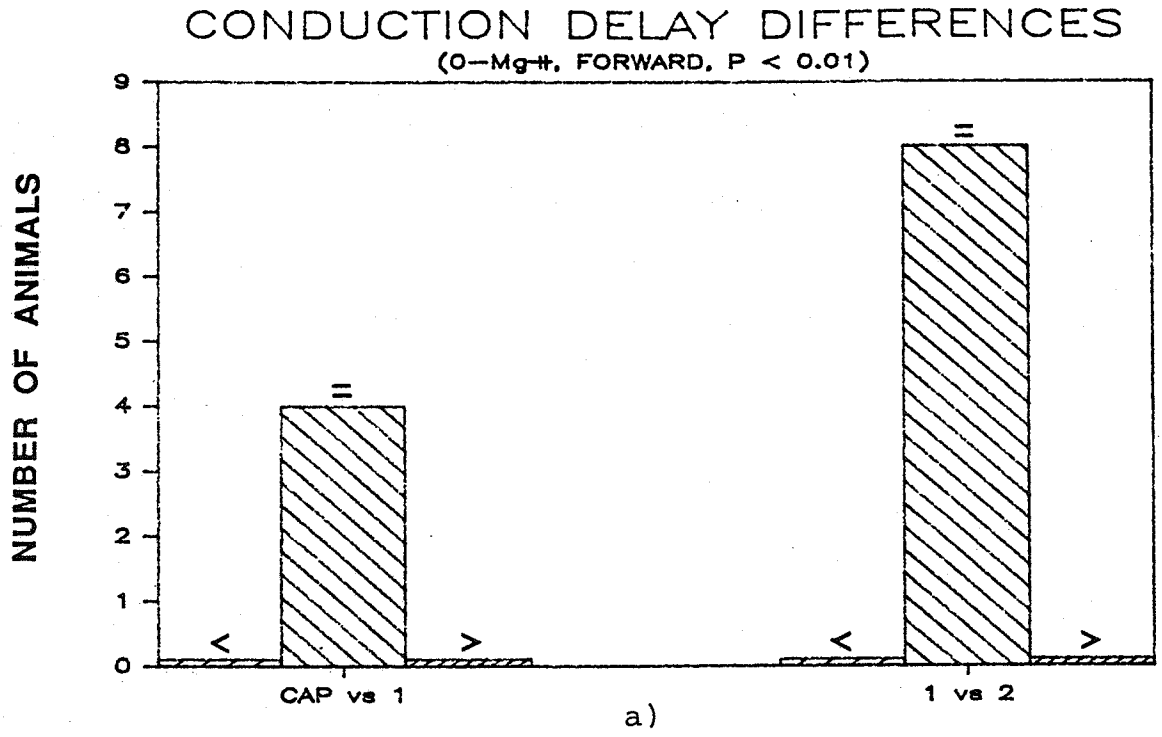

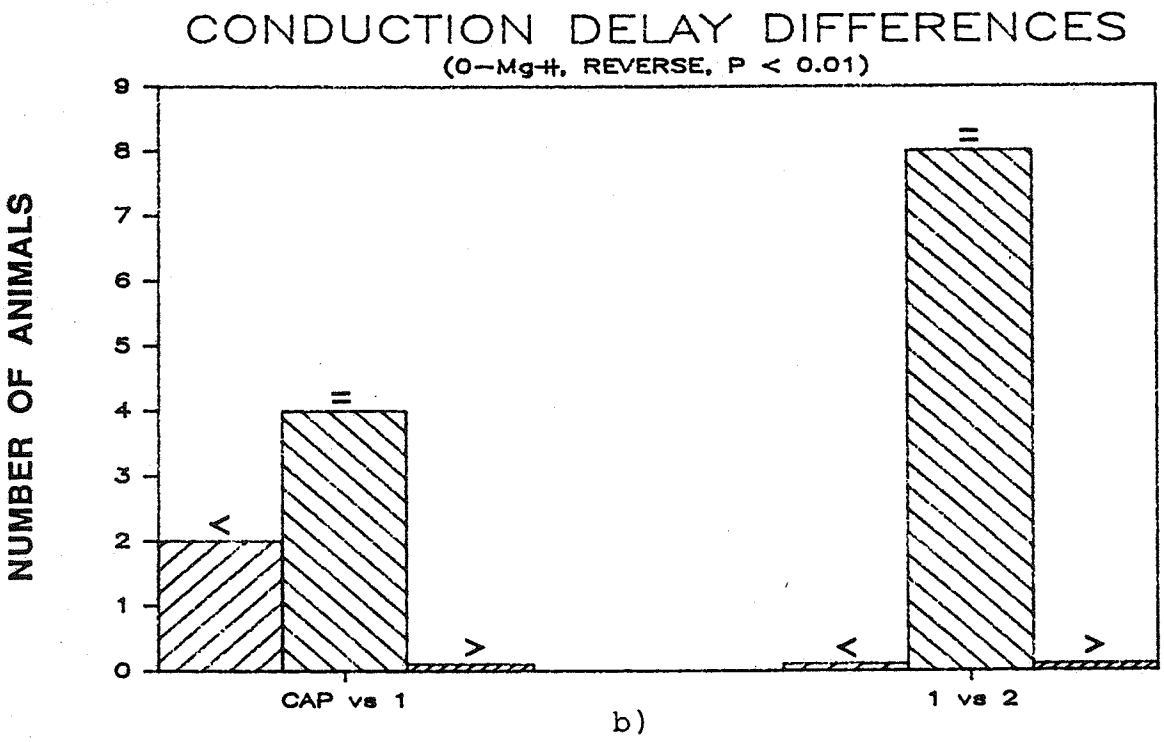

Figure 6.18 Conduction delay comparisons for the 0-Mg^{++} model. Forward conduction is shown in a), reverse conduction in b), and a comparison of forward versus reverse delays is given in c). The data are from 8 slices obtained from 8 animals on separate occasions.

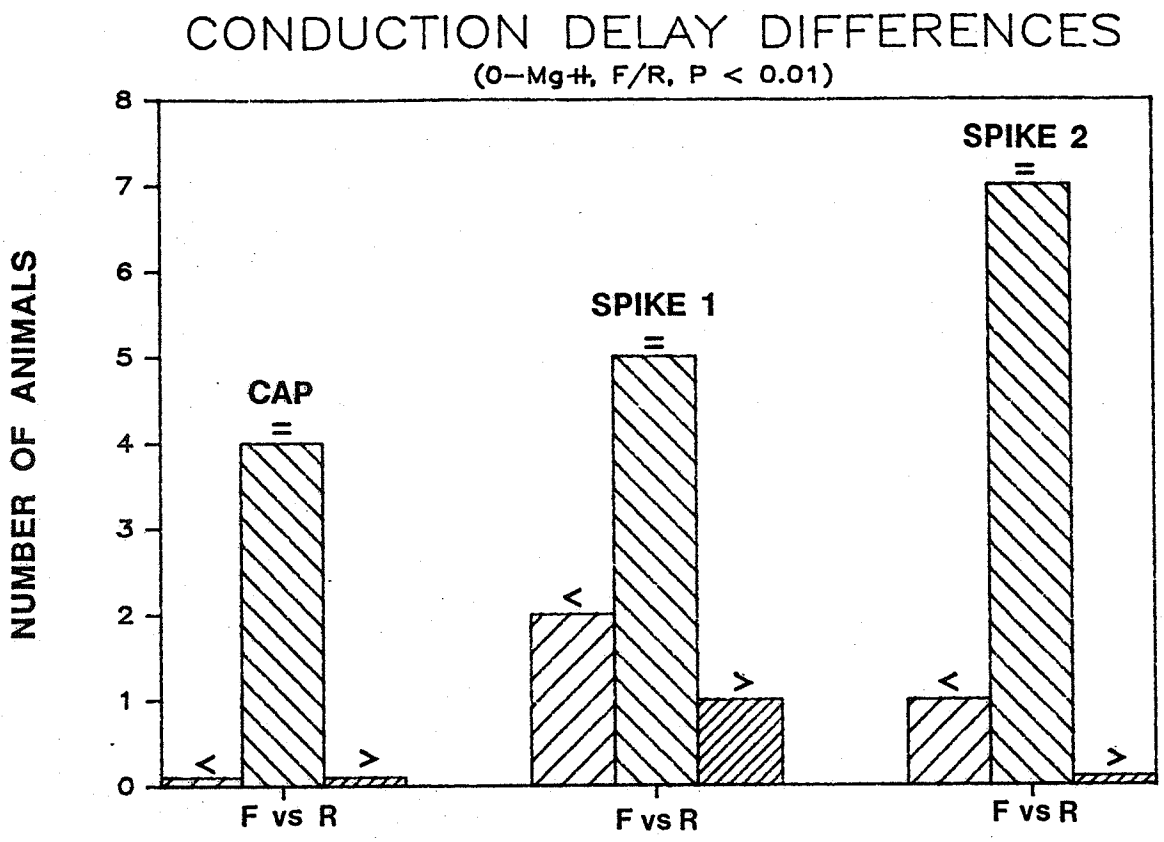

c)

Figure 6.18 Continued.

and were "tuned" for faster propagation in the forward direction. Propagation mechanisms for spike 2 appeared to be isotropic, conducting equally well in both directions.

Interestingly, in the other GABA-inhibitor model, PTZ, similar results were observed (Figure 6.17). Although the CAP was not observed in response to forward stimulation, the histograms were quite similar to those for the PTX model. The conduction delays seemed to be functions of the common GABA-antagonist properties of the convulsant agents.

Experiments performed using 0-Mg^{++} medium displayed markedly different results (Figure 6.18). In contrast with the above data, no difference was observed in delays between any of the components of the bursts propagating in either the forward or reverse directions. Bursts in the 0-Mg^{++} model seemed to remain intact as they propagated, and maintained fixed delays between the three components. This model, in which excitation is enhanced, possessed propagation symmetry which was not present in the reduced-inhibition PTX or PTZ models.

The correlation between peak amplitude and peak time was measured for each slice to investigate the relationship of signal strength and propagation (Table 6.1). The relatively small number of significant cases failed to demonstrate strong involvement of field potential amplitude-dependent propagation coupling mechanisms, such as ephaptic coupling.

Finally, for each of the slices used in the experiments described above, the CSD peak amplitudes of the CAP, spike 1, and spike 2 were recorded for the electrode location displaying the

Table 6.1 Correlation between amplitude and peak time.

Number of slices with significant ($p < 0.05$) correlation between amplitude and peak time

	Forward direction		
PTX	1/3	0/7	2/7
PTZ	---	2/5	0/5
0-Mg^+	2/4	0/8	1/8
	Reverse direction		
PTX	1/5	1/5	1/5
PTZ	4/5	2/5	2/5
0-Mg^+	2/5	1/8	2/8

largest amplitude CSD profile for spike 1. These peak amplitudes provided more reliable indicators of underlying neural activity than those of population spikes because they were minimally affected by adjacent activity. The peak values were averaged across slices to obtain a value for each of the three models of epilepsy studied (Table 6.2). Interestingly, the 0-Mg^{++} model produced population spikes which were considerably smaller than those of either the PTX or PTZ models ($p < 0.025$). The reduction in local inhibition might have permitted tighter synchronization among a local neural population than the 0-Mg^{++} treatment.

Table 6.2 Comparison of maximum peak amplitudes.

Peak amplitudes of burst components (mV /mm^2)
(mean $\pm$ s.d. (N))

Forward direction

	PTX	PTZ	0-Mg^{++}
CAP:	26.6 $\pm$ 14.2 (7)	---	18.2 $\pm$ 9.0 (4)
Spike 1:	134. $\pm$ 73.7 (11)	204. $\pm$ 36.3 (5)	85.3 $\pm$ 78.0 (8)
Spike 2:	68.9 $\pm$ 41.0 (11)	81.9 $\pm$ 21.6 (5)	38.1 $\pm$ 34.4 (8)

Reverse direction

	PTX	PTZ	0-Mg^{++}
CAP:	52.2 $\pm$ 46.0 (5)	28.7 $\pm$ 20.3 (5)	22.5 $\pm$ 12.3 (5)
Spike 1:	141. $\pm$ 103. (5)	208. $\pm$ 51.2 (5)	78.4 $\pm$ 64.0 (8)
Spike 2:	75.2 $\pm$ 54.9 (5)	87.3 $\pm$ 27.3 (5)	37.8 $\pm$ 35.1 (8)

Summary of peak amplitude relationships ($p = 0.025$)

Forward direction

CAP: 0-Mg^{++} < PTX

SPIKE 1: 0-Mg^{++} < PTX < PTZ

SPIKE 2: 0-Mg^{++} < PTX = PTZ

Reverse direction

CAP: 0-Mg^{++} = PTX = PTZ

SPIKE 1: 0-Mg^{++} < PTX = PTZ

SPIKE 2: 0-Mg^{++} < PTX = PTZ

CHAPTER 7

DISCUSSION

7.1 Instrumentation Required for Multichannel Neural Recording

The use of this multiple electrode array brings with it significant potential for new experimental observations. Although no small number of surface array electrode performs as well as the same number of strategically placed conventional electrodes, the slice can be easily positioned on the array so that a large number of regularly spaced electrodes are in good position for simultaneous stimulation and recording.

The potential for mass fabrication, their durability compared to hand-fashioned arrays, and their applicability to tissue culture work make it possible that arrays will be commercially available in the near future. Procedural advantages include the ease with which the electrodes are positioned (i.e., by positioning the slice once) and the fact that the array uses none of the valuable space above the preparation needed for viewing and for positioning other electrodes or applicators.

The experiments described here would not have been possible without the support of a powerful computer-based data acquisition and analysis system. Little multichannel neurophysiological instrumentation was available at reasonable cost/performance ratios. Much of the circuitry was locally constructed after determining that combining many single or dual channel components to produce a 32-channel system was expensive, and often would not work. For example, the 32 independent differential

preamplifiers became unbalanced if all were connected to a single return electrode. Also, because of the relatively high bandwidth required, storage of 32 channels of evoked responses on FM tape was impractical. But the most critical element of the system was the graphics display of 32 amplitude-versus-time functions. The ability to evoke a response and to view it on the monitor within seconds at arbitrary time and amplitude scales provided the feedback necessary to interpret the data so as to maximize productivity. In particular, the CSD profiles could be viewed with only a 2 s delay, effectively "closing the loop" involved in using them to determine acceptability of both slice health and position.

7.2 Performance of the Array with Hippocampal Slices

The results of the previous chapter demonstrate that field potentials may be recorded at the surface of a hippocampal slice using a planar array of electrodes. The techniques described overcome some of the problems associated with the presence of the dead cell layer and the presumably hypoxic nature of the bottom of the slice. The duration of slice viability is sufficient to perform a variety of tests, including establishing electrophysiological stability, observing wash-in of convulsant drugs, positioning of electrodes based upon response, and stimulating at multiple sites with the array. These capabilities meet the fundamental requirements of a new recording/stimulating electrode technology.

Signals recorded by the array can be compared directly with those recorded using conventional electrodes. The only consistent difference is in the amplitudes of the field potentials recorded with the array. They are typically two to five times smaller than signals acquired with conventional electrodes. Initial fears that the presence of the dead layer between the array electrodes and active cells would permit significant dispersion of current flow, reducing field potentials at the surface to below the noise level, are unfounded. It is now believed that, although the dissipation probably does occur to some extent, signals are enhanced by the presence of the insulating electrode array itself. Consider the model in which neurons are current sources in a resistive medium. The interposition of a nonconducting plane (the array) at the recording surface effectively doubles the recorded potentials as though an image current source were present (Jobling, 1981). This also appears to be the case in conventional hippocampal slice recording, as the largest signals are present at the upper surface of the slice, just at the medium/gas interface (F.E. Dudek, personnal communication).

Uniform sampling of extracellular field potentials permits the calculation of the CSD profiles versus time at many points on the slice. The use of the 2-D CSD calculation to estimate the locations of the active neural current sources eliminates errors arising from misinterpretation of field potential data. Additionally, the similarity of CSD profiles derived with the array to those published serves to confirm the relationship

between array and conventional recordings, as well as establishing the uniqueness of surface potential records. The CSD calculations exhibit source/sink relationships, which would not occur if the array recorded surface potentials reflected gross and not local activity.

The creation of spatio-temporal CSD maps is a potentially powerful method of observing spatial processing in the nervous system. Creating these maps using conventional electrodes relies on an averaging and a step-and-repeat process whereby the recording electrodes are moved between stimuli (Freeman and Nicholson, 1975; Swann et al., 1986). Problems in interpretation of these experiments arise from the dynamic and time-varying hippocampal physiology since tissue stationarity must be assumed between as many as 80-100 stimuli and for as long as 2 h (Swann et al., 1986). Additionally, positioning errors and some degree of tissue damage seem unavoidable over such a large number of penetrations.

The technique presented in this thesis offers the advantage of obtaining simultaneous multipoint data for a single stimulus. The slice is positioned once, and evoked responses at 32 sites can be used to create a spatio-temporal CSD map for that particular stimulus. No averaging or assumption of tissue stationarity is necessary, and the interelectrode spacing is fixed. If the tissue shifts or spreads, the anatomical location of the CSD profile will change, but the calculation will remain correct.

Acquiring multiple channels in two dimensions also permits the estimation of 2-D CSD profiles, and not only 1-D profiles as is currently done (Swann et al., 1986; Miyakawa and Kato, 1986). The rationale for using 1-D estimates is based upon the observation that much of the current flow during synchronous activation is along the major axis of pyramidal cells. Although this appears to be accurate, the field potential also depends on the conductivity of the surrounding tissue. A recent report by Holsheimer (1987) shows that the conductivity in the middle of s. pyr. in CA1 is approximately half that of the borders. Conductivity increases smoothly toward the s. rad. and decreases toward the alveus. Unfortunately, conductivities normal to the major axis of the pyramidal cells, parallel to the Schaffer collaterals, are not reported. One might expect significantly smaller conductivities since the paths for current flow are much more restricted in this direction. This enhances the contribution of smaller currents parallel to the Schaffer collaterals to the field potential, particularly those within s. pyr. In light of these arguments, it can be concluded that the 2-D calculation is more accurate since it assumes equal conductivities along both major axes in the slice plane, while 1-D calculations are degenerate cases in which the conductivities in the normal direction have been set to zero.

In addition to the recording potential, this array is capable of stimulating at multiple sites in the slice. The results of stimulation experiments in Chapter 6 demonstrate that relatively localized stimulation may be performed using the array

electrodes with 200 μm resolution. This capability is potentially extremely useful in investigations utilizing stimulation to alter an ongoing epileptiform event (Durand, 1986), as well as in associative conditioning experiments in which multiple pathways are stimulated sequentially (Barrionuevo and Brown, 1983). Also, if the slice is appropriately positioned over the array, one could observe the response of many of the hippocampal subpopulations to direct stimulation, activation via presynaptic fibers, and more natural activation by stimulation of a presynaptic cell population.

The most important limitation to the use of the array/hippocampal slice preparation is the 2 h duration of useful recordings, although this is presently sufficient to establish baseline recordings and to perform solution changes. Modelling studies indicate that the array records only from the bottom half of the slice (Wheeler and Novak, 1986), while recordings can be made for many more hours with conventional electrodes in the upper layers of the slice. Slices presumably die from the bottom up due to the impermeability of the array. Additionally, the phenomenon of slice spreading affects the ability to record from the same location for an extended period of time. Slice spreading has not been reported in the literature as a problem; however, it does occur to some extent in conventional protocols, particularly when recording for extended periods (J. W. Swann, personal communication).

7.3 Implications of Conduction Delay Studies

The experiments presented in Section 6.5 comprise one of the first attempts to quantify the characteristics of propagating epileptiform activity in brain slices. While a wide variety of manipulations to induce epileptiform bursting have been reported in the literature, these studies are concerned with the objective of better understanding the mechanisms which permit the generation of population bursts. Elegant pharmaceutical and ionic alterations allow conclusions to be drawn regarding the cell membranes, local synaptic circuits, and local coupling mechanisms present in a particular model. However, it appears that propagation of epileptiform bursts in slices must also be considered if one is to make accurate extrapolations to other systems. Data relating to propagation are particularly relevant for the development of anticonvulsant drug therapies to reduce the spread of abnormal activity without impairing normal function. This study focuses on one aspect of burst propagation through CA1 by comparing the conduction delays and peak amplitudes for individual components of an epileptiform burst.

A possible explanation for the differences observed in peak amplitudes and conduction delays between the GABA-antagonist and 0-Mg^{++} models is that the generation and propagation mechanisms are separable, and may be manipulated with some degree of independence. Both models sufficiently alter the hippocampal slice system to permit synchronization of individual cells to form population bursts. However, their primary effects are quite different, and appear to differentially alter processes involved

in the spread of abnormal activity.

The generation of population spikes requires synchrony between the firing times of local populations of cells. The degree of synchrony affects the amplitudes of the population spikes. The peak amplitudes in the PTX and PTZ-treated slices are considerably larger than those in 0-Mg^{++}. By reducing local inhibition, the former treatments permit much larger populations of cells to fire in synchrony, resulting in larger summated current flows and population spikes. The 0-Mg^{++} model, which promotes activation of NMDA receptors as well as possibly reducing divalent cation screening charges, preserves the local inhibition. This reduces synchrony within a population by altering firing thresholds. The smaller CSD estimates for the 0-Mg^{++} model suggest that while the manipulation raises the overall level of excitability, it does not promote local synchronization to as great an extent as the other models.

The lack of strong correlation between CSD peak amplitude and peak times argues against involvement of ephaptic or electric field interactions at this spatial resolution, although local involvement during generation and synchronization of population bursts has been demonstrated (Snow and Dudek, 1984). Systems in which ephaptic coupling is dominant in propagation would be expected to propagate with least delay near areas of large signal amplitude, resulting in a strong negative correlation between the two measurements. The interelectrode distances used here appear to be too great for ephaptic coupling to play a significant role.

The propagation of population bursts in CA1 can be explained by treating the slice as a system which propagates the components of a burst with delays reflecting the coupling mechanisms involved. Propagation of the CAP depends only on the physical properties of the Schaffer collateral pathway itself. This is reflected in the similarity of forward and reverse delays in all models. Population spike coupling mechanisms, on the other hand, can be considered to have spatial distributions which describe the extent of excitatory or inhibitory coupling. Computer simulations have shown that as the spatial distribution of an excitatory mechanism becomes larger, the delays for propagating population spikes decrease until they reach the limiting conduction velocity of the axons (Traub et al., 1987). If the distribution of inhibitory mechanisms is increased, e.g., inhibitory interneurons are modelled as projecting to cells more distant, propagation is slowed. Thus, manipulations of these spatial coupling distributions can cause changes in the apparent conduction delays for population spikes. In addition, because spikes 1 and 2 appear to be inherently different, as discussed in Chapter 2, distributions for each of these components may be unique and may be differentially affected by experimental manipulations.

The symmetrical conduction of spike 2 in the GABA-antagonist models implies that largely isotropic coupling mechanisms are involved. The longer conduction delays for spike 2 relative to the CAP could be due to both the absence of excitatory synaptic activation and the residual inhibition. Excitatory coupling

mechanisms for spike 2 are similar to those involved with spike 1 except for the lack of direct synaptic activation via the Schaffer collaterals. Additionally, after the generation of spike 1, the long time course of the PTX resistant IPSPs would reduce excitability. Based upon the above modelling studies, this reduction in excitability would have predicted this observed increase in conduction delays.

In contrast, the asymmetrical conduction of spike 1 in the PTX and PTZ models suggests the influence of a directional coupling mechanism which aids or reduces the resistance to transmission in the forward direction. Two candidate mechanisms are feed-forward excitation and antagonized feed-forward inhibition. Because CA1 possesses a large amount of recurrent and feed-forward inhibition and apparently lacks excitatory interpyramidal cell connections, the latter mechanism appears more likely. As mentioned in Chapter 2, PTX-sensitive synapses are part of the feed-forward synaptic circuitry in CA1. If feed-forward inhibition is preferentially antagonized, transmission in the forward direction would increase. Assuming that the remaining isotropic excitatory coupling mechanisms such as local ion fluxes and electrotonic coupling are sufficiently strong, propagation of the spike 1 in PTX (or PTZ) might occur at the speed of the CAP. Reverse propagation would occur more slowly, since the normal amount of inhibition would be present.

The similarities in conduction delays for spikes 1 and 2 propagating in the reverse direction imply that the two processes

are related. This might be the result of common mechanisms dominating the coupling for each component with changes in conduction delays being mediated by the activation of the Schaffer collaterals and inhibitory circuitry. Thus, propagation through CA1 would occur at a "natural" rate if insufficient modulatory excitation were present. The net modulation due to spike 1 propagating in the reverse direction would be insufficient possibly due to concurrent synaptic inhibition or a lack of coherency among the arriving action potentials. Processes involved with spike 2 do not involve excitation via the Schaffer collaterals and also would not affect conduction delays. In both of these cases, propagation would occur at the "natural" rate. Only during forward activation of the Schaffer collaterals would sufficient modulatory excitation be present to decrease delay times.

Using these ideas, the symmetrical nature of the conduction delays in the 0-Mg^{++} model could be explained as the result of powerful long-duration excitation of the pyramidal cell population. Unmasking long-lasting NMDA-mediated EPSPs would provide sufficient modulatory excitation during the entire burst to decrease conduction delays to that of the CAP. In this manner, the propagation characteristics of the slice as a system have "saturated" and will follow the CAP in either direction. The symmetrical properties of the CAP result in the observed symmetry between all burst components.

7.4 Future Work

Future work with the recording system consists of 1. testing the hypotheses regarding propagation as well as other interesting phenomena with new experiments; 2. investigating other analysis techniques to derive new information, particularly those methods utilizing the spatial domain; and 3. improving technical aspects of the system hardware and software. This thesis serves to establish the multichannel recording technique as a useful tool in the investigation of the spread of abnormal activity. With this technological foundation, it should prove fruitful to perform both scientific and engineering investigations.

The relationship between the generation and propagation of epileptiform activity in CA1 could be explored by first using combinations of the PTX, PTZ and 0-Mg^{++} models. For example, if Mg^{++} levels were lowered gradually in a medium containing a convulsant drug, the conduction delay for spike 2 would be expected to decrease to the point where it saturated to the levels for the CAP and spike 1. Peak amplitudes would not be expected to change since local synchronization is hypothesized to be already maximal due to the antagonized inhibition. Conversely, one would expect to see significant increases in peak amplitudes if a convulsant was added to a 0-Mg^{++} medium. However, since propagation was already maximal, no changes would be observed in the conduction delay for any burst component. These experiments would support the notion that the PTX and PTZ models are more effective in promoting local synchronization, while the 0-Mg^{++} model promotes propagation to a greater extent.

The pharmacological dissection techniques used by Coan and Collingridge (1985) to abolish spike 2 while retaining spike 1 could be profitably utilized to examine the effect of NMDA receptor involvement in propagation. Because the model demonstrating greatest propagation speed (0-Mg^{++}) enhances the activity of NMDA receptors, it seems likely that the addition of small amounts of DAPV, the NMDA antagonist, would result in variations in conduction delays. Furthermore, if NMDA receptors are principally involved in propagation of spike 2 in GABA-antagonist models, addition of DAPV to media containing either PTX or PTZ would be expected to further slow the conduction of spike 2. Spike 1 during reverse propagation would also be slowed, since it appears to be subject to the same propagating mechanisms as spike 2.

Two interesting phenomena observed seem to merit additional study. First, in the PTX and PTZ models, the peak amplitude profiles plotted as a function of the electrode position often increase and then decrease with distance from the stimulating electrode. The rate of the increase is occasionally quite large, and gives the impression of "hot spots" or local foci in which activity was maximal. The results of experiments using 0-Mg^{++} medium do not show this effect. This supports the notion of the existence of local increases in cellular synchronization. Although local pacemaker populations within CA1a exhibiting spontaneous seizure-like activity have been observed in PTX (Hablitz, 1984) and a 0-Ca^{++} model (Konnerth et al., 1986), no reports foci during evoked population bursts are available.

In a few preliminary experiments using PTX (not included among those reported here), there is some evidence of nonuniform conduction of population spikes between electrode locations. Conduction delays increase uniformly to a position at which the delay would either increase or decrease significantly. This type of conduction is present in the neocortical slice model of epileptiform activity and is thought to result from local anatomical differences (Gutnick and Wadman, 1986). Two measures used unsuccessfully to quantify this nonsmooth conduction are the coefficient of variation (mean conduction delay/standard deviation) and the correlation coefficient derived during the linear regression. However, analyses of multiple slices are not consistent, and these measures often obscure cases of obvious saltatory conduction. These two measures are relatively insensitive from a statistical point of view as they rely on only six peak measurements. Perhaps another more sensitive measure can be developed to ascertain whether this phenomenon is real in hippocampal slices.

The potential for using the array with other slice preparations is greatest for those that exhibit large amounts of population activity. Models of epileptiform behavior appear to offer the greatest promise due to the nature of the synchronized neural firing. An obvious application is with longitudinal hippocampal slices. The Schaffer collaterals are severed in slices in this orientation, which prevents serial activation via a common pathway (Traub et al., 1987). Neocortical slices, with multiple layers of cortical organization, can also be used as

models for a variety of studies (Connors and Gutnick, 1984). As mentioned in Chapter 2, studies of propagating epileptiform activity recently have been performed in neocortical slices bathed in a medium containing PTX (Chervin and Connors, 1986; Connors and Chervin, 1986; Gutnick and Wadman, 1986). More detailed analyses of conduction delays using CSD profiles could easily be performed with the array technology.

The derivation of the CSD calculation can be formulated in the time domain, as in Chapter 5, in the temporal frequency domain, or as an algebraic system of equations. The time-domain formulation uses integer arithmetic on information only from adjacent electrodes. The other approaches require floating-point operations and information from a larger region around the point under consideration. However, the temporal frequency-domain approach can be optimized for sources located a given depth into the slice (Wheeler and Novak, 1986), while the algebraic method appears to offer better estimates of CSD profiles at the edge electrodes. Although the discrete Laplacian approach used here provides a good estimate of the CSD profiles, direct comparisons of the results of the three computations may provide insight into situations for which one of the three is optimal.

Another method of analyzing the data which may be applied to slice data involves using spectral decomposition techniques adapted from those used in EEG studies. The cross spectrum between signals on two channels reveals the magnitude and phase relationships at various temporal frequencies. Using this

information, one can reconstruct linear delay relationships between frequency components in a waveform. Still, the relationship between the results of these analyses and the physiology is somewhat unclear. Further work to determine the usefulness of this technique is necessary.

Finally, there are a number of technical improvements which could be made to the system to provide immediate and long-term benefits. First, the recording duration is too short to permit multiple solution changes without losing signal strength. It is believed that hypoxia at the array/slice interface plays a major role in the signal loss. A perforated array, through which oxygen may diffuse to the slice surface, is being developed. This should lead to improvements in slice stability and viability.

The addition of additional electrodes and associated analog hardware is potentially quite useful. Finer recording resolution (e.g., 100 μm) or increased size of covered tissue area will provide information useful in understanding the slice as a neural system. Specialized geometries for other areas of the hippocampal or other slice preparations could easily be laid out using a computer-aided-design (CAD) system for making masks. Standard connectors would permit the use of the same analog and digital instrumentation. Since a 64-channel DMA A/D board was designed and built to permit digitizing field potentials at a 10 kHz/channel rate (Novak and Wheeler, 1987a), only the additional analog circuitry remains to be constructed for the complete recording system.

As the volume of data acquired grows, the techniques for communicating with the experimenter and manipulating the information must become more sophisticated. The system as a whole could be improved through the restructuring of old subroutines and the addition of new functions to support additional I/O peripherals. Additional menus for choosing analysis techniques as well as help screens will aid rapid mastery of the system by nonprogrammers. Timer-driven interrupt routines to permit sampling and data collection in parallel with analysis should also prove quite useful. Implementation of the two additional CSD calculation algorithms discussed above is necessary before comparisons may be made. Displaying this large amount of data using color graphics could aid comparison of multiple waveforms and derived functions. If a 64-channel version of the system is desired, either a windowing technique in which only a subset of data is viewed at one time or multiple monitors appear necessary.

REFERENCES

Aitken, P. G. and Somjen, G. G. (1986) The sources of extracellular potassium accumulation in the CA1 region of hippocampal slices, Brain Res., 369:163-167.

Alger, B. A. (1984) Hippocampus: Epileptiform activity in vitro, in Brain Slices, R. Dingledine, ed., Plenum Press, NY.

Alger, B. A. and Nicholl, R. A. (1982a) Feed-forward dendritic inhibition in rat hippocampal pyramidal cells studied in vitro, J. Physiol., 328:105-123.

Alger, B. A. and Nicholl, R. A. (1982b) Pharmacological evidence for two kinds of GABA receptor on rat hippocampal pyramidal cells studied in vitro, J. Physiol., 328:124-138.

Andersen, P., Bliss, T. V. P., and Skrede, K. K. (1971a) Lamellar organization of hippocampal excitatory pathways, Exp. Brain Res., 13:222-238.

Andersen, P., Bliss, T. V. P., and Skrede, K. K. (1971b) Unit analysis of hippocampal population spikes, Exp. Brain Res., 13:208-221.

Andersen, P., Silfvenius, H., Sundberg, S. H., Sveen, O., and Wigstrom, H. (1978) Functional characteristics of unmyelinated fibers in the hippocampal cortex, Brain Res., 144:11-18.

Andersen, P., Gjerstad, L., and Langmoen, I. A. (1978) A cortical epilepsy model in vitro, in Abnormal Neuronal Discharges, N. Chalazonitis and M. Buisson, eds., Raven Press, NY, pp. 29-36.

Anderson, W. W., Lewis, D. V., Swartkwelder, H. S., and Wilson, W. W. (1986) Magnesium-free medium activates seizure-like events in the rat hippocampal slice, Brain Res., 398:215-219.

Ault, B., Evans, R. H., Francis, A. A., Oakes, D. J., and Watkins, J. C. (1980) Selective depression of excitatory amino acid induced depolarizations by magnesium ions in isolated spinal cord preparations, J. Physiol., 307:413-428.

Bach, M. and Kruger, J. (1986) Correlated neuronal variability in monkey visual cortex revealed by a multi-microelectrode, Exp. Brain Res., 61:451-456.

Balestrino, M., Aitken, P. G., and Somjen, G. G. (1986) The effects of moderate extracellular K+ and Ca++ on synaptic and neural function in the CA1 region of the hippocampal slice, Brain Res., 377:229-239.

Barnes, C. A., Rao, G., and McNaughton, B. L. (1987) Increased electrotonic coupling in aged rat hippocampus: A possible mechanism for cellular excitability changes, J. Comp. Neurol., 259:549-558.

Barrionuevo, G. and Brown, T. H. (1983) Associative long-term potentiation in hippocampal slices, Proc. Nat. Acad. Sci. USA, 80:7347-7351.

Bement, S. L., Wise, K. D., Anderson, D. J., Najafi, K., and Drake, K. L. (1986) Solid-state electrodes for multichannel multiplexed intracortical neuronal recording, IEEE Trans. Biomed. Eng., BME-33:230-241.

Bragin, A. G., Zhadina, S. D., Vinogiadara, O. S., and Kozhechkin, S.N. (1977) Topography and some characteristics of the dentate fascia-field CA3 relations investigated in hippocampal slices in vitro, Brain Res., 135: 55-66.

Breckow, J., Kalmring, K., and Eckjorn, R. (1982) Multichannel recordings and real-time current source density (CSD) analysis in the central nervous system of insects, Biol. Cybern., 45:115-121.

Chervin, R. D. and Connors, B. W. (1986) Lateral propagation of synchronized paroxysmal discharges in the disinhibited neocortex, Proc. Soc. Neurosci., Washington, DC, p. 350.

Coan, E. J. and Collingridge, G. L. (1985) Magnesium ions block an N-methyl-D-aspartate receptor-mediated component of synaptic transmission in rat hippocampus, Neurosci. Let., 53:21-26.

Collingridge, G. L., Kehl, S. J., and McLennan, H. (1983) Excitatory amino acids in synaptic transmission in the Schaffer collateral-commisural pathway of the rat hippocampus, J. Physiol., 334:33-46.

Connors, B. W. and Chervin, R. D. (1986) Physiological evidence for periodicity and directionality of lateral excitatory connections in rat neocortex, Proc. Soc. Neurosci., Washington, DC, p. 350.

Connors, B. W. and Gutnick, M. J. (1984) Neocortex: cellular properties and intrinsic circuitry, in Brain Slices, R. Dingledine, ed., Plenum Press, NY.

Cotman, C. W. and Iversen, L. L. (1987) Excitatory amino acids in the brain-focus on NMDA receptors, TINS, 10:263-265.

Cotman, C. W., Monaghan, D. T., Ottersen, O. P., and Storm-Mathisen, J. (1987) Anatomical organization of excitatory amino acid receptors and their pathways, TINS, 10:273-280.

Dichter, M. A. and Ayala, G. F. (1987) Cellular mechanisms of epilepsy: a status report, Science, 237:157-164.

Dingledine, R. and Gjerstad, L. (1979) Penicillin blocks hippocampal IPSPs, unmasking prolonged EPSPs, Brain Res., 168:205-209.

Dingledine, R. and Langmoen, I. A. (1980) Conductance changes and inhibitory actions of hippocampal recurrent IPSPs, Brain Res., 185:277-287.

Dingledine, R. (1984) Hippocampus: synaptic pharmacology, in Brain Slices, R. Dingledine, ed., Plenum Press, NY, pp. 87-112.

Dingledine, R. (1986) NMDA receptors: what do they do?, TINS, 9:47-49.

Droge, M. H., Gross, G. W., Hightower, M. H., and Czisny, L. E. (1986) Multielectrode analysis of coordinated, multisite, rhythmic bursting in cultured CNS monolayer networks, J. Neurosci., 6:1583-1592.

Durand, D. (1986) Electrical stimulation can inhibit synchronized neuronal activity, Brain Res., 382:139-144.

Ficht, D. A. (1987) Electrode array development for advanced brain slice recording, M.S. thesis, University of Illinois, Urbana-Champaign.

Fisher, R. A. (1954) Statistical Methods for Research Workers, Hafner Publishing Company, New York, NY, pp. 217-223.

Freeman, W. J. and Stone, J. (1969) A technique for current density analysis of field potentials and its application to the frog cerebellum, in Neurobiology of Cerebellar Evolution and Development, R. Llinas, ed., Amer. Med. Assoc., Chicago, IL, pp. 421-430.

Freeman, W. J. and Nicholson, C. (1975) Experimental optimization of current source-density technique for anuran cerebellum, J. Neurophys., 38:369-382.

Freeman, W. J. (1980) Use of spatial deconvolution to compensate for distortion of EEG by volume conduction, IEEE Trans. Biomed. Eng., BME-27:421-429.

Fujita, Y. and Iwasa, H. (1977) Electrophysiological properties of so-called inactivation response and their relationship to dendritic activity in hippocampal pyramidal cells of rabbits, Brain Res., 130:89-100.

Grinvald, A. (1985) Real-time optical mapping of neuronal activity: From single growth cones to the intact mammalian brain, Ann. Rev. Neurosci., 8:263-305.

Gross, G. W. (1979) Simultaneous single unit recording in vitro with a photoetched laser deinsulated gold multimicroelectrode surface, IEEE Trans. Biomed. Eng., BME-26:273-279.

Gross, G. W., Williams, A. N., and Lucas, J. H. (1982) Recording of spontaneous activity with photoetched microelectrode surfaces from mouse spinal neurons in culture, J. Neurosci. Meth., 5:13-22.

Gutnick, M. J. and Wadman, W. J. (1986) Intrinsic neuronal connectivity in neocortical brain slices as revealed by non-uniform propagation of paroxysmal discharges, Proc. Soc. Neurosci., Washington, DC, p. 349.

Haas, H. L., Schaerer, B., and Vosmansky, M. (1979) A simple perfusion chamber for the study of nervous tissue in vitro, J. Neurosci. Meth., 1:323-325.

Hablitz, J. J. (1984) Picrotoxin-induced epileptiform activity in hippocampus: role of endogeneous versus synaptic factors, J. Neurophys., 51:1011-1027.

Hamon, B., Stanton, P. K., and Heinemann, U. (1987) An N-methyl-D-aspartate receptor-independent excitatory action of partial reduction of extracellular Mg++ in CA1 region of rat hippocampal slices, Neurosci. Let., 75:240-245.

Herron, C. E., Williamson, R., and Collingridge, G. L. (1985a) A selective N-methyl-D-aspartate antagonist depresses epileptiform activity in rat hippocampal slices, Neurosci. Let., 61:255-260.

Herron, C. E., Lester, R. A. J., Coan, E. J., and Collingridge, G. L. (1985b) Intracellular demonstration of an N-methyl-D-aspartate receptor mediated component of synaptic transmission in the rat hippocampus, Neurosci. Let., 60:19-23.

Holsheimer, J. (1987) Electrical conductivity of the hippocampal CA1 layers and application to current-source-density analysis, Exp. Brain Res., 67:402-410.

Hotelling, H. (1953) New light on the correlation coefficient and its transforms, J. Roy. Stat. Soc., 15:193-232.

Jefferys, J. G. R. (1984) Current flow through hippocampal slices, Proc. Soc. Neurosci., Wash., DC, p. 1074.

Jobling, D. T., Smith, J. G., and Wheal, H. V. (1981) Active microelectrode array to record from the mammalian central nervous system in vitro, Med. and Biol. Eng. and Comput., 19:553-560.

Kim, S. J., Kim, M., and Heetderks, W. J. (1985) Laser-induced fabrication of a transsubstrate microelectrode array and its neurophysiological performance, IEEE Trans. Biomed. Eng., BME-32: 497-502.

Knowles, W. D. and Schwartzkroin, P. A. (1981) Local circuit synaptic interactions in hippocampal brain slices, J. Neurosci. 1:318-322.

Knowles, W. D., Funch, P. G., and Schwartzkroin, P. A. (1982) Electrotonic and dye coupling in hippocampal CA1 pyramidal cells in vitro, Neurosci., 7:1713-1722.

Knowles, W. D., Schneiderman, J. H., Wheal, H. V., Stafstrom, C. F, and Schwartzkroin, P. A. (1984) Hyperpolarizing potentials in guinea pig hippocampal CA3 neurons, Cell. and Molec. Neurobiol. 4:207-230.

Knowles, W. D., Strowbridge, B. W., and Traub, R. D. (1985a) Initiation and spread of epileptiform bursting in the hippocampal slice, Proc. Soc. Neurosci., Dallas, TX, p. 1230.

Knowles, W. D., Traub, R. D., Wong, R. K. S., and Miles, R. (1985b) Properties of neural networks: Experimentation and modeling of the epileptic hippocampal slice, TINS, 8:73-79.

Koerner, J. F. and Cotman, C. W. (1982) Response of Schaffer collateral-CA1 pyramidal cell synapses of the hippocampus to analogues of acidic amino acids, Brain Res., 251:105-115.

Konnerth, A., Heinemann, U., and Yaari, Y. (1986) Nonsynaptic epileptogenesis in the mammalian hippocampus in vitro. I. Development of seizurelike activity in low extracellular calcium, J. Neurophys., 56:409-423.

Kruger, J. and Bach, M. (1981) Simultaneous recording with 30 microelectrodes in monkey visual cortex, Exp. Brain Res., 41:191-194.

Kruger, J. (1982) A 12-fold microelectrode for recording from vertically aligned cortical neurones, J. Neurosci. Meth., 6:347-350.

Kuperstein, M. and Eichenbaum, H. (1985) Unit activity, evoked potentials and slow waves in the rat hippocampus and olfactory bulb recorded with a 24-channel microelectrode, Neurosci., 15:703-712.

Kuperstein, M., Eichenbaum, H., and VanDeMark, T. (1986) Neural group properties in the rat hippocampus during the theta rhythm, Exp. Brain Res., 61: 438-462.

Llinas, R. and Nicholson, C. (1974) Analysis of field potentials in the central nervous system, in Handbook of Electroencephalography and Clinical Neurophysiology, Part B, vol. 2, C.F. Stevens, ed., Elsevier, Amsterdam, The Netherlands.

Lorente de No, R. (1934) Studies on the structure of the cerebral cortex II. Continuation of the study of the Ammonic system, J. Psychol. Neurol. (Lpz.) 46:113-177.

Lucas, J. H., Kirkpatrick, J. B., and Gross, G. W. (1985) A photoetched cell relocation matrix for long-term quantitative observations of selected individual neurons in culture, J. Neurosci. Meth., 14:211-219.

MacVicar, B. A. and Dudek, F. E. (1980a) Local synaptic circuits in rat hippocampus: Interactions between pyramidal cells, Brain Res., 184:220-223.

MacVicar, B. A and Dudek, F. E. (1980b) Dye-coupling between CA3 pyramidal cells in slices of rat hippocampus, Brain Res., 196:494-497.

Masukawa, L. M., Bernardo, L. S., and Prince, D. A. (1982) Variations in electrophysiological properties of hippocampal neurons in different subfields, Brain Res., 242:341-344.

Mayer, M. L., Westbrook, G. L., and Guthrie, P. B. (1984) Voltage-dependent block by Mg++ of NMDA responses in spinal cord neurones, Nature, 309:261-263.

Mesher, R. A. and Schwartzkroin, P. A. (1980) Can CA3 epileptiform discharge induce bursting in normal CA1 hippocampal neurons?, Brain Res., 183:472-476.

Miyakawa, H. and Kato, H. (1986) Active properties of dendritic membrane examined by current source density analysis in hippocampal CA1 pyramidal neurons, Brain Res., 399:303-309.

Mody, I., Lambert, J. D. C., Heinemann, U. (1987) Low extracellular magnesium induces epileptiform activity and spreading depression in rat hippocampal slices, J. Neurophys., 57:869-888.

Monaghan, D. T. and Cotman, C. W. (1985) Distribution of N-methyl-D-aspartate-sensitive L-[H^3]Glutamate-binding sites in rat brain, J. Neurosci., 5:2909-2919.

Nicholson, C. (1973) Theoretical analysis of field potentials in anisotropic ensembles of neuronal elements, IEEE Trans. Biomed. Eng., BME-20:278-288.

Nicholson, C. and Freeman, J. A. (1975) Theory of current source-density analysis and determination of conductivity tensor for anuran cerebellum, J. Neurophysiol., 38:356-358.

Novak, J. L. and Wheeler, B. C. (1985) Multi-site stimulation and recording from rat hippocampal slices using a microelectrode array, Proc. IEEE Eng. in Med. and Biol., Chicago, IL, p. 1275.

Novak, J. L. and Wheeler, B. C. (1986a) Recording from the Aplysia abdominal ganglion with a planar microelectrode array, IEEE Trans. Biomed. Eng., BME-33:196-202.

Novak, J. L. and Wheeler, B. C. (1986b) Local synchronous epileptiform activity in CA1 recorded using a 32 element planar microelectrode array, Proc. Soc. Neurosci., Wash., DC, p. 1528.

Novak, J. L. and Wheeler, B. C. (1987a) A fast-sampling multichannel neural data acquisition system for IBM PC compatibles, J. Neurosci. Meth., submitted.

Novak, J. L. and Wheeler, B. C. (1987b) Multisite hippocampal slice recording and stimulation using a 32 element microelectrode array, J. Neurosci. Meth., in press.

Novak, J. L. and Wheeler, B. C. (1987c) Epileptiform activity recorded simultaneously at multiple sites on the surface of a hippocampal slice with a planar microelectrode array. In A. Schurr, T. J. Teyler, and M. Tseng, eds., Brain Slices: Fundamentals, Applications and Limitations, S. Karger, Basel, Switzerland, pp. 177-183.

Novak, J. L. and Wheeler, B. C. (1987d) Differences in conduction velocities of components of epileptiform bursts in the rat hippocampal slice, Brain Res., in preparation.

Novak, J. L., Wheeler, B. C., and Chang, F. -L. (1987) Variations in the delays between peaks within population bursts in CA1 recorded with a 32 element array, Proc. Soc. Neurosci., New Orleans, LA, p. 942.

Olverman, H. J., Jones, A. W., and Watkins, J. C. (1984) L-Glutamate has higher affinity than other amino acids for [^{3}H]-D-AP5 binding sites in rat brain membranes, Nature, 307:462-464.

Pickard, R. S. (1979) A review of printed circuit microelectrodes and their production, J. Neurosci. Meth., 1:301-318.

Pine, J. (1980) Recording action potentials from cultured neurons with extracellular microcircuit electrodes, J. Neurosci. Meth., 2:19-31.

Plonsey, R. (1969) Bioelectric Phenomena, McGraw-Hill, NY, pp. 202-233.

Pochay, P., Wise, K. D., Allard, L. F., and Rutledge, L. T. (1979) A multichannel depth probe fabricated using electron-beam lithography, IEEE Trans. Biomed. Eng., BME-26:199-206.

Prince, D. A. (1978) Neurophysiology of epilepsy, Ann. Rev. Neurosci., 1:395-415.

Rall, W. (1973) Time constants and electrotonic length of membrane cylinders and neurons, Biophys. J., 13:648-688.

Rutecki, P. A., Lebeda, F. J., and Johnston, D. (1985) Epileptiform activity induced by changes in extracellular potassium in hippocampus, J. Neurophys., 54:1363-1374.

Saggau, P., Galvan, M., and Bruggencate, G. T. (1986) Long-term potentiation in Guinea pig hippocampal slices monitored by optical recording of neuronal activity, Neurosci. Lett., 69: 53-58.

Schneiderman, J. H. (1986) Differences in penicillin-induced synchronous bursts in the CA1 and CA3 regions of the hippocampus, Epilepsia, 27:3-9.

Schwartzkroin, P. A. (1975) Characteristics of CA1 neurons recorded intracellularly in the hippocampal in vitro slice preparation, Brain Res., 85:423-436.

Schwartzkroin, P. A. and Mathers, L. H. (1978) Physiological and morphological identification of a nonpyramidal hippocampal cell type, Brain Res., 157:1-10.

Schwartzkroin, P. A. and Prince, D. A. (1978) Cellular and field potential properties of epileptogenic hippocampal slices, Brain Res. 147:117-130.

Schwartzkroin, P. A. (1986) Regulation of excitability in hippocampal neurons, in The Hippocampus, vol. 3, R.L. Isaacson and K.H. Pribram, eds., Plenum, NY.

Shamma-Donoghue, S. A., May, G., Cotter, N. E., White, R. L., and Simmons, F. B. (1982) Thin-film multielectrode arrays for a cochlear prosthesis, IEEE Trans. Electronic Devices, ED-29: 136-144.

Snow, R. W. and Dudek, F. E. (1984) Electrical fields directly contribute to action potential synchronization during convulsant-induced epileptiform bursts, Brain Res., 323:114-118.

Sokal, R. R. and Rohlf, F. J. (1969) Biometry: The Principles and Practice of Statistics in Biological Research, W. H. Freeman and Co., San Francisco, CA, pp. 404-493.

Somjen, G. G. and Giacchino, J. L. (1985) Potassium and calcium concentrations in interstitial fluid of hippocampal formation during paroxysmal responses, J. Neurophys., 53:1098-1108.

Swann, J. W., Brady, R. J., Friedman, R. J., and Smith, E. J. (1986) The dendritic origins of penicillin-induced epileptogenesis in CA3 hippocampal pyramidal cells, J. Neurophys., 56:1718-1738.

Swartzwelder, H. S., Lewis, D. V., Anderson, W. W., and Wilson, W. A. (1987) Seizure-like events in brain slices: suppression by interictal activity, Brain Res., 410:362-366.

Teyler, T. J. (1980) Brain slice preparation: hippocampus, Brain Res. Bull., 5:391-403.

Thomas, C. A., Springer, P. A., Loeb, G. W., Berwald-Netter, Y., and Okun, L. M. (1972) A miniature microelectrode array to monitor the bioelectric activity of cultured cells, Exp. Cell Res., 74:61-66.

Thomson, A. M. and West, D. C. (1985) Picrotoxin-induced epileptiform discharge in slices of rat cerebral cortex is not blocked by NMA antagonists, J. Physiol. (Lond.), 364:31P.

Traub, R. D., Wong, R. K. S., Miles, R., and Knowles, W. D. (1985) Neuronal interactions during epileptic events in vitro, Fed. Proc., 44:2953-2955.

Traub, R. D., Miles, R., and Wong, R. K. S. (1987) Studies of propagating epileptic events in the longitudinal hippocampal slice, Proc. Soc. Neurosci., New Orleans, LA, p. 1159.

Turner, D. A. and Schwartzkroin, P. A. (1980) Steady-state electrotonic analysis of intracellularly stained hippocampal neurons, J. Neurophys., 44:184-199.

Wheeler, B. C. and Novak, J. L. (1986) Current source density estimation using microelectrode array data from the hippocampal slice preparation, IEEE Trans. Biomed. Eng., BME-33:1204-1213.

Wheeler, B. C. and Smith, S. R. (1987) High-resolution alignment of action potential waveforms using cubic spline interpolation, J. Biomed. Comput., in press.

Wise, K. D. and Angell, J. B. (1975) A low-capacitance multielectrode probe for use in extracellular neurophysiology, IEEE Trans. Biomed. Eng., BME-22:212-219.

Wong, R. K. S. and Prince, D. A. (1979) Dendritic mechanisms underlying penicillin-induced epileptiform activity, Science, 204:1228-1231.

Wong, R. K. S., Prince, D. A., and Basbaum, A. I. (1979) Intradendritic recordings from hippocampal neurons, Proc. Nat. Acad. Sci. USA, 76:986-990.

Wong, R. K. S. and Traub, R. D. (1983) Synchronized burst discharge in disinhibited hippocampal slice: I. Initiation in CA2-CA3 region, J. Neurophys., 49:442-458.

VITA

James Lawrence Novak was born on April 19, 1961, in Berwyn, Illinois. From 1979 to 1983, he attended the University of Illinois at Urbana-Champaign and was awarded a Bachelor of Science degree in Electrical Engineering in 1983.

In 1983, Mr. Novak entered the Graduate College of the University of Illinois at Urbana-Champaign in the Department of Electrical and Computer Engineering. He received a University Fellowship in 1983 and a GTE Fellowship in 1985. He served as research assistant under Professor B. C. Wheeler, fabricating multielectrode arrays for neural recording from 1983 to 1986.

During the academic year 1986-1987 he was a teaching assistant for a course on linear integrated circuits, under the supervision of Professor R. W. Burtness. During the fall of 1987, Mr. Novak again served as a research assistant to Professor Wheeler, performing his doctoral research on multichannel neural signal recording and analysis.